UCLouvain

epl

École polytechnique de Louvain

Low tech solar collector for tiny houses

Authors: **Arnaud Philippart, Pierre Balhaut**
Supervisor: **Francesco Contino**
Readers: **Francesco Contino, Geoffrey Van Moeseke, Philippe Hébert**
Academic year 2023–2024
Master [120] in Electro-mechanical Engineering

Acknowledgments

This master thesis would not have been possible without the support and guidance of many individuals.

First and foremost, we would like to express our gratitude to our supervisor, Dr. Francesco Contino, for his support and his guidance which helped us throughout the research and writing of this thesis.

We are also deeply grateful to Philippe Hébert and the Hellow team, for their valuable comments and suggestions which enhanced the quality of our work. We thank them also for proposing this fascinating subject and for providing the necessary resources and support such as their solar collector and their measurement instrumentation.

We are really thankful to the Institute of Mechanics, Materials, and Civil Engineering for providing the necessary instrumentation to conduct our experiments.

Our sincere thanks go to the École polytechnique de Louvain for subsidizing the construction of the collectors used in our research. Additionally, we appreciate the generous contributions from those who donated the glasses for the collector covers and to Jean-Luc Willems, the roofer, for supplying all the necessary slates for the absorbers.

We would like to extend our appreciation to our friends for their encouragement and for making our time at the École polytechnique de Louvain a memorable experience. And last but not least to our family for their continuous support and for enduring the numerous experiments conducted during this research.

Thank you all for your contributions and support.

This master thesis subject has been proposed by Hellow, a company specialized in sustainable tiny houses who explores the impact of innovative construction techniques on housing affordability and environmental sustainability.
Given its perpetually available nature, solar energy emerges as a leading solution to address future energy problems, given the anticipated depletion of fossil fuels. Low-tech air solar collectors are promising in harnessing this energy due to low maintenance and long life cycles.

This thesis evaluates the power output of such devices, focusing on the geometry and impact of the materials. Python simulations were conducted, alongside validation with experimental data from built collectors. The goal is to assess the performance and optimize the design of low-tech air solar collectors for domestic purposes.

Our research showed that the behavior is highly dependent on the irradiance. For a given mass flow rate, a collector with an area 1.84 larger than another one outperforms the latter of 14.6 % for a mean irradiance of 234 $\frac{W}{m^2}$ and it increases to 61.86 % of additional power output with a mean irradiance of 598 $\frac{W}{m^2}$. An efficiency improvement of up to 20 % is achievable through the insulation of the collector.
The yield is found to increase with the mass flow rate and can be kept constant around 50 % of the irradiation from spring to autumn by forcing a variable mass flow rate thanks to a small fan. In this configuration a collector with an area of 0.658 m^2 harnesses 280.84 [kWh] throughout the year with a global yield of 49.54 %. The simulation uses heat exchanger transfer coefficients computed experimentally for a collector of 0.658 m^2 and 1.212 m^2 at different mass flow rate.
A natural convection set up experimentally achieved a yield of 5.75 %. We assessed experimentally the optimum number of baffles to 5 for the collector of 0.658 m^2 which leads to an expected yield of 50.82 % Edges have a heat transfer coefficient of 3.05 $\frac{W}{m^2}$, the back face a coefficient of 1.52 $\frac{W}{m^2}$ with insulator and the front 7.22 $\frac{W}{m^2}$[1]. The losses through the front face therefore represent on average more than 40 % of the total losses.
The global heat transfer for the losses is found to be 6.275 [W] on average for the 0.658 m^2 collector.

These findings demonstrate that low-tech solar collectors can significantly contribute to reducing energy consumption in tiny houses. While not a complete replacement for traditional heating systems, they provide a substantial supplementary solution that promotes sustainable living practices. AI has been used to enhance the turning of sentences, correct the text, and improve the vocabulary.

[1] 0.658 m^2 collector

Contents

Chapter 1

Introduction

In the context of increasing emphasis on reducing carbon footprints and adopting sustainable lifestyles, the concept of tiny houses has gained considerable attention. These small dwellings promote a minimalist approach to living, non-conforming to the conventional norms, encouraging an evolution towards more eco-friendly habits. Belgium, like many other regions, faces a growing need to address energy consumption.

Addressing heating concerns becomes thus a priority. Solar collectors emerge as a promising solution, offering a sustainable alternative to traditional CO2-emitting heating sources.
Indeed, by capturing solar energy and converting it into usable heat, solar collectors can significantly reduce dependence on wood stove or other heating system.
This is not intended to replace completely actual heating system but rather to serve as one component among others contributing to overall heating. Moreover, they save space by being mounted on the walls. In reality, due to the intermittent nature of solar radiation, relying solely on these panels for autonomy would not be feasible.

Another challenge for homes and especially minimalist ones is thermal inertia. Thermal inertia refers to a material's ability to retain heat, such as walls, and is characterized by its thermal capacity. The purpose of thermal inertia in a wall is to release stored heat or coolness with a delay relative to thermal fluctuations outside and inside the building. Thus, it's a more efficient way to utilize thermal energy.

Consequently, the higher the thermal inertia of a house, the longer it takes to heat

or cool it. This characteristic is very important to guarantee comfort, in summer to avoid overheating and in winter to absorb and store heat during the day and release it slowly at night.

Indeed, this capability enables to limit the effects of a "rapid" variation in outside temperature on the indoor climate, by creating a phase shift between the outside temperature and the inside surface temperature of the walls, and by damping the amplitude of this variation. A sufficient phase shift in summer means that outside heat only arrives inside at the end of the day. At the same time, it is much easier to cool the house by simply opening the windows. The house thus maintains a cool temperature throughout the day.

Unlike traditional houses in which the stone walls have a high inertia, the walls of a tiny house are mainly composed of wood and insulators which have a low inertia.

It is intended, among others, to analyze the power output evolution with an absorber of higher inertia than those materials, such as a slate absorber.

In summary, these collectors enable one to reduce the impact of one's lifestyle while simultaneously enhancing their standard of living. It strengthens collective resilience and strives for sobriety, efficiency, and sustainability with this system.

1.1 The low-tech solar collector

Low-tech solar collector stands for a low technology level solar collector which is simple yet effective. It consists of basic materials such as glass or plastic foil, slates or black painted surfaces, aluminum foil or reflective surfaces, optionally wood for the frame and even polystyrene or polyethylene foam for the insulation. Its design is straightforward, the dark heat-absorbing surface is enclosed within a light framework behind a cover.

The glass or plastic foil aims to reduce infrared heat losses and to protect the absorber from dust, debris, rain, and wind, preserving its effectiveness and prolonging gespan.
One has to consider the fact that regular glass poses a significant risk of breaking when there is a temperature difference of 30 °C or more between its two sides. For example, if the absorber reaches temperatures over 70 °C, the inside glass surface

might be around 45 °C according to our measurements. Then, if the outside surface is suddenly cooled by a rain shower, this can create internal stress and cause the glass to shatter.

Tempered glass can address this problem. It is subjected to a special thermal process: it is heated to over 600 °C after being cut to size and then rapidly cooled with cold air jets, which induces compressive stress in the outer layers. This treatment significantly enhances its strength, giving it a flexural strength of about 200 N/m^2 compared to just 40 N/m^2 for ordinary glass of the same thickness and its main advantage in this situation, it can handle temperature fluctuations of up to 200 °C which eliminate the risk we previously stated. Its light transmission remains similar to those of regular glass but it cannot be cut or drilled after tempering without the risk of breaking which is not handy if one needs to resize the glass for the collector dimensions.

The goal of the slates or black painted surfaces is to collect heat in order to transfer it to the working fluid. Slates present the advantage of having a high inertia. Indeed, the higher the density and volume, the higher the inertia and consequently the ability to release heat during a long period of time after sun exposure and to smooth the release of energy. In return, the system needs more time to heat up before reaching a sufficient working temperature.
Black painted surfaces in contrast have a relatively low inertia which allows a heat transfer directly after solar radiation exposure. The importance of the heat transfer is highly dependent on the instant radiation and is sensitive to small radiation fluctuations.
Aluminum foil or reflective surfaces are used to increase radiative transfers to the air and have to be placed opposite the absorber to radiate its power efficiently. The framework can be built in wood for an easy to do and cheap solution. It can also be done directly in the polystyrene foam to lighten the collector while isolating it but this leads to a less attractive and more fragile prototype. This foam primarily serves to insulate the back of the collector to reduce heat losses from the air flow.

Wood sticks or polyethylene foam can possibly be used in order to build baffles to divert the air flow, increasing the contact time with the hot surface and creating turbulences which increase heat transfers.

It operates on the principle of converting sunlight into heat and absorbing it in the slate or the dark surface, taking advantage of the greenhouse effect thanks to the

glass screen, producing heat energy during the day which allows decreasing the load of the conventional heating system. Here below one can see such a system made by NightHawkIngLight. This version is a very basic and cheap one to understand the concept of solar thermal collector but it is not suitable for long-term usage. The cover is made of a plastic film held on a window frame, the absorber is an aluminum black painted foil, the frame a pipe insulator, foam for the baffles and eventually a polystyrene piece for the base.

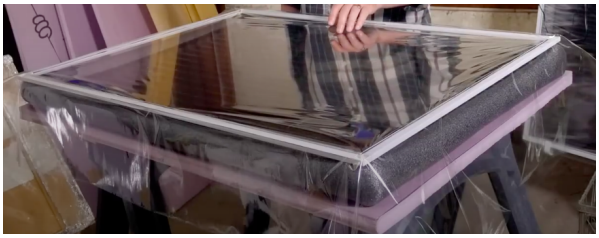

Figure 1.1: DIY collector from NightHawkIngLigth

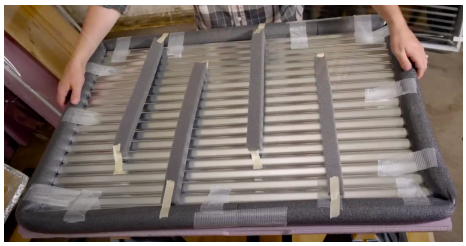

Figure 1.2: Baffles of the DIY collector from NightHawkIngLigth

1.2 Properties of materials

When radiation, such as solar radiation, interacts with a material, the material will absorb, reflect, or transmit a portion of the incident radiation. These characteristics depend on the surface properties, temperature, as well as the angle and wavelength of the incident radiation, and are linked by the following expression :

$$\rho + \tau + \alpha = 1 \tag{1.1}$$

ρ being the reflectance, τ the transmittance, and α the absorptance.

Absorptivity

Solar absorptance is characterized by the ratio of the radiation absorbed by a material, to that of the solar radiation incident to the material. An ideal absorber would then absorb all the incident solar radiation and is known as a 'blackbody'. The reflectance and the transmittance of a blackbody are $\rho = \tau = 0$

Reflectivity

Reflectivity indicates how much incoming radiation is reflected away rather than absorbed. 0% indicates a perfectly absorbing material and 100% indicates a perfectly reflective material.
High reflectivity therefore means less energy absorbed by the material, often leading to a colder material or a material that requires more energy to maintain the target temperature since the latter reflects a part of the incoming heat. Reflectivity is a property useful in a solar collector, on the base facing the absorber.

Indeed, the absorber emits infrared radiation towards the working fluid. A reflective coating allows the base to re-radiate part of this heat back to the air, leading to a lower increasing of the temperature of the base, fewer losses and thus a higher increasing of air temperature.

Speed of heat storage or release

The speed of heat storage or release is determined by two factors: diffusivity and effusivity.
Diffusivity is a measure of how quickly temperature differences smooth out within a material, affecting how rapidly heat spreads through it. Therefore, diffusivity indirectly influences the speed of heat storage or release by affecting how quickly heat can move through a material.

Effusivity is a thermal property that combines the effects of both thermal conductivity and heat capacity. It characterizes how readily a material can exchange heat with its surroundings, taking into account both its ability to conduct heat and its capacity to store heat.

They can be expressed as:

- $D = \frac{\lambda}{\rho \cdot C_P}[\frac{m^2}{s}]$
- $\epsilon = \sqrt{\rho \cdot \lambda \cdot C_p}[\frac{W}{\sqrt{mK}}]$

To build an effective solar collector, its absorber must have a good absorptivity to capture heat and a good diffusivity for a uniform heat distribution and an efficient spreading of the absorbed heat to the air.
A high emissivity at the back of the absorber is also desirable to transfer heat efficiently to the air.
The slate shows a good absorptance and emissivity in the infrared range at room temperature and a low reflectivity.

Selectivity

There are mainly two types of absorbers used in solar collectors : The selective ones and the non-selective ones.

A selective surface presents the advantage of prevailing a high absorptance for radiation in the solar energy spectrum while keeping the long-wave emittance (on the infrared range) of the surface as low as possible, which shrinks the related heat losses. A high absorbing surface also is a high emitting one, hence, selective surfaces change their emissivity depending on the wavelength of the incident radiation.

In order to build such an absorber, coatings possessing high absorption for solar radiation and high transmittance for long-wave radiation can be applied to substrates exhibiting low emittance. These coatings allow absorbing solar radiation efficiently, while the substrates act as poor emitters of long-wave radiation. Metal oxides can typically serve as common coating materials, while metals, such as aluminum or copper, function as the substrates (for instance, copper oxide applied on aluminum).

Material	ϵ/T [K]	α
Black chrome on Ni steel	0.09	0.95
Cu black on Cu	0.17	0.89
Ni black on galvanized steel	0.17	0.81

Table 1.1: Examples of selective materials (12)

Surfaces or coatings that are non-selective maintain a consistent level of emissivity across the entire spectrum. Consequently, as the temperature of the device rises, more energy is lost owing to thermal emittance.

The greenhouse effect

The greenhouse effect is a fundamental atmospheric process that warms the Earth's surface to a life-supporting average of approximately 15°C.
Solar radiation reaches the Earth's surface predominantly in the form of visible and ultraviolet light, which the surface absorbs and then re-emits as infrared radiation. Greenhouse gases absorb a significant portion of this infrared energy and re-radiate it in all directions, including back towards the Earth's surface.
This re-radiation is the key to the warming of the Earth's lower atmosphere and surface. Examples of greenhouse gases are water vapor, carbon dioxide (CO2),

methane (CH4), nitrous oxide (N2O), and fluorinated gases.

This principle also applies in a solar collector, the cover acts as a greenhouse and traps solar radiation, warming the air and absorber inside.
In fact, the glass used is typically highly transparent to short-wavelength solar radiation, including visible and ultraviolet light. When sunlight strikes the collector, this radiation passes through the glass cover and is absorbed by the dark-colored absorber plate.

Once the solar energy is absorbed and converted to heat, the heated surfaces inside the collector re-emit this energy as long-wavelength infrared radiation.
Unlike short-wavelength solar radiation, this long-wavelength infrared radiation cannot pass easily through the glass cover due to its different optical properties.
Besides trapping heat through the greenhouse effect, the glass cover also serves as a physical barrier against heat loss by conduction and convection.

1.3 Characterization of the sunlight resource

The solar radiation is a particle flow. Photons are particles present in electromagnetic waves that carry energy. A light beam is a flow of these particles and each photon carries a specific amount of energy based on the wavelength of the light beam. This amount is given by:

$$E_{ph} = \frac{\mathrm{hc}}{\lambda} \tag{1.2}$$

Moreover, the energy carried by each photon in a light beam, is also characterized by the number of photons per square meter and per second, called here ϕ and is the photon flux contained in the beam. It is the same for solar radiation and the resulting power density or **Irradiance** is written as:

$$\mathrm{H} = \phi \frac{\mathrm{hc}}{\lambda} \tag{1.3}$$

After that, one can model most common light sources, as the Sun, as black-body emitters. It means that this body absorbs all radiation incident on its surface and emits radiation based on its temperature. Planck's radiation law defines the spectral irradiance from a blackbody as:

$$F(\lambda) = \frac{2\pi hc^2}{\lambda^5 (exp(\frac{hc}{k\lambda T}) - 1)} \tag{1.4}$$

Based on the Stefan-Boltzmann law that introduced a constant σ (equivalent to $\sigma = 5.670337442 \cdot 10^{-8}[\frac{\mathrm{W}}{m^2K^4}]$), one has to integrate the Planck's law over all wavelengths from 0 to ∞, and one simply obtains an expression for the total power density from a blackbody equal to:

$$\mathrm{H} = \sigma \mathrm{T}^4 \tag{1.5}$$

In the literature, astronomers agree that sun can be considered as a blackbody of 5778[K] but it is usual to approximate it to 5800[K]. The surface power can be computed based on the equation 1.5 and the value found is approximately:

$$H = 64 \cdot 10^6 \frac{\mathrm{W}}{\mathrm{m}^2} \tag{1.6}$$

Blackbodies, like the sun, have some properties and especially one, which is that they are "*diffuse emitters*". It means that the energy emitted is radiated isotropically and the direction of radiation does not affect it. One can therefore compute the irradiance on an incident object at a given distance D from the center of the sun. The total power emitted from the sun is equal to the irradiance at the border of the resource $H_{sun} = 64 \cdot 10^6[\frac{\mathrm{W}}{\mathrm{m}^2}]$ multiplied by the surface, $S_{sun} = \pi \mathrm{R}^2_{sun}$. The power is conserved until the distance D of the object and the irradiance at this distance is:

$$H_o = \frac{{R_{sun}}^2}{D^2} \mathrm{H}_{sun} \tag{1.7}$$

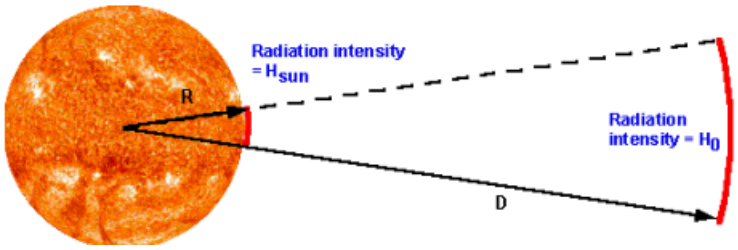

Figure 1.3: Irradiance of an object at a distance D from the center of the sun

The solar constant, G_{sc}, is defined as the energy from the Sun, per unit time, received on a unit area perpendicular to the direction of the radiation's propagation at the average Earth-Sun distance, outside the atmosphere. Its value is $G_{sc} = 1368$ W/m^2.

The radiation emitted by the sun and its solar relationship to the earth, results in an almost fixed intensity of solar radiation outside the Earth's atmosphere.

The solar constant varies trough in tandem with the 11-year solar cycle, which is also observed in other solar phenomena like sunspots, which are dark spots occasionally visible on the solar surface. Therefore, extraterrestrial radiation fluctuates throughout the year. However, variations due to sunspot activity are limited to $\pm 0.02\%$.

Another factor affecting variations in extraterrestrial radiation is the Earth's elliptical orbit. The Earth's orbital eccentricity is about 1.7%, causing the maximum extraterrestrial radiation to occur at perihelion (the point of minimum Earth-Sun distance) and the minimum at aphelion.

One can see on this graph how it evolves :

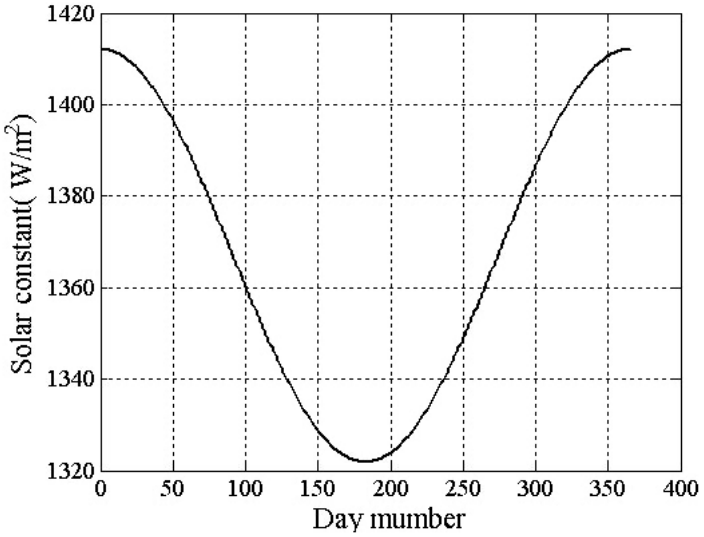

Figure 1.4: Evolution of the solar constant throughout a year

Although those variations on Earth's atmosphere are still relatively low, the amount of solar radiation that reaches the Earth's surface at a perpendicular angle undergoes variations due to the atmosphere acting as an absorber of the emitted power, meaning that the radiation on a collector placed on Earth's surface is lower than

the power at the top of the atmosphere. These changes are brought by two primary phenomena: atmospheric scattering and atmospheric absorption.

Atmospheric scattering occurs when solar radiation interacts with particles in the atmosphere, such as air molecules, water (both in liquid and vapor form), and dust. The extent to which scattering happens is influenced by the quantity of particles the radiation encounters on its path and how large these particles are in comparison to the radiation's wavelength. Those effects are driven by what is called the *Air Mass*. The latter is a parameter which represents the ratio of the path length through the atmosphere that sunlight takes and the path length that sunlight would have taken if the sun was directly overhead the collector or the surface receiving the emitted power. One can compute this factor as :

$$AM = \frac{1}{\cos\theta} \tag{1.8}$$

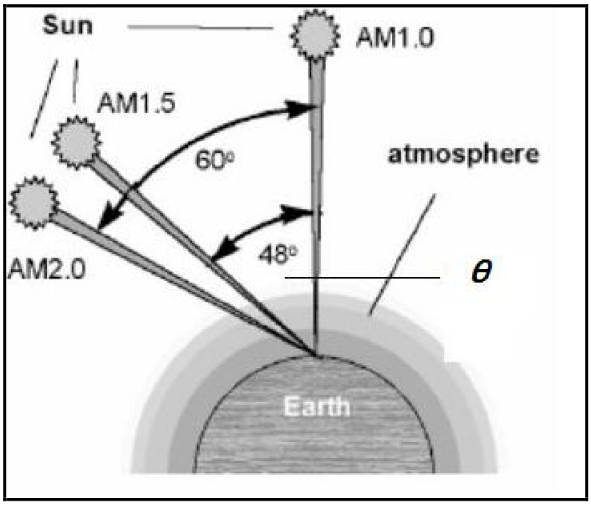

Figure 1.5: Air mass of 1, 1.5 and 2

Chapter 2

Methodology

2.1 Calculation of the incident solar radiation

The power that can be extracted from the solar air collector is directly linked with the irradiance. The angle θ_z can be defined to characterize the irradiance of the sunlight on the collector and analyze how the angle or the position of the collector on the tiny house impacts the irradiance obtained by the solar air collector.

The Sun path relative to a specific location on Earth's surface changes throughout the time of the day and throughout the year and season. The angle that the sunlight strikes an object on Earth can be characterized using different angles.

Longitude

Longitude is the angular distance measured from the prime meridian through Greenwich, England, to the west or east to a point on the surface of the Earth. Any location west of the prime meridian is positive and any location east is negative.

Latitude ϕ

Latitude is the angular distance measured along a meridian from the equator, North or South, to a point on the Earth's surface. Any location towards the North is considered having positive latitude and towards the South as negative latitude. The North and South poles are +90 and -90, respectively. Latitude values are important as they define the relationships with the sun.

Declination angle δ

The angle formed by the line connecting the Earth and the Sun and the equatorial plane is called the declination angle. This is a date-dependent angle, and location does not matter. The declination reaches the minimum or maximum ($\pm 23.45°$) at summer and winter solstices, and it is zero at the equinoxes. It is computed as follows:

$$23.45 \cdot \sin\left(\frac{360}{365} \cdot (N - 81)\right) \qquad \text{N being the day number}$$

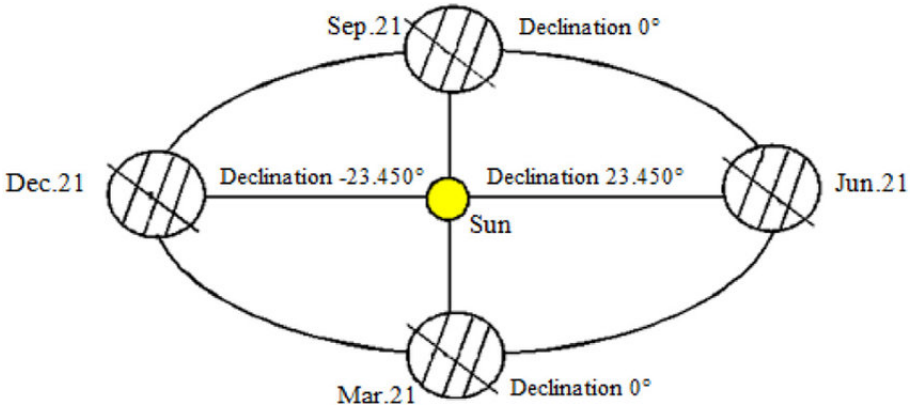

Figure 2.1: Declination angle evolution

Surface azimuth angle γ

The deviation of the projection on a horizontal plane of the normal to the surface from the local meridian, with zero due south, east negative and west positive $-180° \leq \gamma \leq 180°$.

Slope of surface β

The angle between the surface plane and the horizontal is within the range of $0° \leq \beta \leq 180°$. If β exceeds 90°, the surface is inclined downward, which won't happen for this application. For a vertically mounted collector, the angle β is set to 90°.

Hour angle

This is the angle between a line pointing directly at the sun and a line pointing at the position of the sun at solar noon. It is equal to 15 degrees multiplied by the number of hours from local solar noon. This is based on the nominal time of 24 hours for one earth revolution. Morning values are positive in the north hemisphere (east to south) and afternoon values are negative (south to west).

It is defined as :

$$\omega = \frac{(h-12)\cdot 360}{24}$$

With h being the watch time equal to :

$$h = \text{solar time} + \text{daylight saving} - \frac{1}{15}\left(L_{\text{st}} - L_{\text{loc}}\right) - E$$

The solar time is the time based on the apparent angular motion of the sun across the sky, with solar noon being when the sun crosses the meridian of the observer. The rest of the equation is composed of correcting factors. The daylight saving is equal to 1 in winter and 2 in summer, L_{loc} is the longitude between reference meridian and local meridian and L_{st} is a correction due to perturbations in earth rotation.

E, the equation of time is governed by :

$$E = 229.18\cdot(0.000075 + 0.001868\cos(B) - 0.032077\sin(B) - 0.014615\cos(2B) - 0.040849\sin(2B))$$

It is expressed in hours and the angle B is the day of the year in radians :

$$radians(\frac{\text{day of the year } \cdot \ 360}{365})$$

Incidence angle θ

The solar radiation received from the sun without having been scattered by the atmosphere is called beam radiation. The angle at which this beam radiation strikes a surface, relative to the perpendicular of that surface, is known as the angle of incidence θ.
The incidence angle can be calculated using a formula that incorporates the previous angles defined :

$$\begin{aligned}\theta = \arccos\big(&\sin(\delta)\cdot\sin(\phi)\cdot\cos(\beta) - \sin(\delta)\cdot\cos(\phi)\cdot\sin(\beta)\cdot\cos(\gamma)\\ &+ \cos(\delta)\cdot\cos(\phi)\cdot\cos(\beta)\cdot\cos(w) + \cos(\delta)\cdot\sin(\beta)\cdot\sin(\gamma)\cdot\sin(w)\\ &+ \cos(\delta)\cdot\sin(\phi)\cdot\sin(\beta)\cdot\cos(\gamma)\cdot\cos(w)\big)\end{aligned}$$

However, since the irradiance of the data used is the one hitting the horizontal surface of the ground, it is necessary to adjust this irradiance to account for the inclined surface. One can define the angle θ_z as the angle between the beam radiation and the perpendicular to the horizontal surface. It is a form expression of the θ angle.

$$\theta_z = \arccos(\cos(\phi)\cos(\delta)\cos(\omega) + \sin(\phi)\sin(\delta))$$

The irradiance on the tilted surface is therefore :

$$I = I_{horizontal} \cdot \frac{\cos(\theta)}{\cos(\theta_z)})$$

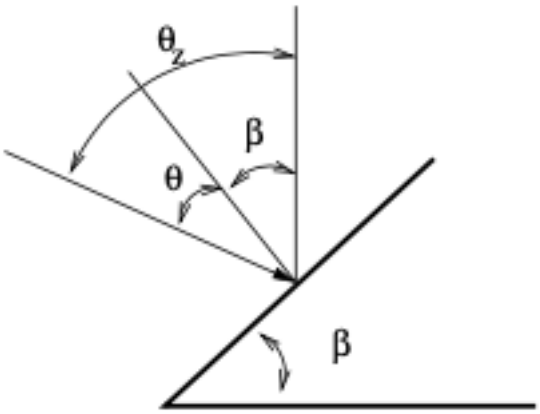

Figure 2.2: Angles

Optimum slope of the collector

The maximum solar gain is obtained when the surface is perpendicular to the direction of solar radiation. It is obvious that to obtain the maximum radiation throughout the day it is necessary to move the surface following solar direction which is tough not relevant for an application like this one due to the non profitability and because it makes the system less resilient. Taking into account that maximum radiation occurs when the sun passes the local meridian, surfaces must be oriented to the south ($\gamma = 0°$) to maximize solar gains. At solar noon, the solar incidence angle θ can be evaluated as:

$$\theta = \phi - \beta - \delta$$

Since the optimal condition is to have radiation perpendicular to the collector which means θ=0, the optimum slope of the collector is $\beta = \phi - \delta$. At first glance, the collector is most useful in winter, as homes generally don't require significant heating in summer. One could thus set the collector with consideration of the winter solstice declination, -23.45. With the current latitude 50.67°, this results in an optimal tilt of 74.12°. A mounted collector has a tilt angle of 90° which is not far from the optimum while being the simplest to achieve.

Multiple reflections

When solar rays strike the cover, the interaction with the cover occurs in three ways: some rays are immediately reflected, some are absorbed, and the rest are transmitted through the cover.

The transmitted rays hit the absorber, which absorbs the major part but also reflects a portion back towards the cover.
The same scheme takes place and the cover transmits, absorbs and reflects some of the rays.
The reflected rays continue to bounce between the cover and the absorber, with the intensity of the rays diminishing with each subsequent interaction.

To calculate the transmittance of the cover, it is necessary to determine its reflectance and absorptance.

When a ray hits a glass plate at an angle θ with θ_1 as the angle of incidence and θ_2 as the angle of refraction, the reflectance at a single interface is the ratio of the reflected beam's radiative component to the incident beam's radiative component:

$$\rho = \frac{I_r}{I}$$

$$\rho = \frac{1}{2}\left[\frac{\sin^2(\theta_2 - \theta_1)}{\sin^2(\theta_2 + \theta_1)} + \frac{\tan^2(\theta_2 - \theta_1)}{\tan^2(\theta_2 + \theta_1)}\right]$$

The angles θ_1 and θ_2 are related by Snell's law:

$$\frac{n_1}{n_2} = \frac{\sin\theta_2}{\sin\theta_1}$$

For normal incidence ($\theta = 0$), the reflectance for a single surface is given by:

$$\rho = \left(\frac{n_1 - n_2}{n_1 + n_2}\right)^2$$

For instance, for a glass cover with $n_2 = 1.52$ and $n_1 = 1$, the refraction index of air, the reflectance $\rho = 0.044$, implying that 4.2% of incident radiation is reflected by one surface. Therefore, for the two surfaces of the cover, the loss is then approximately 8.4%.

Neglecting absorption, the cover's transmission is shown below :

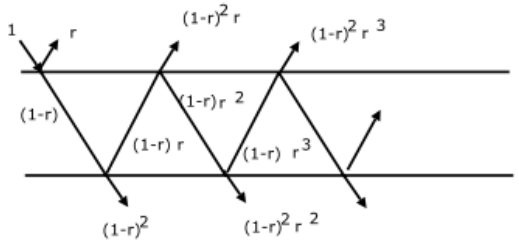

Figure 2.3: Transmission through a single cover

Considering the transmittance for both perpendicular and parallel components of initially unpolarized radiation:

$$\tau_r = \frac{1}{2}\left(\frac{1 - r_n}{1 + r_n} + \frac{1 - r_p}{1 + r_p}\right)$$

where

$$r_n = \frac{\sin^2(\theta_2 - \theta_1)}{\sin^2(\theta_2 + \theta_1)}$$

$$r_p = \frac{\tan^2(\theta_2 - \theta_1)}{\tan^2(\theta_2 + \theta_1)}$$

If we have the same material with multiple layers N, we can compute the global transmittance as :

$$\tau_{r,N} = \frac{1}{2}\left(\frac{1 - r_n}{1 + (2N - 1)r_n} + \frac{1 - r_p}{1 + (2N - 1)r_p}\right)$$

However this is a simplified formula since it doesn't consider the absorptance of the cover. The absorptance of a partially transparent medium follows Bouguer's law, stating that the absorbed radiation is proportional to the intensity in the medium and the distance traveled by the radiation :

$$\tau_a = \exp(-KL/\cos(\theta_2))$$

where K is the extinction coefficient of the medium, and $L/\cos(\theta_2)$ is the path length in the medium. Here, θ_2 is the angle between the normal to the surface and the direction of radiation.

The transmittance of covers can be approximated as:

$$\tau = \tau_a \cdot \tau_r$$

The absorptance can be approximated as:

$$\alpha = 1 - \tau_a$$

Eventually, using the relation between the reflectance, absorptance and transmittance :

$$\rho + \alpha + \tau = 1$$
$$\rho = \tau_a(1 - \tau_r)$$
$$\rho = \tau_a - \tau$$

Part of the energy reaching the absorber

Using the previous results, the fraction of the incident radiation that is finally absorbed by the absorber is given by:

$$(\tau_c\, \alpha_a) = \tau_c \alpha_a \sum_{n=0}^{\infty} [(1-\alpha_a)\rho_c]^n = \frac{\tau_c \alpha_a}{1-(1-\alpha_a)\rho_c}$$

Using the convergence of geometric sums. The subscript c stands for cover and a for absorber and the sum describes all the subsequent reflections on the absorber and the cover.

For solar collectors this can be approximated by

$$(\tau\, \alpha) \approx 1.01\, \tau_c\, \alpha_a \quad (22)$$

Meaning that approximately 101% of the initial transmitted and absorbed energy will be eventually absorbed by the absorber due to the multiple reflections. For a slate absorber with an absorptance of 0.89 and a glass cover of transmittance 0.90 one obtains the following energy eventually absorbed :

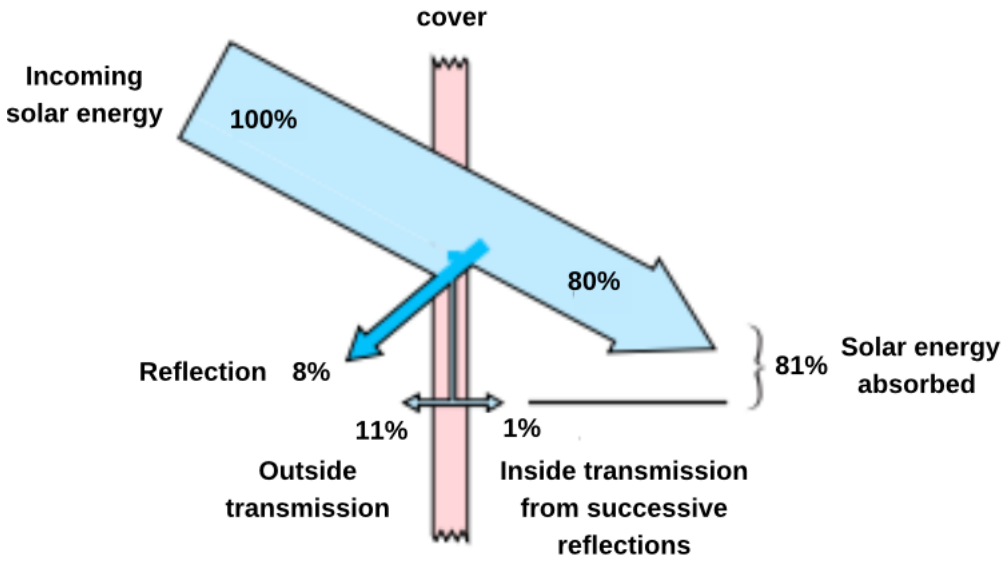

Figure 2.4: Global absorption of solar radiation transmitted through a cover

2.2 Data

The simulation utilizes meteorological data for the year 2023 for Meeffe (Hannut), the place where all the experiments were made. It was provided by Solcast (24) for research purposes. The granularity of the data sets is of 5 minutes. We used the irradiance (striking one square meter on the ground), the atmosphere temperature and the wind speed at 10 meters height. Since we need a ground wind speed, the data have to be adapted. We can use the wind profile power law which gives the wind speed at a certain height depending on the wind speed at 10 meters.

$$v(z) = v_{10} \cdot (\frac{z1}{10})^{\alpha} (25)$$

Where α is the wind shear exponent. For urban areas with high surface roughness, it is typically around 0.3 (25), value that we will use in this simulation, and z1 is taken as the mean height of the collectors, approximately 0.65 m.

A closer look at the bar charts below reveals a comparison of the annual variations in irradiance and temperature. It's evident that during winter, the collector's ability to harness heat is limited due to high thermal losses caused by the low outdoor temperature and due to low irradiation. This observation suggests that the collector is likely to be more effective during the intermediate seasons.

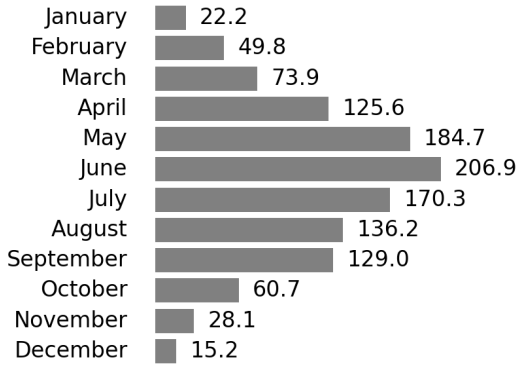

(a) Monthly irradiance in kWh/m^2

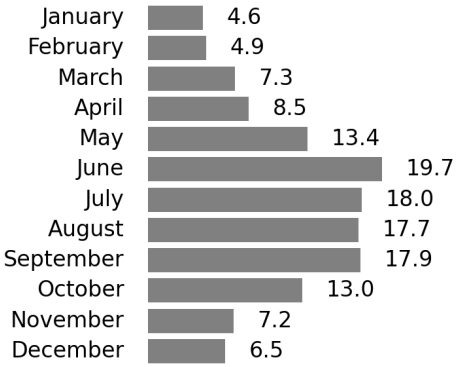

(b) Monthly temperature [°C]

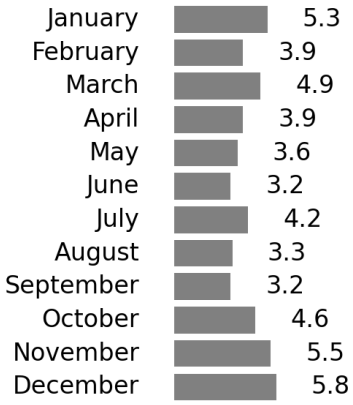

Figure 2.6: Monthly wind speed at 10 meters height [m/s]

2.3 Overall heat transfer

2.3.1 Thermal network of a collector with one cover

The system can be seen as an electrical circuit where the different media and heat transfer phenomena play the role of resistances between the analyzed bodies[1].

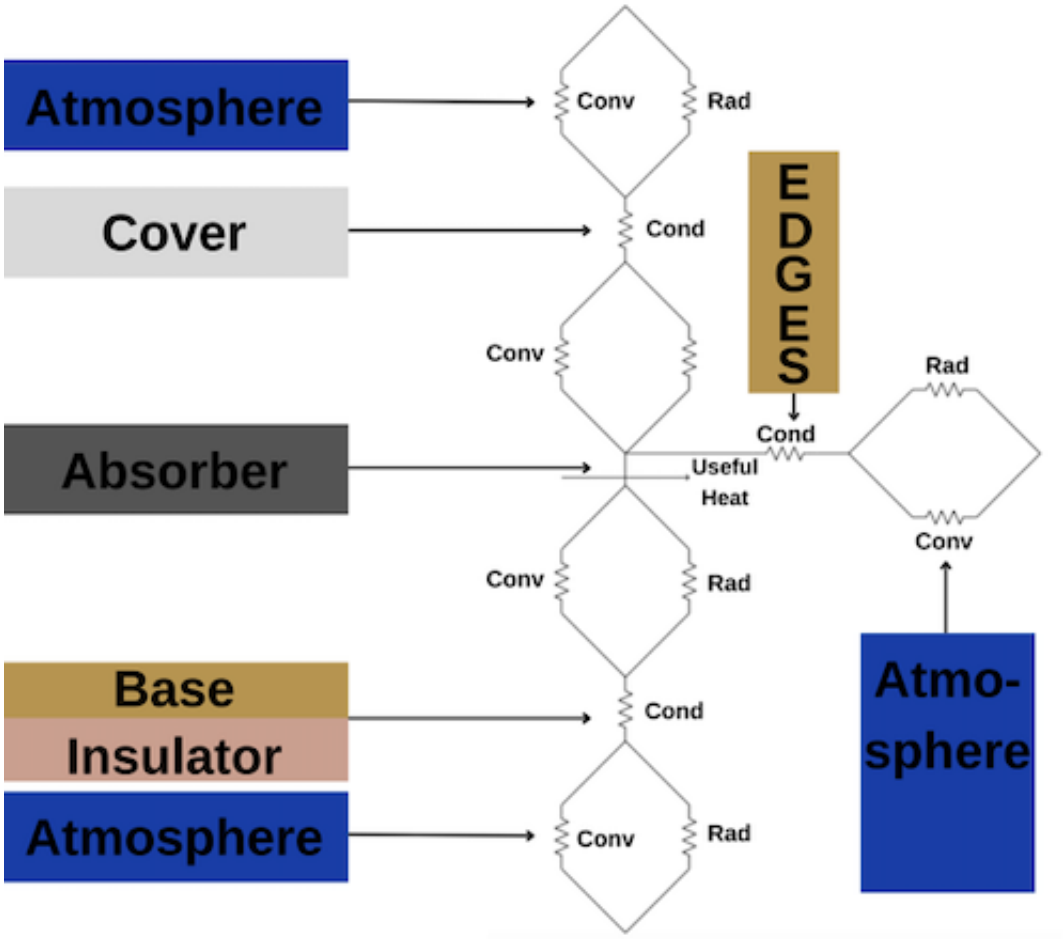

Figure 2.7: View of the collector as an electric circuit with the related heat transfer

The different bodies that exchange heat are the atmosphere, the front cover, the absorber, the back cover and the edges.

[1] conv = convection, cond = conduction, rad = radiation

We analyze here three different heat transfer phenomena : the convection, the conduction and the radiation.

The convection here relates the flow of heat due to the movement of air whose resistances are denoted by $\frac{1}{h_c}$.
We observe here convection between the atmosphere and the cover, the cover and the absorber mwhich is more or less strong depending on the thickness of the insulating air layer. There is also useful convection that occurs at the back of the absorber with the circulating air coming from the house.
This convection is intended to be maximized to enhance the performances of the collector
There is optionally a convection which occurs at the back of the collector which depends on how the collector is adhered to the wall, which enables or does not enable an air flow detrimental to the performances of the collector.

The conduction describes the exchange of heat due to a difference of temperature through the materials such as the cover, wood frame, or insulator.

The radiation for its part characterizes the thermal transfer resulting from heat wave emissions, the latter being absorbed, transmitted, or reflected through a colder body.
Radiation from the sun is transmitted to the absorber because of this phenomenon, and some of this energy is radiated back to the atmosphere.
The radiation from the rear side of the absorber is partially absorbed by the working fluid and the insulator. We immediately understand the use of a reflective foil to increase reflectivity toward the air.
Due to the lower emissivity of aluminum than wood, the radiative heat transfer from the absorber to the base is reduced, meaning less heat is transferred from the slate to the base.
This makes the collector more effective at retaining heat in the absorber and heating the air. We will assume the surfaces to be diffuse and gray. Considering them as diffuse means that they scatter radiation uniformly in all directions. It simplifies the radiative heat transfer calculations since the directional dependence of radiation can be ignored. Sky will also be considered as a blackbody. It simplifies the modeling of radiative heat exchange between the collector and the sky since we can use the blackbody radiation laws for the sky.

2.3.2 Computation of the Heat Transfer Coefficients

Here, we will consider each part of the collector one after another and analyze the related heat transfer coefficients.

Front face : $h_{conv,a-c}$, $h_{conv,c-s}$, $h_{rad,a-c}$, $h_{rad,c-s}$, k_c [2]

Edges : k_w, $h_{conv,a-e}$, $h_{rad,a-e}$ [3]

Back : $h_{conv,s-b}$, $h_{rad,s-b}$, k_w, $h_{conv,a-b}$, $h_{rad,a-b}$ [4]

Front face of the collector

When the slate heats up, heat transfer from the latter to the environment occurs through the front face of the collector.
Between the cover and the absorber, radiation, convection and conduction occur. Convection might be leading over conduction depending on the conditions.

The slate radiates towards the cover and the cover radiates back to the absorber with a lower intensity since its temperature is lower and optionally its emissivity. This is the case for glass with an emissivity of 0.92 while that of the slate, for instance, is 0.97.(20)

If the temperature difference between the absorber and the cover is high enough and the gap separating them as well[5], convection occurs and the fluid ascends along the heated vertical surface and descends along the cooled surface. The core becomes nearly stagnant, although additional cells can develop in the corners and the sidewall boundary layers eventually undergo transition to turbulence.

If on the contrary these conditions are not met, conduction will lead over convection through the air layer thickness.

Conduction occurs through the glass. However the glass being a good conductor[6], this effect on the global heat transfer is limited. This heat flow is considered as one-dimensional. This reduces the complexity of the heat transfer equations and

[2] a = atmosphere, c = cover, s = slate to refer to the absorber without mixing up with the a of atmosphere

[3] w = wood, e = edges

[4] b = base

[5] We will develop further what "enough" is.

[6] k $\approx 1[W/mK]$

lead to a single spatial dimension which is easier to solve.

The ambient air flowing against the outside face of the cover induces convective heat transfer from the glass to the environment and eventually, the cover exchanges radiation with the sky, which will be hypothetically considered as a blackbody. It simplifies the modeling of radiative heat exchange between the collector and the sky since we can use the blackbody radiation laws for the sky.

Convection Coefficient between air and the cover ($h_{conv,a-c}$)

This coefficient relates the convection between the air and the cover and is taken from a correlation valid for wind speed ranging from 2 to 20 [m/s] :

$$h_c = 12.12 - 1.16v + 11.6\sqrt{v} \quad (18)$$

v being the wind speed [m/s] of the air along the cover.

Convection Coefficient between Cover and Absorber ($h_{conv,c-s}$)

This is the heat transfer coefficient between the cover and the absorber, considering the convective effects due to the thickness of the air layer and the heat released by the plate.

In a rectangular cavity, for Rayleigh numbers less than a critical value of $Ra \leq 1708$(17), buoyancy forces cannot overcome the resistance imposed by viscous forces, and heat transfer occurs by conduction and radiation. The Rayleigh number is defined as:

$$Ra = \frac{g \cdot \beta \cdot (T_{absorber} - T_{cover}) \cdot L^3}{\nu \cdot \alpha}$$

Where:

- β is the coefficient of volume expansion (approximately $1/T$ for ideal gases).
- L is the characteristic length (thickness of the air layer).

- ν is the kinematic viscosity.
- g is the gravitational acceleration.

All properties are evaluated at the average temperature:

$$T_{bulk} = \frac{T_{cover} + T_{absorber}}{2}$$

From measurements, the temperature delta average between cover and absorber is around 11.8°C (for the large collector) with a maximum of 24.9°C.
Using the average temperature of these conditions ($T_{bulk} = 31.8$°C) and the maximum delta temperature, we find $Ra = 1437$ for the small collector and $Ra = 85242$ for the large collector.
This difference is due to the characteristic lengths of 0.01 m (small collector) and 0.039 m (large collector).

Collector Type	$T_{abs} - T_c$ (°C)	T_{bulk} (°C)	(Ra)	L_{chara}
Large Collector	11.8 (avg), 24.9 (max)	31.8	85242	0.039
Small Collector			1437	0.01

Table 2.1: Comparison Rayleigh number between large and small collectors

Other scenarios for the small collector have been tested, and none exceeds the Rayleigh number limit. Therefore, convection is considered for the large collector but not for the small one. One indeed finds a limit value for the characteristic length of 1.06 cm for the small collector.

The correlation used for the Nusselt number made by Hollands et al. describes natural convection in inclined enclosures, such as solar collectors whose aspect ratio $\frac{H}{L} \geq 12$:

$$Nu = 1 + 1.44\left[1 - \frac{1708(\sin(1.8\beta))^{1.6}}{Ra\cos\beta}\right]\left[1 - \frac{1708}{Ra\cos\beta}\right]^{+} + \left[\frac{Ra\cos\beta^{1/3}}{5830} - 1\right]^{+} \quad (2.1)$$

The "+" superscript indicates that the term is zero if the value inside the brackets is negative. The implication is that, if the Rayleigh number is less than the critical value, there is no flow within the cavity.
Afterwards, using the fact that the dimensionless Nusselt number is the ratio of a pure convection resistance to a conduction resistance, the convective coefficient can be easily deduced :

	Critical angle for inclined rectangular cavities				
$\frac{H}{L}$	1	3	6	12	≥ 12
$\tau^*[^\circ]$	25	53	60	67	70

Table 2.2: Critical angle for inclined rectangular cavities to use Holands et al. correlation

$$h_{conv,c-s} = \frac{Nu \cdot k_{air,layer}}{L} \tag{2.2}$$

with L the absorber-cover distance.

This correlation is nevertheless valid under a certain condition between the tilt angle and the aspect ratio :

For panels with a tilt higher than 70 ° , this correlation no longer stands.

With increasing Rayleigh number, the cellular flow intensifies and becomes concentrated in thin boundary layers adjoining the sidewalls.

One can therefore use the Churchill and Chu correlation which is a widely accepted method for estimating the Nusselt number in natural convection scenarios, including vertical surfaces. The correlation is given by:

$$Nu_L = \left[0.825 + \frac{0.387 Ra_L^{1/6}}{\left(1 + (0.492/Pr)^{9/16}\right)^{8/27}}\right]^2$$

This correlation is applicable for a wide range of Rayleigh numbers and Prandtl numbers and is suitable for both laminar and turbulent flows. Specifically, for a vertical rectangular enclosure:

- The Rayleigh number Ra should be within 10^4 to 10^{12}.
- The Prandtl number Pr can vary widely, making it suitable for air with $Pr < 1$.

For the large collector, the aspect ratio is $\approx \frac{1.325}{0.039} = 33.97$. The flow dynamics might therfore be more complex, but the general form of this correlation can still be applied as it adjusts to various flow conditions. For high aspect ratios, the correlation remains valid because it inherently considers the boundary layer development along the vertical surface.

The Prandtl number is a dimensionless number that provides a measure of the efficiency of transport by momentum diffusivity to thermal diffusion and in this case it is approximately :

$$Pr = \frac{nu}{\alpha} \approx= 0.48$$

Radiative heat transfer coefficient between cover and absorber/slate ($h_{rad,c-s}$)

Using a new hypothesis, which stipulates that the two faces are considered as infinite plates, no other bodies are to be taken into account. Let's then write down the equations of the system to compute the radiative heat transfer coefficient between the cover and the slate or absorber :

$$J_s = \sigma\, \epsilon_s\, T_s^4 \; + \; \rho_s\, G_s = \sigma\, \epsilon_s\, T_s^4 \; + \; (1 - \epsilon_s)\, G_s \tag{2.3}$$

$$G_s = J_c \tag{2.4}$$

$$J_c = \sigma\, \epsilon_c\, T_c^4 \; + \; \rho_c\, G_c = \sigma\, \epsilon_c\, T_c^4 \; + \; (1 - \epsilon_c)\, G_c \tag{2.5}$$

$$G_c = J_s \tag{2.6}$$

After solving this system, the radiative exchange per m^2 between the two surfaces can be found to be :

$$Q_{rad,s-c} = \frac{\sigma \; \cdot \; (T_s^4 - T_c^4)}{\frac{1}{\epsilon_s} + \frac{1}{\epsilon_c} - 1} \tag{2.7}$$

Dividing this result by $T_s - T_c$, we end up with the radiative heat transfer coefficient which is :

$$h_{rad,s-c} = \frac{Q_{rad,s-c}}{T_s - T_c} = \frac{\sigma \cdot (T_s^2 - T_c^2) \cdot (T_s + T_c)}{\frac{1}{\epsilon_s} + \frac{1}{\epsilon_c} - 1} \tag{2.8}$$

Radiative Heat Transfer Coefficient between Atmosphere and Cover ($h_{rad,a-c}$)

The radiative heat transfer coefficient between the atmosphere and the cover considers the sky as a blackbody with its radiosity therefore equal to its emissive power:

$$J_{sky} = E_b(T_{sky}) = \sigma \cdot T_{sky}^4$$

For the cover:

$$J_c = \sigma \cdot \epsilon_c \cdot T_c^4 + \rho_c \cdot G_c$$

Where G_c is the radiosity from the sky intercepted by the cover, with view factor $F_{c\,sky} = 1$:

$$G_c = J_{sky} = E_b(T_{sky}) = \sigma \cdot T_{sky}^4$$

Using Kirchhoff's law and the diffuse and gray property of the surface:

$$J_c = \sigma \cdot \epsilon_c \cdot T_c^4 + (1 - \epsilon_c) \cdot \sigma \cdot T_{sky}^4$$

The net radiative exchange per m² between the cover and the atmosphere is:

$$Q_{rad,a-c} = \sigma \cdot \epsilon_c \cdot (T_c^4 - T_{sky}^4)$$

Dividing by $T_c - T_a$, the radiative heat transfer coefficient is:

$$h_{rad,a-c} = \frac{\sigma \cdot \epsilon_c \cdot (T_c^4 - T_{sky}^4)}{T_c - T_a}$$

The sky temperature T_{sky} is correlated as(23):

$$T_{sky} = 0.0553 \cdot T_a^{1.5} \quad \text{with } T_a \text{ in Kelvin}$$

Edges of the collector

These losses will not be of a paramount interest, they are low and won't change the behavior of the collector. Conduction from the absorber to the environment occurs through the thickness of the frame of the collector. This heat transfer depends on the thickness and the conductivity of these edges and its resistance is written as $\frac{t_{wood}}{k_{wood}}$.

Outside, convection and radiation occur between the outer surface of the edges and the environment.

The convection heat transfer coefficient between the atmosphere and edges ($h_{rad,a-e}$) is the same as the one between the atmosphere and the cover ($h_{rad,a-c}$).

Radiative heat transfer coefficient between atmosphere and edges ($h_{rad,a-e}$)

To compute the radiative heat transfer coefficient between the edges and the environment, one can use the development of the heat transfer coefficient between the sky and the cover.
The sky is again considered as a blackbody exchanging radiation with the edges or back of the frame. Following the same procedure,

$$Q_{rad,a-e} = J_{edges} - J_{sky} = \sigma \cdot \epsilon_{wood} \cdot (T_{edges}^4 - T_{sky}^4) \tag{2.9}$$

Dividing this result by $T_{edges} - T_a$, we end up with the radiative heat transfer coefficient which can be used for the global heat transfer from the plate to the atmosphere :

$$h_{rad,a-e} = \frac{Q_{rad,a-e}}{T_{edges} - T_{sky}} = \frac{\sigma \cdot \epsilon_c \cdot (T_c^4 - T_{sky}^4)}{T_{edges} - T_a} \tag{2.10}$$

Back of the collector

These losses will also be paramount and will be analyzed experimentally later. The absorber exchanges heat with the base by radiation and convection. Indeed, the flow rate of air captures calories from the absorber and loses part of this energy to the base. At the same time, the absorber emits infrared radiation towards the base, thus heating up the base and the air. Part of the energy reaching the base is radiated back to the absorber depending on the reflectivity of the base, and another part is transmitted by conduction through the base and will be considered as a one-dimensional heat flow. The absorber and base planes can be approximated by infinite parallel plates which eliminates edge effects. This conductive resistance is written as $\frac{t_{wood}}{k_{wood}}$.

Outside, convection and radiation occur in the same manner as for the edges. If one considers that the collector is hung up on the wall, one can consider that no convection occurs since no air can flow. The heat nevertheless spreads through the wall of the tiny house like a wave whose source is the collector. It thus slightly contributes to the insulation of the house.

In these experiments, the collector was leaned against the wall but not hanging on it.

The convection heat transfer coefficient between the atmosphere and the base ($h_{rad,a-b}$) is therefore the same as the one between the atmosphere and the cover ($h_{rad,a-c}$).

The radiative heat transfer coefficient between atmosphere and the base ($h_{rad,a-b}$) can also be computed using the development of the heat transfer coefficient between the sky and the cover, considering again the sky as a blackbody. We successively obtain :

$$Q_{rad,a-b} = J_{back} - J_{sky} = \sigma \cdot \epsilon_{wood} \cdot (T_{back}^4 - T_{sky}^4) \tag{2.11}$$

Dividing this result by $T_{back} - T_a$, we end up with the radiative heat transfer coefficient which can be used for the global heat transfer from the plate to the atmosphere :

$$h_{rad,a-b} = \frac{Q_{rad,a-b}}{T_{back} - T_{sky}} = \frac{\sigma \cdot \epsilon_c \cdot (T_c^4 - T_{sky}^4)}{T_{back} - T_a} \tag{2.12}$$

Radiative heat transfer coefficient between absorber and base ($h_{rad,s-b}$)

The absorber temperature is considered uniform. Following the same calculation as for the radiative heat transfer coefficient between the cover and the absorber, one replaces the equation by the adequate emissivities and temperature and obtains :

$$Q_{rad,slate-base} = \frac{\sigma \cdot (T_s^4 - T_b^4)}{\frac{1}{\epsilon_s} + \frac{1}{\epsilon_{wood}} - 1} \tag{2.13}$$

Dividing this result by $T_s - T_b$, we end up as well with the radiative heat transfer coefficient which is :

$$h_{rad,s-b} = \frac{Q_{rad,s-b}}{T_s - T_b} = \frac{\sigma \cdot (T_s^2 - T_b^2) \cdot (T_s + T_b)}{\frac{1}{\epsilon_s} + \frac{1}{\epsilon_w} - 1} \tag{2.14}$$

Slate emissivity is ≈ 0.97 and wood emissivity ≈ 0.94(19)(20), valid for temperature ranging from room temperature to 100 °C in the infrared range. This leads to a denominator of 1.095. Polished aluminum emissivity is however around 0.05 for these conditions, which leads to a denominator of 20.03.
The use of a reflective aluminum foil therefore decreases the global radiative heat transfer from the absorber to the base by a factor 20.
However, the absorber actually still radiates towards the base, but a major amount is now radiated back to the absorber. This increases the absorber and air temperature instead of the base temperature, reducing heat losses through the base.

Convective heat transfer coefficient between absorber and base ($h_{conv,s-b}$)

The flow rate through the collector is controlled by a fan. Knowing the flow rate and the cross section of the air path, one can compute the flow speed and use the same correlation as used for the outer surfaces.

$$h_c = 12.12 - 1.16v + 11.6\sqrt{v}(18)$$

With v the wind speed $[\frac{m}{s}]$ of the air flow in the collector, ranging from 1.5 to 4.25 $[\frac{m}{s}]$.

2.3.3 Thermal Losses through the Top, Edges, and Back

Top Losses :

$$R_{tot} = (R_{conv,a-c} // R_{rad,a-c}) + R_{cond,c} + (R_{conv,c-ab} // R_{rad,c-ab})$$

$$R_{tot} = \frac{1}{h_{conv,a-c} + h_{rad,a-c}} + \frac{t_c}{k_c} + \frac{1}{h_{conv,c-ab} + h_{rad,c-ab}}$$

$$U_{front} = \frac{1}{R_{tot}}$$

$$Q_{front,losses} = U_{front} \cdot A_{cover} \cdot (T_{slate} - T_{outside})$$

Edge Losses :

$$R_{tot,edges} = R_{cond,wood} + R_{conv,a-c} // R_{rad,a-e}$$

$$R_{tot,edges} = \frac{t_{wood}}{k_{wood}} + \frac{1}{h_{conv,a-c} + h_{rad,a-e}}$$

$$U_{edges} = \frac{1}{R_{tot,edges}}$$

$$Q_{edges,losses} = U_{edges} \cdot A_{edges} \cdot (T_{slate} - T_{outside})$$

Back Losses :

$$R_{tot} = R_{conv,s-b}//R_{rad,s-b} + R_{cond,poly} + R_{cond,wood} + R_{conv,a-b}//R_{rad,a-b}$$

$$R_{tot} = \frac{1}{h_{conv,s-b} + h_{rad,s-b}} + \frac{t_{poly}}{K_{poly}} + \frac{t_{wood}}{K_{wood}} + \frac{1}{h_{conv,a-c} + h_{rad,a-b}}$$

$$U_{back} = \frac{1}{R_{tot}}$$

$$Q_{back,losses} = U_{back} \cdot A_{back} \cdot (T_s - T_a)$$

Global Heat Transfer Coefficient

Redefine previous heat transfer coefficients:

$$U_{edges} = U_{edges} \cdot \frac{A_{edges}}{A_{cover}}$$

$$U_{back} = U_{back} \cdot \frac{A_{back}}{A_{cover}}$$

The global heat transfer coefficient is:

$$U_{total} = U_{edges} + U_{back} + U_{front}$$

Thus, the overall heat losses can be written as:

$$Q_{losses} = U_{total} \cdot A_{cover} \cdot (T_{slate} - T_{outside})$$

2.4 Crafting a DIY Solar Collector

The construction of a DIY solar collector involves a step-by-step process aimed at understanding its performance under various conditions. The initial phase involves constructing the collector and conducting measurements under different scenarios. Subsequently, the data collected help in analyzing the impact of altering specific collector parameters.

2.4.1 The materials

To assemble a basic solar collector, readily available materials are utilized. The frame is crafted from wood, and plywood serves as a base for cost-effectiveness. To withstand outdoor exposure, the plywood requires treatment. Alternatively, opting for treated wood planks prolongs the collector's lifespan, although at a higher expense.

Baffles are affixed to the base with screws and right angles. They consist of rectangular wood pieces of uniform dimensions in order to modify the air path throughout the collector.

One also needs slates or metal sheet depending on the absorber chosen. These are preferably sourced from recycled materials to align with sustainability goals. In this case the slates used are leftover that were picked up from a slate living in the nearby village.
By grinding an old metal shelf, one obtained the metal sheets.

After that, one needs a transparent glass to cover the collector. Here again we found glasses on the market that people were going to throw away.

The seals are fashioned from the leftover EPDM liner from a previous pond construction project.
Only two sizes of screws were enough to fix all the pieces together.

2.4.2 Tools

Drill: Essential for creating holes in wood and slates for screw fixation.

Screwdriver: For driving screws during assembly.

Router: Used to create rebates to accommodate the glass.

Slate Shear: For cutting slate pieces to size.

Scissors: Needed to cut liner strips for sealing.

Pencil and Ruler: For marking and measuring distances for cutting.

Glass Cutter with Turpentine: Optional tool for resizing glass if not a safety glass, with turpentine used as a lubricant.

Screws : Long ones for the frame and rebates and short ones for the baffles and slates/metal sheets.

Vacuum cleaner : To regularly vacuum the collector and avoid sawdust accumulation.

2.4.3 Step-by-step construction

We determined the size of the panels based on the dimensions of available glass pieces. We practiced glass cutting using remnants from a broken window, using a glass cutter and lubricating the wheel with turpentine. However, we found one large glass and a smaller one with suitable dimensions for our application which allows us to evaluate the impact of the collector surface.

The large glass is a safety glass that measures 137x100 cm and is 5 mm thick. We chose a base size of 145x105 cm, using wood pieces measuring 70x70 mm and opted for thick wood ensuring a thick air layer behind the slates, aiding in efficient circulation. The base is made of plywood of 18mm thickness.

(a) Sealing of the frame

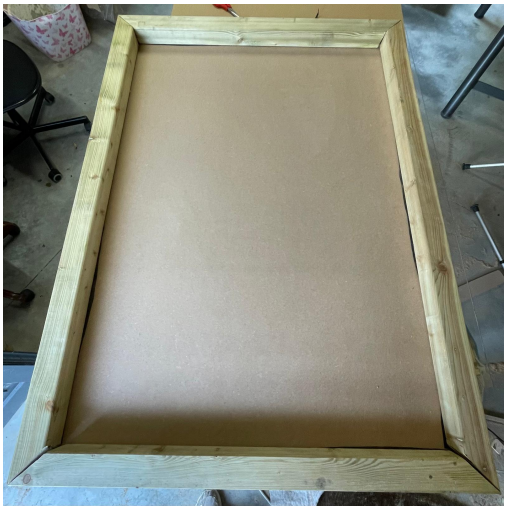

(b) Frame and base

Once we had gathered all the necessary materials and tools, we started cutting the planks and wood pieces to the desired dimensions.
EPDM liner strips, 5 cm in width and slightly narrower than the wood, were employed. The upper strip covers the entire width, while the side strips extend down to the base to prevent infiltration of rainwater.
We drilled from the back of the base and used four long screws vertically and three horizontally.

One cut two holes for the inlet and outlet of the collector, each measuring 11 cm in diameter to match the PVC pipes, a suitable size for the fitting of an electric fan at the entrance .
Subsequently, we covered the base with aluminum foil tape for its reflective properties, which help to reduce heat loss by reflecting some of the heat back towards the working fluid.

We fixed baffles to deflect the air path and increase contact time with the slate, thereby achieving higher final temperatures. These baffles measure 64.5 cm in length, 2.5 cm in height, and 4.5 cm in width. They are spaced 27 cm apart from the frame's edge and 12.60 cm apart from each other. We used three right angles to secure each baffle and used small screws to prevent drilling through the entire base which could lead to water infiltration and premature wear of the collector. This also facilitates changing the number of baffles and their placement.

In order to accommodate the glass, we created rabbets of 6 mm depth with the router and refined them with a sander for improved aesthetics and glass fitting. Given the heavy weight of the glass, we made sure it is safely held by the rebates. The rabbet dimensions are thus 2.25 cm for the top and bottom wood pieces and 4.25 cm for the sides.

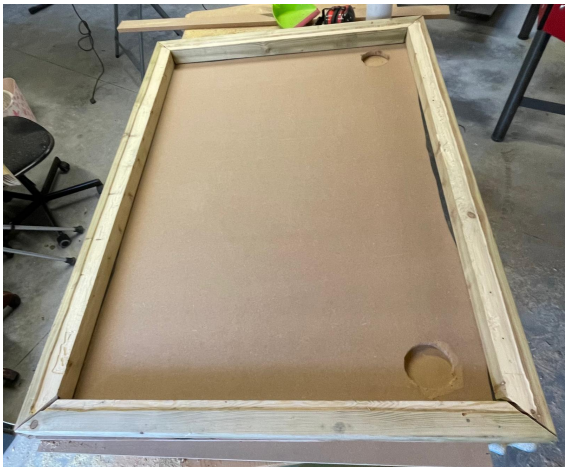

(a) Inlet and outlet openings

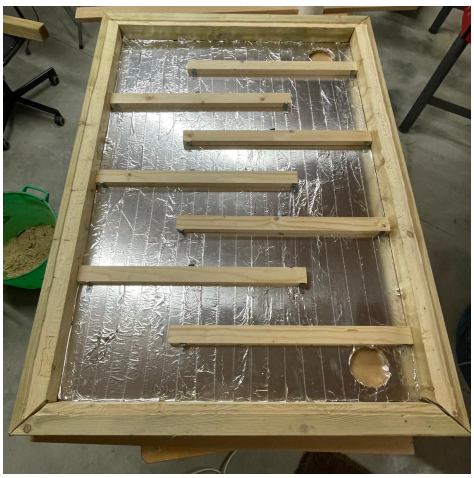

(b) Baffles and aluminium foil

When the temperature inside the heated room reaches its upper comfort limit, the collector must be closed to prevent further heating.
However, simply shutting the outlet and inlet hatches would result in an accumulation of heat inside the collector, as no airflow would cool it down. This excess of heat could indirectly heat up the room by conduction losses through the wall during the day and hinder the room's cooling process by conduction towards the environment after the sunny time due to the inertia of the slate that would keep its temperature above the indoor temperature for a while.

To address this, a hatch has been knocked off at the top of the collector. Therefore, convection can still occur and cools down the slates when the outlet hatch is closed. This heat regulator hatch is manually closed using a waterproof flap.

It is possible to leave the inlet hatch open. Indeed, the collector is likely to be south-oriented for optimal efficiency. Therefore, we can take advantage of natural convection within the panel to draw the air upwards from the inlet to the outside while opening a north-oriented window of the room to replace this air by a cooler one.

We knocked off some slate supports and screwed them to the base to level and fix the slates better. These supports were designed to be as small as possible to minimize their impact on airflow redirection and thus to neglect them in the analysis.

(a) Summer hatch and flap

(b) Supports to hold the slates

The traditional laying of the roofer is not required here and almost the entire surface of a slate (22 x 44 cm) will be exploited. Initially, we attempted cutting the slate with an ice axe, but the results lacked precision. We therefore tried a graphite saw with a jigsaw, which actually yielded excellent results. This approach also minimizes air leakage from the back to the front of the collector by increasing the accuracy of the finishes. The surface covered by the slates is 91.5x132.5 cm.

Here, the beveled surface of the slate is facing the basej unlike on a roof installation. This arrangement helps to minimize the gap between two adjacent slates, thereby reducing airflow leakage in front of the slates. We used a concrete bit to drill the slates and two to three small screws per slate fixed to the baffles or slate supports. Each slate has been cleaned before laying to avoid dust inside the panel.

(a) Slate cutting

(b) Slate accommodation

Once more, we cut EPDM strips to seal the glass-frame interface. As for the base sealing, the upper strip spans the entire width, while the side strips extend down to the base to prevent water infiltration from rain. These are 1.5 cm in width and are positioned as closely as possible to the side of the frame.

(a) Sealing of the front glass

(b) Final prototype

The dimensions in cm are gathered in the table below :

Safety glass	137x100x0.5
Base	145x105x1.8
Frame wood pieces	145x70x70 and 105x70x70
Rabbets	4.25x0.6 along the height and 2.25x0.6 along the width
Rebates	143.5x5.5 and 103x5.5
Hatch	14.5x5
Hatch flap	19x6.5
EPDM strips for the base	two of 140x5 , one of 95x5 and one of 105x5
EPDM strips for the glass	two of 135.5x1.5 , one of 100x1.5 and one of 97x1.5x1.5
Number of baffles	7
Baffles dimension	64.5x2.4x4.5
Spacing between baffles	12
Slates thickness	0.4
Spacing glass-slates	3.9
Overall weight	67.2 kg
Useful surface	91.5x132.5 = 1.212 m^2

Table 2.3: Dimension large collector [cm]

2.4.4 Second collector

The second collector smaller, is made in the same way as the first collector. The dimension of each component in cm is listed in the table 2.4.

Since this collector is more handy, it is the one to which modifications will be brought.

Glass (not a safety one) dimension	119.5x59.5x0.6
Base	125.5x65.5x1.8
Frame wood pieces	125.5x45x45 and 65.5x45x45
Rabbets	3x0.7
Rebates	64x4 and 124x4
Hatch	10x3.5
Hatch flap	14x4
EPDM strips for the base	119.5x3 and 65.5x3
EPDM strips for the glass	118.5x1 and 59.5x1
Number of baffles	5-7-9
Baffles dimension	40.5x2.4x3.5
Spacing between baffles	16.5-11.5-8.5
Slates thickness	0.4
spacing glass-slates	1
Overall weight	37 kg
Useful surface	56.5x116.5 = 0.658 m^2

Table 2.4: Dimension small collector [cm]

(a) Sealing of the base and frame

(b) Final prototype

2.4.5 Collector lended by Hellow

In order to analyse the behavior of a collector with an aluminum absorber, Hellow nicely lended us their aluminum prototype for the semester. It is an horizontal collector designed with a reflective aluminium foil on the base as well as on the back of the absorber. The dimensions are the following :

Glass (not a safety one) dimension	116x65.5x0.4
Base	114.5x63x1.4[7]
Polystyren insulator	114.5x63x1.6
Frame wood pieces	122.2x8.8x3.8 and 70.8x8.8x3.8
Hatch	15x2.5
Number of baffles	4
Baffles dimension	104x3x2
Spacing between baffles	10.4
Aluminum thickness	0.2
spacing glass-slates	2.9
Overall weight	24.5 kg
Useful surface	114.5x63 = 0.721 m^2

Table 2.5: Dimension Aluminum absorber collector from Hellow [cm]

2.4.6 Changes in the design realized

Reflective aluminium foil

The first modification made to the collector is the reflective aluminium foil. This change aims to observe the increase in the air's temperature resulting from the additional heat being reflected toward the absorber and therefore the fluid.

Figure 2.14: Adding of the aluminium foil

Insulation

The next change involves insulating the collector. Since a 18mm MDF board only separates the hot air from the atmosphere, one can expect to have an enhancement of the collector's performance due to reduced heat loss through the base.

Figure 2.15: Isolation with polystyrene foam

Figure 2.16: Side view of the foam

Baffles increasing

Adding baffles to deflect the air is a known technique to increase contact time with the hot absorber, create slight turbulences that enhance heat transfer, and ensure the air absorbs heat from the maximum surface area of the absorber. However, there is an optimal mass flow rate at which heat transfer is most efficient. This change aims to find that optimal configuration.

Figure 2.17: Change from 5 to 7 baffles

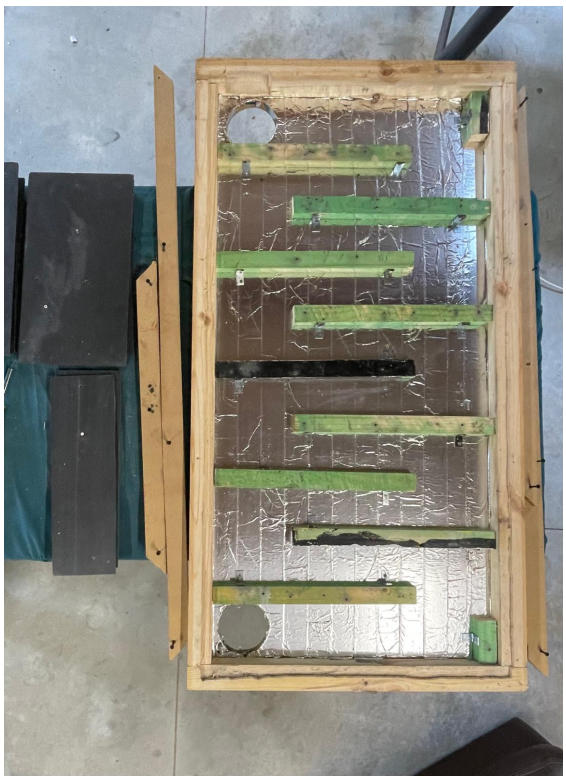

Figure 2.18: Change from 7 to 9 baffles

2.5 Mass flow rate

2.5.1 Natural convection

In the following analysis, we will evaluate the evolution dependence of the (mass) flow rate with the temperature to know how to approximate this function with different flow rate measurements.

$$\dot{m} = \rho \times A \times v \ [\frac{\text{kg}}{\text{s}}] \tag{2.15}$$

where ρ represents the density, A the flow area, and v the velocity of the flow.

In the previous terms:

- The area obviously does not depend on the temperature difference between the air and the slate.

- The density ρ depends on temperature as $\rho_{\text{air}} = \rho_0(1 - \beta(T_{\text{slate}} - T_0))$.
- The velocity also depends on temperature through the conservation of momentum equations.

However, for the second point, the Boussinesq approximation allows us to neglect the temperature dependence. For ideal gases, the thermal expansion coefficient is $\beta = \frac{1}{T}$, making the temperature-dependent term negligible compared to 1.

Therefore, the temperature dependence of the mass flow rate $\dot{m}$ is solely proportional to the temperature dependence of the velocity v.

To determine how the velocity varies with the temperature difference, we must examine the order of magnitude of the terms in the momentum conservation equation along the plate. These equations are:

$$\rho_0(1 - \underbrace{\beta(T - T_0)}_{\ll 1})\left(u\frac{\partial v}{\partial x} + v\frac{\partial v}{\partial y}\right) = -\underbrace{\frac{\partial p}{\partial y}}_{\rho_0 g} + \mu\left(\frac{\partial^2 v}{\partial x^2} + \frac{\partial^2 v}{\partial y^2}\right) - \rho_0\left(1 - \beta(T - T_0)\right)g \tag{2.16}$$

$$\rho_0\left(u\frac{\partial v}{\partial x} + v\frac{\partial v}{\partial y}\right) = \mu\left(\frac{\partial^2 v}{\partial x^2} + \frac{\partial^2 v}{\partial y^2}\right) + \rho_0\beta(T - T_0)g \tag{2.17}$$

The assumption that the pressure field is hydrostatic (valid for air) allows us to transition from equation 2.16 to equation 2.17. Furthermore, the term $\beta(T - T_0)$ can generally be neglected for the flow of air or water. The term β is of the order of magnitude $\mathcal{O}(10^{-3})$. In the case of an air slate collector, for a slice of the air flow, the temperature difference does not rise beyond a maximum of 10[°C]. This results in a maximum approximation of 3%, which demonstrates that the term is negligible compared to 1.

By examining the orders of magnitude and knowing that the thickness (along x) of the boundary layer is much smaller than the length of the plate, we can neglect the inertia terms compared to the buoyancy and viscous friction terms.

$$\underbrace{u\frac{\partial v}{\partial x} + v\frac{\partial v}{\partial y}}_{\ll \frac{V}{\delta^2}} = \beta g(T - T_0) + \nu\frac{\partial^2 v}{\partial x^2} \tag{2.18}$$

By analyzing the orders of magnitude of the remaining terms, we find a temperature-dependent characteristic velocity V:

$$V = \frac{\beta g \Delta T \delta_t^2}{\nu}, \tag{2.19}$$

where δ_t^2 represents the thickness of the thermal boundary layer.

To find an order of magnitude for δ_t^2, we use the continuity and energy conservation equations (eq. 2.20 and 2.21):

$$\frac{\partial u}{\partial x} + \frac{\partial v}{\partial y} = 0 \tag{2.20}$$

$$u\frac{\partial T}{\partial x} + v\frac{\partial T}{\partial y} = \alpha\frac{\partial^2 T}{\partial x^2} \tag{2.21}$$

The order of magnitude is expressed as:

$$\delta_t^2 = \sqrt{\frac{\alpha L}{V}} = \left(\frac{\nu\alpha}{\beta g \Delta T L^2}\right)^{1/2}, \tag{2.22}$$

where L represents a characteristic length of the slate in the vertical plane (usually the length). Substituting the order of magnitude found for δ_t^2 into relation 2.19, we find:

$$V = \sqrt{\frac{\beta g \Delta T}{\nu L^2}}, \tag{2.23}$$

which allows us to assert that the velocity v is proportional to the square root of the temperature difference and, consequently, so is the mass flow rate $\dot{m}$.

2.5.2 Forced convection

In order to control the mass flow rate through the collector and extract more power from it, one need to assess its sweet spot according to the slate temperature and instant irradiation. To this aim, we used a fan controlled by a variable voltage source supplying the load at 6, 7.5, 9 and 12 volts and a second fan, less powerful which was used for the small collectors that we supplied at 12 volts and that we will call '12 V bis' from now.

After multiplying this result by the density at the collector's inlet, one can have a theoretical value for the mass flow rate. The datasheet shows(6) that the maximum

flow rate is 1.3 $[\frac{m^3}{min}]$, so 0.0217 $[\frac{m^3}{s}]$ at 13.8V and evolves linearly with the voltage around its nominal value of 12 volts. For the second fan, this value is 0.0090 $[\frac{m^3}{s}]$ at 12 volts.

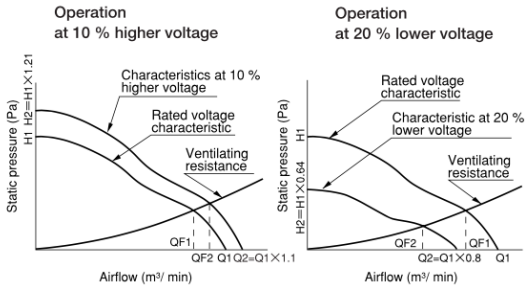

Figure 2.19: Flow rate static pressure curves for different voltages

As seen in the datasheet, the fan is highly sensitive to downstream pressure. Indeed, as the static pressure increases, the flow rate decreases. In the collector, the path imposed by the baffles and the boundary effects acts that way and decrease the flow rate. In order to evaluate these effects, one can measure the outlet flow rate at each voltage, which allows to compute the real heat transfer exchange without overestimating it.

To address this problem, the Log-Tchebycheff method, used for flow measurement in ducts or pipes, ensures a representative sampling of the entire area while minimizing measurement bias.

Using this method, the duct is divided into concentric circles, each containing equal area. This approach facilitates the acquisition of an optimal average through an equal allocation of readings across each circular section.

We drilled 3 holes in the duct at 60° angles from each other and took measurements of the wind speed with a hot wire anemometer at the locations on the picture 2.20. Typically, ducts with a diameter of 25.4cm or less, which is our case, with a 10cm diameter, utilize three concentric circles, resulting in six measuring points per diameter. Afterwards, we averaged the measurements to compute the estimation of the wind speed through the duct and then multiplied it by the cross section of the duct which is 78.54 cm^2.

Configuration	6V	7.5V	9V	12V	12Vbis
Theoretical FR without resistance	0.00940	0.01180	0.01410	0.01880	0.0900
Outlet FR small collector 9 baffles	0.00273	0.00364	0.00396	0.00492	0.00348
Outlet FR small collector 7 baffles	0.00402	0.00526	0.00643	0.00820	0.00451
Outlet FR Aluminum collector	0.00392	0.00549	0.00746	0.00963	0.0450
Outlet FR large collector	0.00456	0.00654	0.00720	0.01034	/
Outlet FR small collector 5 baffles	0.00598	0.00761	0.00922	0.01206	0.00570

Table 2.6: Flow rate (FR) $[\frac{m^3}{s}]$ according to the Log-Tchebycheff method

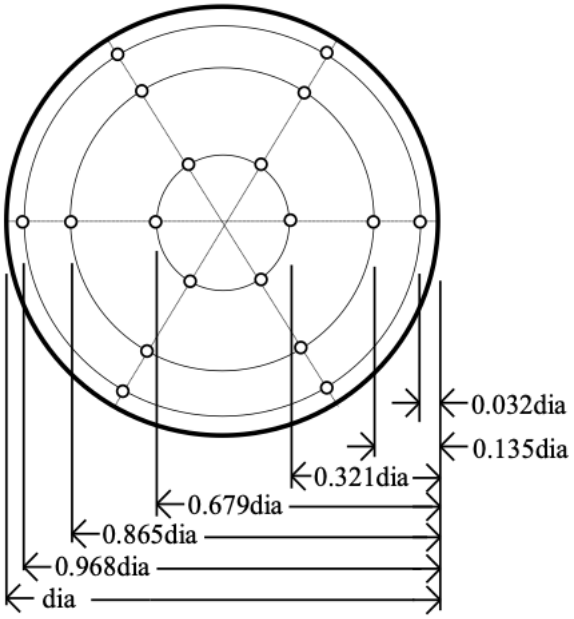

Figure 2.20: Location of measuring points using log-Tchebycheff method

Applying this method to the three collectors, one obtains the average speed in $[\frac{m}{s}]$ for every configuration. The results for each circle are gathered in tables that can be found in appendix A:

All the results expressed in $[\frac{m^3}{s}]$ have been gathered in the tabular here below :

Configuration	6V	7.5V	9V	12V	12V bis
Theoretical MFR without resistance	0.01132	0.01420	0.01698	0.02263	0.01080
Outlet MFR small collector 9 baffles	0.00415	0.00439	0.00477	0.00593	0.00418
Outlet MFR small collector 7 baffles	0.00484	0.00633	0.00774	0.00987	0.005411
Outlet MFR Aluminum collector	0.00472	0.00661	0.00898	0.01159	0.0540
Outlet MFR large collector	0.00559	0.00802	0.00882	0.01265	/
Outlet MFR small collector 5 baffles	0.00732	0.00932	0.01129	0.01478	0.00684

Table 2.7: Mass flow rate (MFR) $[\frac{kg}{s}]$ according to the Log-Tchebycheff method

By applying conservation of mass, the flow rate evolves as well as the density but the mass flow rate is kept constant. The measurements have been done indoor to have no external wind and at an average temperature of 15 °C for the large collector and the smaller one with 5 baffles and at 20 °C for the other ones. One can thus multiply these flow rates by the density of the air at 15 °C and 20 °C respectively to have a good approximation of the mass flow rate at any condition.

The evolution of this mass flow rate as function of the voltage applied evolves linearly. The increase in flow rate and thus mass flow rate due to an increase in the voltage is similar to the case in theory. One can see on the graph that the slope is steeper in theory than experimentally observed which compensates for having a proportional increase of the flow for each configuration :

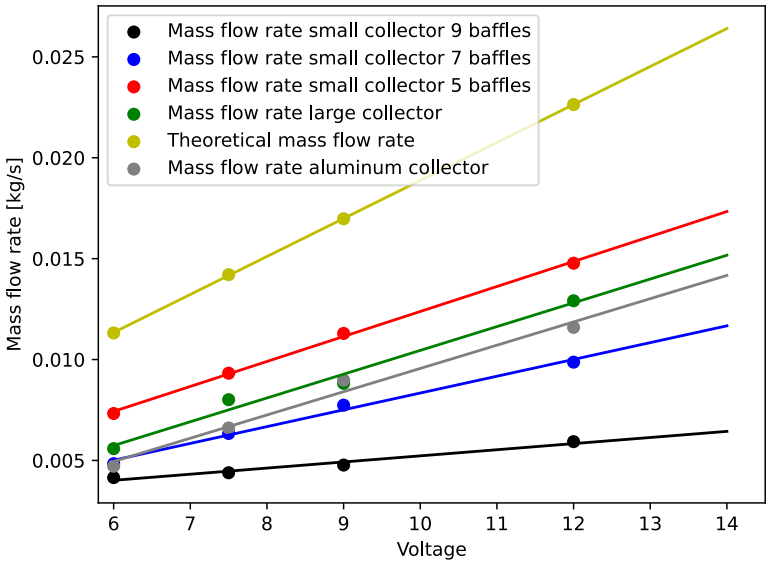

Figure 2.21: Flow rates evolution for the larger fan [kg/s]

Given in percentage of the maximum theoretical mass flow rate, this gives :

Configuration	6V	7.5V	9V	12V	12V bis
Theoretical flow rate without resistance	100.0	100.0	100.0	100.0	100
Outlet MFR small collector 9 baffles	36.6	30.9	28.1	26.2	38.7
Outlet MFR small collector 7 baffles	42.8	44.6	45.6	43.6	50.1
Outlet MFR Aluminum collector	41.7	46.6	52.9	51.2	50
Outlet MFR large collector	49.4	56.5	51.9	55.9	/
Outlet MFR small collector 5 baffles	64.7	65.6	66.5	65.3	63.3

Table 2.8: Percentage of the maximum theoretical mass flow rate [%] for each configuration

One can expect slightly better results in working conditions since natural con-

vection due to temperature gradients will be added to the forced one and because air will be slightly less viscous due to the temperature increase. Therefore, the pressure losses will be reduced when working at higher temperatures.

For the same working temperature, one can observe that there are fewer pressure losses in the smaller collector configured with 5 baffles because, among others, the air path is shorter, thus slowing down less the air flow due to edge effects.

Indeed, the mean air path = 8x0.645 + 7x0.165 = 6.315 meters for the large collector, 6x0.405 + 5x0.21 = 3.48 for the smaller one with 5 baffles and 8x0.405 + 7x0.15 = 4.29 for its configuration with 7 baffles.

In addition, there is more deflection of the air in the bigger panel, resulting in 14 bends with 7 baffles versus 10 for 5 baffles (2 per baffle). These bends induce singular pressure losses.

In order to evaluate friction losses, one needs to calculate pressure losses. These latter are influenced by the resistance to air flow within the ducts, resulting from friction with the walls and disturbances due to changes in direction or cross-section. We can break down pressure losses in two parts :

Regular/linear losses $w_{f,reg}$: Pressure losses in straight pipes with constant section.

Singular pressure losses $w_{f,sing}$: Local presence of an obstacle or an abrupt change in the geometry of the pipe. This is directly related to the bends in the collector.

With a differential pressure meter, we computed the pressure losses between the inlet (right after the fan) and the outlet of the collectors for several voltages i.e. different flow rates :

Pressure losses [Pa]	6V	7.5V	9V	12V
small collector aluminium absorber	4.25	7.05	9.83	16.1
large collector	4.45	7.37	10.84	18.02
small collector 7 baffles	6.07	10.15	14.98	24.73
small collector 9 baffles	6.89	10.41	15.82	23.92

Table 2.9: Pressure losses [Pa]

In the following analysis, we will have a theoretical approach of the pressure losses and we will compute them for the large collector with an air flow rate of 0.00456 $\frac{m^3}{s}$ (6 volts configuration).

Linear/Regular Pressure Losses

The linear pressure losses, ΔP_{lin}, in a duct can be determined using the Darcy-Weisbach equation:

$$\Delta P_{\text{lin}} = f \cdot \frac{L}{D} \cdot \frac{\rho V^2}{2} \tag{2.24}$$

where:

- f is the friction factor, dependent on the flow regime, impacted by the Reynolds number and the relative roughness.
- L is the length of the duct.
- D is the diameter of the duct.
- ρ is the density of the air.
- V is the average velocity of the air.

The velocity V is related to the volumetric flow rate Q by the relation:

$$Q = V \cdot A \tag{2.25}$$

where A is the cross-sectional area. Therefore, $V = \frac{Q}{A}$.

We can therefore write the Darcy-Weisbach equation in terms of flow rate, as:

$$\Delta P_{\text{lin}} = f \cdot \frac{L}{D} \cdot \frac{\rho \left(\frac{Q}{A}\right)^2}{2} \tag{2.26}$$

The linear pressure losses are therefore proportional to the square of the flow rate:

$$\Delta P_{\text{lin}} \propto Q^2 \tag{2.27}$$

The friction coefficient, f, evolves with the flow rate in a manner that depends on the flow regime within the duct or pipe. The flow regime is determined by the Reynolds number (Re), a dimensionless quantity representing the ratio of inertial forces to viscous forces in the fluid flow. The Reynolds number is given by:

$$\text{Re} = \frac{\rho V D}{\mu} \tag{2.28}$$

where:

- ρ is the fluid density,
- V is the flow velocity,
- D is the characteristic diameter of the pipe or duct,
- μ is the dynamic viscosity of the fluid.

D_h, the hydraulic diameter, is a concept used in fluid mechanics. It is often used for non-circular ducts or channels. The hydraulic diameter is defined to estimate fluid flow in these non-standard conduits, enabling comparison with a circular duct that would have the same area using this diameter.

When the flow evolves horizontally between two baffles, it represents the configuration of a duct flow. This diameter is equal to $\frac{4A}{P}$ with A the cross section and P the wet perimeter, $2 \cdot (L+l)$. For the large collector this is equal to $\frac{4 \cdot L \cdot l}{2 \cdot (L+l)} = 0.04\ m$.

Considering a fluid temperature of 20 °C to match the conditions of measurements of the pressure losses and the flow rates, and the speed ranges from 0.580 to 1.321 $[\frac{m}{s}]$ one obtains a Reynolds number range of :

$$Re = \frac{1.204 \cdot [0.580 \text{ to } 1.321] \cdot 0.04}{1.94 \cdot 10^{-5}} = 1439 \text{ to } 3279$$

For laminar flow (Re $<$ 2000), f is given by :

$$f = \frac{64}{\mathrm{Re}}$$

This corresponds to flow with an average speed below 0.874 $[\frac{m}{s}]$, For turbulent flow (Re $>$ 4000), f can be determined using the Colebrook-White equation :

$$\frac{1}{\sqrt{f}} = -2\log\left(\frac{e/D}{3.7} + \frac{2.51}{\mathrm{Re}\sqrt{f}}\right)$$

where e is the duct roughness. These results can be extracted from the Moody chart :

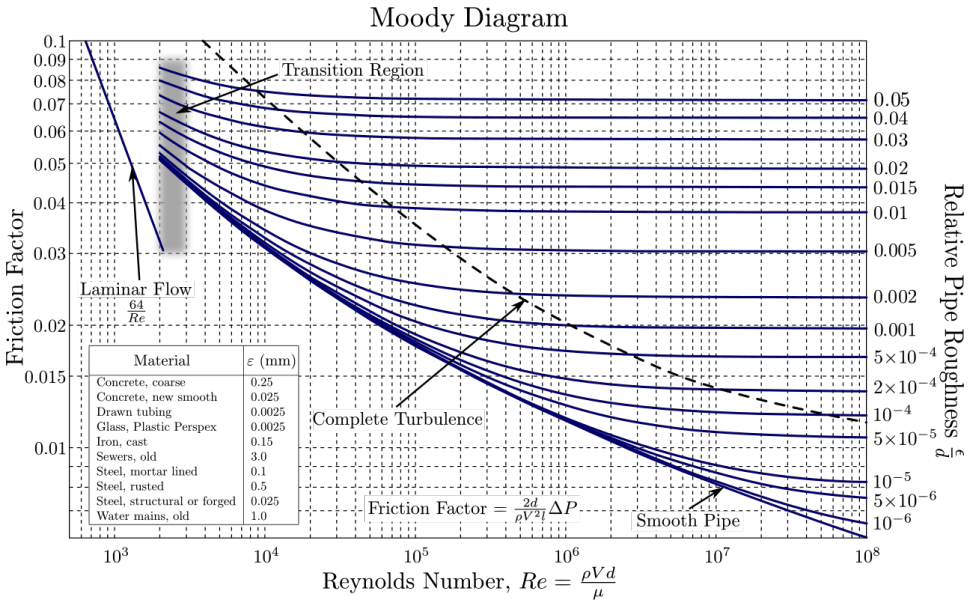

Figure 2.22: Moody chart

For the materials used in this project, the relevant roughness values are listed below :

Material	Roughness
Wood slat	2-3 μm
Medium Density Fiberboard MDF	1 μm
Natural slates	20-50 μm

Table 2.10: Relevant roughness for this application

For the large collector, the mean roughness is $\frac{2.5 \cdot 0.024 \cdot 2 + 1 \cdot 0.12 + 35 \cdot 0.12}{0.12 + 0.12 + 2 \cdot 0.024} = 15.42 \mu\text{m}$

For a flow rate of 0.00456 $\frac{m^3}{s}$ (6V configuration) the friction coefficient is therefore $\frac{64}{1439} = 0.0445$.

$$\Delta P_{\text{lin}} = 0.0482 \cdot \frac{6.315}{0.04} \cdot \frac{1.204 \cdot (0.580)^2}{2} = 1.31\ [Pa]$$

Singular Pressure Losses

Singular pressure losses, ΔP_{sing}, can be expressed as :

$$\Delta P_{\text{sing}} = K \cdot \frac{\rho V^2}{2} \tag{2.29}$$

where K is a loss coefficient specific to the geometry of the obstacle. In terms of flow rate, this becomes:

$$\Delta P_{\text{sing}} \propto Q^2 \tag{2.30}$$

For the flow rate of 0.00456 $\frac{m^3}{s}$, the singular pressure losses are

$$\Delta P_{\text{sing}} = \Delta P_{\text{losses}} - \Delta P_{\text{lin}} = 4.45 - 1.31 = 3.14\ [Pa]$$

The global coefficient K is thus $K = \frac{\Delta P_{\text{sing}} \cdot 2}{\rho \cdot V^2} = \frac{3.14 \cdot 2}{1.204 \cdot 0.580^2} = 15.5$

Overall pressure losses evolution

The overall pressure losses evolve then with the square of the flow rate. If we plot the graphs of the pressure losses as function of the flow rate, one can see this square evolution :

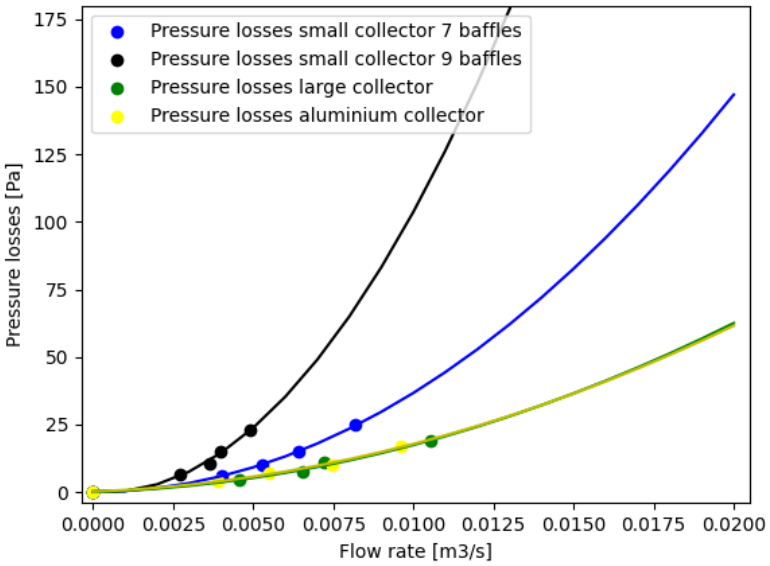

Figure 2.23: Pressure losses evolution with the flow rate

For the small collector with 9 baffles, the function evolves really quickly even though we have similar pressure losses measurements. However the flow rate being much lower for a voltage supplied, this explains the trend of the curves, which might be different if we could take measurements at a higher flow rate.

Impact of natural convection on forced convection

In order to evaluate if the natural convection should be taken into account in the calculations, one can rest on a main rule :

$$\text{The } \frac{Gr}{Re^2} \text{ ratio}$$

- For values ≥ 10, natural convection dominates,
- For $0.1 \leq$ values ≤ 10 mixed convection occurs, one needs to take them both into account
- For values ≤ 10, forced convection dominates

The Grashof is a dimensionless number that approximates the ratio of the buoyancy to viscous forces acting on a fluid :

$$\text{Gr} = \frac{g\beta(T_s - T_\infty)L^3}{\nu^2}$$

- T_∞ is the bulk temperature which is the mean fluid temperature
- T_s is the absorber surface temperature
- L is the characteristic length which is the height of the collector in this case

At a fluid temperature of 32.5 °C and an absorber temperature of 50 °C (a difference of 17.5 °C between the mean air temperature and the absorber is a common value in our measurements), one obtains for the large collector :

$$Gr = \frac{9.81 \cdot \frac{1}{318.15} \cdot 17.5 \cdot 1.325^3}{1.94 \cdot 10^{-5}} \approx 3.33 \cdot 10^9$$

However, this is in a configuration without baffles. The Reynolds number to be considered here is then the one whose characteristic length is the height of the collector. Indeed, for vertical enclosures, the height of the enclosure is typically used as the characteristic length since it represents the vertical distance over which the buoyancy-driven flow develops. One obtains therefore a Reynolds value ranging from 43971 to 100147, underlying the turbulent regime.

The ratio $\frac{Gr}{Re^2}$ ranges therefore from 0.332 to 1.722 which is in the mixed convection range. This suggests that natural convection should be taken into account, even if its impact is less than the one of forced convection since we are far from the value of 10. However, due to the deflection of the air path with the baffles, natural convection is seriously reduced but the regime is less turbulent as well.

One couldn't find any precise correlation to take this into account. However, the longest path encountered by the air going up is at the edges of a baffle. The height is therefore twice the spacing between baffles plus the baffles width so, $2 \cdot 0.12 + 0.045 = 0.285m$. The Grashof number becomes Gr $\approx 3.32 \cdot 10^7$.

The enclosure to be considered for the Reynolds is the one whose top and bottom sides are the top and bottom baffle with respect to the edge baffle considered, one side is the frame wall and the other one is open with the edge of the middle baffle at its center. The characteristic length is 0.285 m for the Reynolds which ranges then from 9458 to 21541 and the ratio ranges from 0.00628 to 0.371. It is at the limit between forced and mixed convection.

One could therefore add up the behavior of the collector working in forced and natural convection. To do so, one can characterize the collector in forced convection

at ambient temperature (when the collector does not produce any power) and characterize the collector while working in natural convection. The fan would encounter less resistance in working conditions, which can be approximated by adding up the two mass flow rates.

Fan model

The model used is the SKUD12B4S silent fan from Servo. A silent model is more suitable for this application in order to limit the acoustic noise in the home, which is a major concern for the comfort of the dwellers.

2.6 Simulation

We coded a *Python* program to simulate the behavior of a solar air collector. It is useful to observe the results that a collector with another configuration (dimensions, materials,...) will produce, without the need to build the latter and measure the outputs of those collectors.

2.6.1 Used parameters

The design parameters of the collector (mass flow rate, thickness, length and width of each part of the collector (wood pieces or insulators), number of baffles and their size, absorber area and thickness and its material, cover parameters and air gap thickness with the absorber) are taken as input given by the user of the code while the properties of materials are implemented as constants that one doesn't need to provide.

2.6.2 Implemented functions

Angle of incidence

According to the orientation and tilt of the collector and the precise time and date of the year, this function computes the incident irradiance on the surface. The irradiance data used is the one hitting 1 m^2 on the ground. One has thus to modulate it on the vertical surface of the collector.

The general equation to compute is the one explained in the methodology :

$$\begin{aligned}\theta = \arccos\big(&\sin(\delta)\cdot\sin(\phi)\cdot\cos(\beta) - \sin(\delta)\cdot\cos(\phi)\cdot\sin(\beta)\cdot\cos(\gamma)\\ &+\cos(\delta)\cdot\cos(\phi)\cdot\cos(\beta)\cdot\cos(w) + \cos(\delta)\cdot\sin(\beta)\cdot\sin(\gamma)\cdot\sin(w)\\ &+\cos(\delta)\cdot\sin(\phi)\cdot\sin(\beta)\cdot\cos(\gamma)\cdot\cos(w)\big)\end{aligned}$$

Irradiance datasets being given on one square meter on the ground, one needs to calculate this angle :

$$\theta_z = \arccos(\cos(\phi)\cos(\delta)\cos(\omega) + \sin(\phi)\sin(\delta))$$

To eventually get the irradiance on a tilted surface :

$$I = I_{horizontal}\cdot\frac{\cos(\theta)}{\cos(\theta_z)})$$

Inside Air Temperature

Since the purpose of such a device is to assess the power output expected throughout the year to heat a dwelling, we computed among others a code that can take input parameters of the dwelling such as the volume, the indoor temperature, the minimum air temperature maintained by an additional heating system and the air renewal rate. However, we didn't analyze the results since one needs to evaluate and add the thermal losses of the dwelling which is out of the scope of this thesis. One can thus modify the code to add them and run the simulation to have the expected evolution.

For health reasons, it is vital to change the air in a tiny house regularly to maintain good air quality. For a tiny house, a benchmark for maintaining good air quality is that the entire air volume should be refilled every 4 hours during the day and every 8 hours during the night. In the simulation, the principle is that every minute the air volume in the tiny house is subject to two heat exchanges:

1. A fraction of the volume,$\frac{1}{240}$ during the day and $\frac{1}{480}$ between 20h and 8h, of the air is replaced by the same volume with the outside air. The volume's temperature decreases from the room temperature to the outside air temperature
2. A volume amount defined by the airflow in the collector. This volume's temperature increases from the room temperature to the output air of the collector temperature, which depends on the properties of the collector and the conditions to which it is subjected.

This implementation can update on every minute the room temperature, with the effect of the indoor air renewal and with the effect of the solar air collector.

Computing of the losses

The irradiance that the Sun gives off is not fully converted to useful heat by the slate. The slate is subject to various losses that need to be calculated in order to simulate the temperature of the slate over time.

Front heat losses

The output of this function represents the losses from the front face of the collector. The front heat transfer coefficient U_{front} is computed following those steps:

1. Compute the sky temperature $T_{sky} = 0.0553 \cdot ((T_a)^{1.5})$
2. Assume an initial candidate for the inside cover temperature: $T^*_{c,in} = \frac{T_s+T_a}{2}$[8] and for the outside cover temperature $T^*_{c,out} = T^*_{c,in} - 3$
3. Based on this estimation, evaluate the radiative heat transfer coefficient between the inside cover face and the absorber $h_{r,s-c} = \frac{\sigma(T_s+T^*_{c,in})(T_s^2+{T^*_{c,in}}^2)}{\frac{1}{\epsilon_s}+\frac{1}{\epsilon_c}-1}$
4. Evaluate the radiative heat transfer coefficient between the outside cover face and the sky $h_{r,c-a} = \frac{\sigma\epsilon_c({T^*_{c,out}}^4-T^4_{sky})}{T^*_{c,out}-T_a}$
5. Evaluate the Rayleigh number to check if the heat transfer is mainly conductive or convective $Ra = \frac{g\cdot\beta_{air}\cdot|T_s-T^*_{c,in}|\cdot L^3}{(\nu\cdot\alpha)}$[9]
6. Evaluate the Nusselt (depending of the Rayleigh number) as $Nu = 1 + 1.44\left[1-\frac{1708(\sin(1.8\beta))^{1.6}}{Ra\cos\beta}\right]\left[1-\frac{1708}{Ra\cos\beta}\right]^+ + \left[\frac{Ra\cos\beta^{1/3}}{5830}-1\right]^+$ if the heat transfer is convective and $Nu = 1$ if the heat transfer is conductive.
7. Compute the convective heat transfer coefficient $h_{conv,c-a} = Nu\frac{k}{L}$
8. Evaluate the top loss coefficient $U_t = \left[\frac{1}{h_{conv,s-c}+h_{r,s_c}} + \frac{1}{h_{c,c-a}+h_{r,c-a}} + \frac{t_c}{k_c}\right]^{-1}$[10]
9. Evaluate the inside heat transfer coefficient $U_{in} = (\frac{1}{h_{conv,s-c}+h_{r,s_c}})^-1$
10. Evaluate the inside cover temperature $T_{c,in,new} = T_s - \frac{U_{front}(T_s-T_a)}{U_{in}}$
11. Evaluate the outside cover temperature $T_{c,out,new} = T_{c,in,new} - \frac{U_{front}(T_s-T_a)}{\frac{k_c}{t_c}}$
12. Evaluate the error $= |T^*_{c,in} - T_{c,in,new}|$

[8] The suffix 's' stands for slate to describe the absorber to avoid confusion with the 'a' of atmosphere.

[9] The characteristic length for the Rayleigh and the Nusselt the air front layer thickness.

[10] $\frac{t_c}{k_c} = \frac{\text{cover thickness}}{\text{cover conductivity}}$

If the error is larger than 0.1 °C, the initial candidates are updated with the new ones and the loop starts over with the new candidates until convergence is reached.

After the coefficient U_{front} is computed by the algorithm, the losses are computed as :

$$Q_{front,losses} = U_{front} \cdot (T_s - T_{air}) \cdot A_{glass}$$

Back Losses

The back losses also include an iterative process using guesses for the inside base temperature and the outside base/foam temperature. The rear section of the simulated DIY solar collector comprises a layer of polystyrene paired with a layer of wood. Adding the convective and radiative resistances. The global heat transfer coefficient is :

$$U_{back} = \frac{1}{h_{conv,sb} + h_{rad,sb}} + \frac{t_{poly}}{k_{poly}} + \frac{t_{wood}}{k_{wood}} + \frac{1}{h_{conv,ca} + h_{rad,ca}})^{-1}$$

. The back losses are defined as

$$Q_{back,losses} = U_{back} \cdot (T_s - T_a) \cdot A_{back}$$

It is calculated in this manner :

- Compute the sky temperature $T_{sky} = 0.0553 \cdot ((T_a)^{1.5})$
- Asses the absorber temperature subjected to losses. Indeed the heat transfer to the working fluid occurs at the same time. A part of the heat taken by the air is lost by convection and radiation to the base and edges and another part is taken out of the collector, considered thus as the useful heat. By withdrawing this energy from the absorber temperature, one ensures that it is not taken into account in the losses. The slate temperature for the back losses is therefore[11]

$$T_{slate} = T_{slate} - C_{p,air} \cdot \dot{m} \cdot \text{ interval } \cdot \frac{(T_{air,out} - T_{air,in})}{C_{p,absorber} \cdot \rho \cdot Vol_{absorber}}$$

- Find a guess for the outside base temperature $T^*_{b,out} = T_a + 2$ and the inside base temperature $T^*_{b,in} = T_s - 10$.

[11]The interval represents the granularity of the data provided, usually 10 seconds

- According to the collector and its configuration, assess the convective heat transfer coefficient arising from the air flow :

$$A_{cross-section} = \frac{\text{heat exchanger height - baffles width} \cdot \text{nbr of baffles}}{\text{Nbr of baffles} + 1} \cdot \text{Baffle thickness}$$

$$v = \frac{mdot}{A_{cross-section}}$$

$$h_c = 12.12 - 1.16 \cdot v + 11.6 \cdot sqrtv$$

- Evaluate the inside radiative heat transfer coefficient between the absorber and the base :

$$h_{r,s-b} = \frac{\sigma(T_s + T^*_{b,in})(T_s^2 + {T^*_{b,in}}^2)}{\frac{1}{\epsilon_s} + \frac{1}{\epsilon_{alu}} - 1}$$

- Evaluate the radiative heat transfer coefficient between the outer face of the base (emissivity adapted if there is an insulator or not) :

$$h_{r,b-a} = \frac{\sigma \epsilon_{poly}({T^*_{b,out}}^4 - T^4_{sky})}{T^*_{b,out} - T_a}$$

- Compute the back heat transfer coefficient[12] :

$$U_{back} = \frac{1}{h_{conv,sb} + h_{rad,sb}} + \frac{t_{poly}}{k_{poly}} + \frac{t_{wood}}{k_{wood}} + \frac{1}{h_{conv,ca} + h_{rad,ca}})^{-1}$$

- Compute the inside heat transfer coefficient :

$$U_{in} = \frac{1}{h_{conv,sb} + h_{rad,sb}}$$

- Evaluate the new inside base temperature :

$$T_{b,in,new} = T_s - U_{back} \cdot \frac{(T_s - T_a)}{U_{in}}$$

- Compute the conductive heat transfer coefficient :

$$U_{cond} = \frac{t_{poly}}{k_{poly}} + \frac{t_{wood}}{k_{wood}}$$

[12]The outside convective heat transfer coefficient is considered constant throughout the day and just taken as a parameter here

- Evaluate the new outside base temperature :

$$T_{b,out,new} = T_{b,in,new} - U_{back} \cdot \frac{(T_s - T_a)}{U_{cond}}$$

- Compute the error for the inside base temperature :

$$|T_{b,in,new} - T^*_{b,in}|$$

  and iterate until convergence is reached.

Edges Losses
The coefficient of the edges of the collector is defined as:

$$U_{edges} = \left(\frac{wood_{thick}}{k_{wood}} + \frac{1}{h_{conv,ca} + h_{rad,ca}} \right)^{-1}$$

And the total losses through the edges are computed as :

$$Q_{edges,losses} = U_{edges} \cdot (T_{slate} - T_a) \cdot A_{edges}$$

1. Compute the sky temperature $T_{sky} = 0.0553 \cdot ((T_a)^{1.5})$
2. Find a guess for the outside edges temperature $T_{e,out} = T_a + 2$
3. Iterate and evaluate the radiative heat transfer coefficient between the edges and the sky $h_{r,e-a} = \frac{\sigma \epsilon_e ({T^*_{e,out}}^4 - T^4_{sky})}{T^*_{e,out} - T_a}$
4. Evaluate the global heat transfer coefficient U_{edges} and the inside coefficient $U_{in} = \frac{k_{wood}}{t_{wood}}$
5. Compute $T_{e,new} = T_s - U_e \cdot \frac{(T_s - T_a)}{U_{in}}$
6. Compute the error $|T_{e,new} - T_{e,out}|$ and iterate until convergence is reached.

Modelling of the outlet temperature

The air sensor is characterized by a heat transfer from the slate to the air. The heat flow per second is mathematically described by the following equation:

$$\dot{Q} = U A_s \Delta T_m$$

In this equation, A_s represents the heat exchange surface area. The term ΔT_m stands for the log mean temperature difference, calculated as an appropriate average between the air temperature and the temperature at the base of the slate. The log

mean temperature difference method is used to determine this average temperature difference. An energy balance on each fluid in a differential section of the heat exchanger can be expressed as each fluid in a:

$$\dot{Q} = \dot{m}_h C_{p,h} dT_h$$

and

$$\dot{Q} = \dot{m}_c C_{p,c} dT_c$$

That is, the rate of heat loss from the hot fluid at any section of the exchanger is equal to the rate of heat gain by the cold fluid in that section. The temperature change of the hot fluid is negative . Solving the equations above for dT_h and dT_c gives:

$$dT_h = \frac{\dot{Q}}{\dot{m}_h C_{p,h}}$$

and

$$dT_c = \frac{\dot{Q}}{\dot{m}_c C_{p,c}}$$

Taking their difference, we get:

$$dT_h - dT_c = d(T_h - T_c) = -\dot{Q}\left(\frac{1}{\dot{m}_h C_{p,h}} + \frac{1}{\dot{m}_c C_{p,c}}\right)$$

The rate of heat transfer in the differential section of the heat exchanger can also be expressed as:

$$\dot{Q} = U(T_h - T_c)dA$$

Substituting those two last equations and rearranging give:

$$d(T_h - T_c) = -UdA\left(\frac{1}{\dot{m}_h C_{p,h}} + \frac{1}{\dot{m}_c C_{p,c}}\right)$$

Integrating from the inlet of the heat exchanger to its outlet, we obtain:

$$\ln\left(\frac{T_{h,\text{out}} - T_{c,\text{out}}}{T_{h,\text{in}} - T_{c,\text{in}}}\right) = -UA\left(\frac{1}{\dot{m}_h C_{p,h}} + \frac{1}{\dot{m}_c C_{p,c}}\right)$$

Finally, after some rearrangement, it gives

$$\dot{Q} = UA\Delta T_{\text{lm}}$$

where

$$\Delta T_{\text{lm}} = \frac{\Delta T_1 - \Delta T_2}{\ln(\Delta T_1 / \Delta T_2)}$$

is the log mean temperature difference, which is the suitable form of the average temperature difference for use in the analysis of heat exchangers. Here ΔT_1 and ΔT_2 represent the temperature difference between the two fluids at the two ends (inlet and outlet) of the heat exchanger. It makes no difference in the direction of flow.

The U coefficient represents the overall heat transfer coefficient, which is unique to each heat exchanger based on its geometry and materials. It is determined through experimental measurements to ensure the best match. A stability condition on irradiance is established to easily obtain data where the panel is not in transition. The optimal coefficient that best matches the retained data is found using a least squares approximation between the data and the function $f(x) = U \cdot A_s \cdot x$. The coefficient U is therefore determined by minimizing the square of the Euclidean norm of the difference between the data and the respective values of the function at these points. U must be chosen such that:

$$\sum_{i=0}^{n} (\dot{Q}_i - U \cdot A_s \cdot \Delta T_{m,i})^2$$

is minimal. This term is called the jacobian $J(U)$ and this condition can be rewritten by deriving the jacobian with respect to U and setting it to zero. This gives the new equation:

$$\frac{\delta J}{\delta U} = 0$$

$$U \cdot A_s \cdot \sum_{i=0}^{n} (\Delta T_{m,i})^2 = \sum_{i=0}^{n} (\dot{Q}_i \cdot \Delta T_{m,i})$$

The instantaneous heat input $\dot{Q}_i$ is defined as $\dot{Q}_i = \dot{m} \cdot C_p \cdot (T_{out} - T_{in})$, which can be easily calculated by measuring the temperatures at the inlet and outlet. The coefficient C_p represents the specific heat capacity at constant pressure and evolves with the temperature. It is taken at the bulk temperature which is the mean air temperature and is expressed in $[\frac{J}{K.kg}]$. The mass flow rate is provided with a certain tolerance in the fan specifications and remains constant according to the conservation of mass principle.

$$\frac{\delta m}{\delta t} = 0$$

For each panel and set of data measured on it, a specific coefficient is defined.

Given that the power output is $\dot{Q} = U * A * \Delta T_m$ and also $\dot{Q} = \dot{m} * C_p * (T_{out} - T_{in})$, a numerical solver (typically fsolve) is used to solve the equation to find the value of T_{out}.

Main Loop

The main part of the simulation is a *for* loop that iterates over each minute of the input irradiance data. For each minute, the program calculates the energy received from the sun by measuring the solar energy and passing it through the function that measures the panel angle's impact on the amount of heat captured. Then, for each minute, the following methodology is followed:

1. Calculate all losses (front, back, edges) based on the temperatures of the current minute.
2. Calculate the slate temperature for the next minute using the equation

$$T_{slate}[i+1] = T_{slate[i]} + \frac{Q_u[i+1] \cdot 60}{C_{p,slate} \cdot \rho_{slate} \cdot Vol_{slate}}$$
$$-C_{p,air} \cdot \dot{m} \cdot 60 \cdot \frac{(T_{air,out}[i+1] - T_{air,in}[i+1])}{C_{p,slate} \cdot \rho \cdot Vol_{Slate}}$$

   , where **i** represents the minutes.
3. Calculate the sensor outlet temperature using the heat exchanger model provided in the dedicated module.
4. Subtract the amount of heat given from the slate to the air to decrease the slate temperature according to

$$T_{slate}[i+1] = T_{slate[i]} - C_{p,air} \cdot \dot{m} \cdot \frac{T_{out} - T_{in}}{C_{p,slate} \cdot \rho_{slate} \cdot Vol_{slate}}$$

5. With the input and output values of the air collector, as well as the outdoor air temperature, the ambient room temperature for the next minute is calculated using the **Inside Air Temperature** function described above in section 2.6.2.

This scheme is then repeated for each minute to simulate the operation of the collector and estimate the indoor temperature. As the objective is to heat a living space, this operating scheme is only used if the ambient temperature is below 25° Celsius. If this temperature is exceeded, the program simulates the behavior where the collector operation is stopped, by equalizing the outlet temperature to the inlet temperature (thus the slate no longer provides any heat to heat up the dwelling).

Daily simulation

The simulation described previously allows one to compute the slate temperature, the losses and the heat transfer coefficient of the heat exchanger that the air and

the absorber represent. However, the purpose being to be able to simulate the behavior of these collectors in a new situation with irradiance and atmospheric data, i.e., inlet temperature.
However, modeldeling this only by simulation lacks of accuracy since the heat transfer of the heat exchanger of the collector varies according to a multitude of parameters. By computing first the heat transfer coefficient for the configuration with experimental data, one can run a simulation with new data sets very precisely.

This simulation aims at evaluating the behavior of a collector using the most appropriate heat transfer coefficient and is an explicit method designed as follows :

- Take as input the irradiance (measured at the tilt angle of the collectors), atmosphere temperature and the design parameters of the collector (mass flow rate, thickness, length and width of each part of the collector (wood pieces or insulators), number of baffles and their size, absorber area and thickness and its material, cover parameters and air gap thickness with the absorber), the properties of materials are implemented as constant one doesn't need to provide.
- Set at the first iteration the temperature of the absorber and the outlet at the value of the inlet temperature.
- Compute the effective irradiance striking the surface and evaluate the subsequent losses using the absorber, inlet and outlet temperature and the design parameters.
- Compute the useful energy of the iteration as the irradiation minus total losses and update the absorber temperature 2.6.2
- Evaluate the outlet temperature for the next iteration using the actual slate temperature and the next inlet temperature, taking the actual outlet temperature as a guess. One computes the Logarithmic mean temperature LMTD and then solves this equation :

  $$mdot \cdot Cp(T_{bulk}) \cdot (T_{out} - T_{in}) - U_{LMTD}(LMTD) \cdot A_{h.exch} \cdot LMTD$$

  where $U_{LMTD}(LMD)$ is a function that takes the LMTD as input and gives the heat transfer coefficient of the exchanger by interpolating between the experimental heat exchanger coefficients.
- The actual slate temperature is re-updated withdrawing the heat given to the air.
- The next initial slate temperature is set to the value of the actual one and the loop starts over.

Full year simulation

The simulation over a year (or more) works similarly to the daily simulation but two features have been adapted :

- The first one concerns the irradiance. Previously, irradiance was manually taken according to the tilt and orientation of the collector. Here the global irradiance (direct and diffuse) is the one striking one square meter on the ground. With a function that takes into account the tilt, azimuth angle and daytime of the year we can precisely assess the irradiance striking the surface of the collector.
- Collectors exhibit different optimum characteristics at a different mass flow rate. At low mass flow rate, the absorber of the collector possibly reaches high temperature. This allows for a high outlet air temperature but so do the heat losses. One does not need high temperature air to warm up their dwelling. We decided therefore to adapt the mass flow rate at each iteration depending on slate and outlet temperature. The latter goes from a natural convection mass flow rate to the values computed for the fan considered at 6,7.5,9 and 12 [V] 2.7. Each iteration increases/decreases the mass flow rate of at most one step (0.00987 ->0.00774 $[\frac{kg}{s}]$ or NC-> 0.00484 $[\frac{kg}{s}]$ for instance).

  We experimentally measured outlet flow rate for natural convection and fitted a square root evolution function. Whenever the absorber temperature is lower than 20 [°C], we decided that forcing the flow through the collector was not beneficial since the outlet temperature would be very low [13] and we therefore compute the natural convection mass flow rate.

  When the slate reaches a temperature higher than 20 degrees, the forced convection starts at the lowest mass flow rate allowed by the fan. If the outlet temperature exceeds 30 °C, the fan is set to the next higher mass flow rate and if it drops below 30 °C, the mass flow rate is decreased. Whenever the absorber temperature drops below 20 [°C], the natural convection mass flow rate is directly computed and set.

  As we can see later in the analysis, this optimizes greatly the yield.

[13] However, this condition could be adapted if air refresh is intended (better to do it with 14 °C than 5 °C air for instance in winter)

Chapter 3

Results

3.1 Measurements methodology

The collectors are south-oriented (175 ° South). Their tilt is kept around 70 °.

The heat regulator hatch is closed and a fan is fixed to each of the air entrances at the bottom of the collectors.

By using a varied voltage source, the speed of rotation of the fan can be adapted. We can thus compute the heat transfer for different mass flow rates.

To conduct the experiment, the temperature of each probe of each data logger is recorded at intervals of 10 seconds for several fan revolution speeds, each for a different day. The probes are offset before the measurements are taken to reduce the underlying uncertainty.

The slate temperature is consistently measured at a specific location for a relevant comparison of the results and is located in the middle of the top left quarter of the collector for front measurements. It is located on the outlet and inlet slate for measurements at the back of the absorber.
A small piece of aluminum foil holds the probes so that heat is efficiently transferred. Bottom slates are likely to have a lower temperature since they are in contact with cooler air while center slates tend to have a higher temperature since they are heated up by adjacent slates and are the lastto be shaded during the sun's path. There is a temperature gradient decreasing from the front to the back of the slates.

Since the most important thing is to be regular in our measurements, we opted for the position mentioned above, which we will discuss later.

A duct is fixed at the outlet and the outlet temperature is measured at the beginning of this outlet pipe in its center, at a spot located within the thickness of the plywood base. This minimizes the influence of heat losses from the pipe on the environment and is more independent of the potential reversal of outside wind into the pipe.

The outdoor temperature is measured behind the collector, ensuring that the probe is not in contact with any surface but only with the air. This also ensures that the probe does not absorb heat from direct sunlight exposure.

Overall, the experimental measurements have been performed over 18 days. The following analysis will focus on a part of these data.

Figure 3.1: Measurement environment

3.2 Experimental and simulation results

3.2.1 Optimal Coefficient for the Heat Exchanger

We now know that the instantaneous heat transfer $\dot{Q}$ between the hot material and the air is modeled using a heat exchanger and is thus given by $\dot{Q} = U \times A_{slate} \times \Delta T_m$. The coefficient U, specific to each panel and for each configuration of that panel, is estimated through experimental measurements.
The ΔT_m corresponds to a specific average between the temperature of the slate and the temperature of the airflow at different points.

Nevertheless, the temperature of the slate is not uniform, and the following measurements were taken by placing a thermocouple on the face directly receiving the irradiance.
This resulted in measurements that significantly deviated from the linearity predicted by the theoretical formula $\dot{Q} = U \times A_{slate} \times \Delta T_m$, as can be seen in the data collected (3.2) on the small collector.
This panel was designed with 7 baffles, and a fan was powered with a voltage of 12 V with the small fan, corresponding in this situation to a mass flow rate of 0.00541 $\left[\frac{kg}{s}\right]$. The data in Figure 3.2 were obtained using the irradiance from Graph

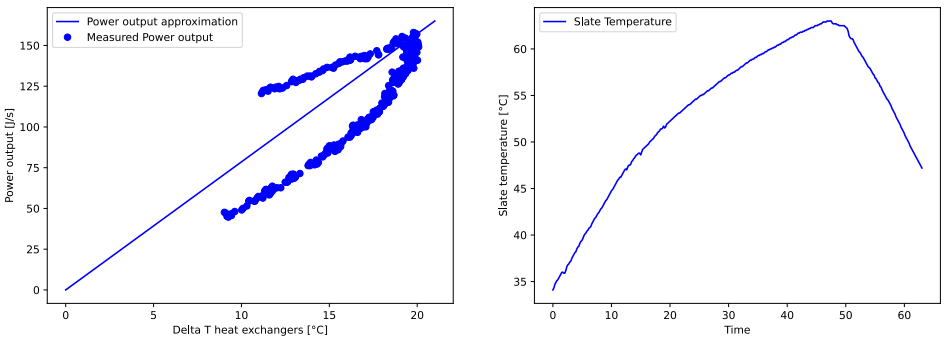

Figure 3.2: Power output w.r.t ΔT_m and associated slate temperature

3.3.

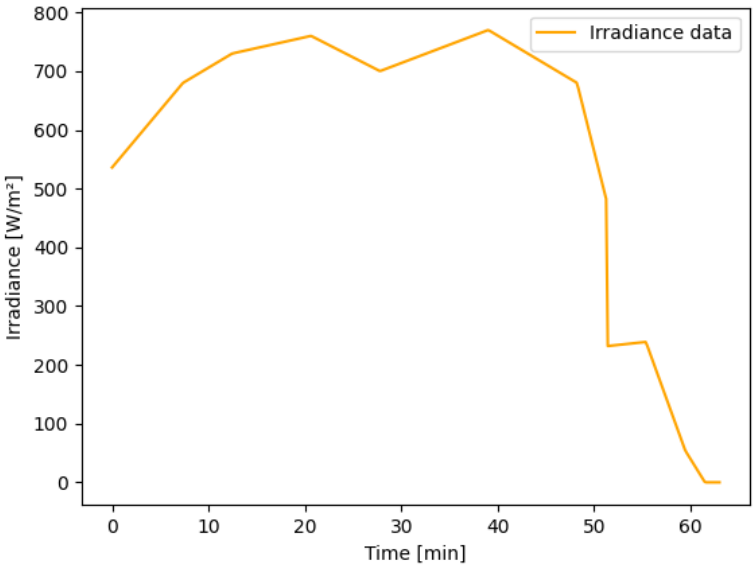

Figure 3.3: Irradiance data

It can be easily observed that some of the data points lie to the right of the linear trend line, while others lie to the left. By analyzing the data more precisely, we can see (see Fig 3.4) that the data points on the right represent the set of data taken when the irradiance is high and the slate temperature is increasing.

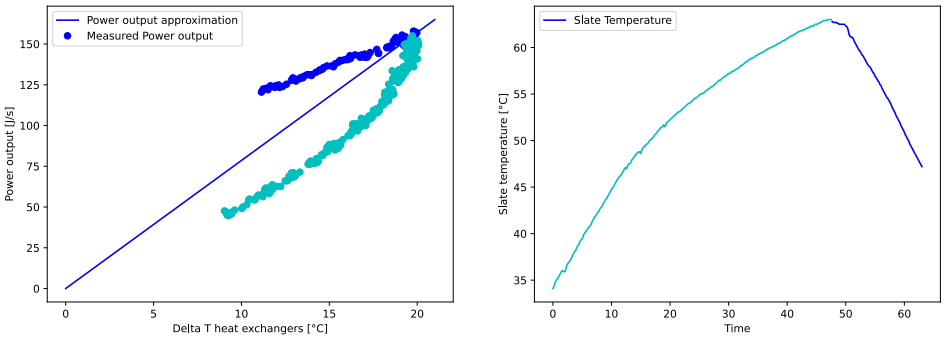

Figure 3.4: Measurement during the heating of the slate

Increase in slate temperature

Theoretically, the ΔT_m is calculated by considering the temperature of the slate surface in contact with the air it heats. When the slate is exposed to sunlight, the

front of the slates, where the measurements are taken, is therefore warmer than the back, which corresponds to the contact surface where the actual heat exchange takes place. This means that for a given measure of extracted power during the temperature rise, the measured ΔT_m (and thus displayed on the graph) is higher than that really corresponding to the heat exchange. This implies that the point will deviate to the right from the $\dot{Q} = U \times A_{slate} \times \Delta T_m$ relation.

Decrease in slate temperature

Similarly, when the sunlight stops illuminating the slate, the losses on the front become greater than the sum of the losses at the back and the amount of heat given to the airflow. This implies that the temperature at the front of the slates will become lower than the temperature at which the heat exchange occurs. In addition, the log-mean ΔT_m needs a slate temperature measurement at the beginning of the heat exchanger and at the end of the heat exchanger. However, as part of the measurements carried out in this thesis, a probe is placed at the front or back of the slates and the equivalent slate temperature is considered at any point on the respective surface. Therefore, for a fixed amount of heat, the measured ΔT_m is lower than the ΔT_m of the heat exchange, which results in a shift of the measurement to the left of the linear heat exchange relation.

3.2.2 Observation of Differences in ΔT_m Based on Measurement Location due to inertia

As previously mentioned, the linearity and heat transfer coefficient U depend on the measurement location. The objective of this subsection is to observe the differences in slate temperatures depending on where the measurements are taken. During an experiment on the large collector, we observed the temperature difference and its implications on ΔT_m, and consequently, the variations in the heat transfer coefficient. Measurements were taken both at the front and the back of the slates. The temperatures at different locations follow the same dynamic. However, the rear surface temperature has a time delay of 50 seconds, demonstrating that if the front of the slates experiences a sharp increase in temperature, this peak reaches the rear surface 50 seconds later. The rear slate surface is also on average 3.96 $[°C]$ lower than the front (see fig. 3.7). It is also observed that for the same irradiance, the higher the mass flow rate, the greater the temperature difference between the two probes, which is logically explained by the fact that the amount of heat supplied to the air increases with the mass flow rate, thus lowering the temperature at the back of the slate.

The irradiance data used are from Figure 3.5.

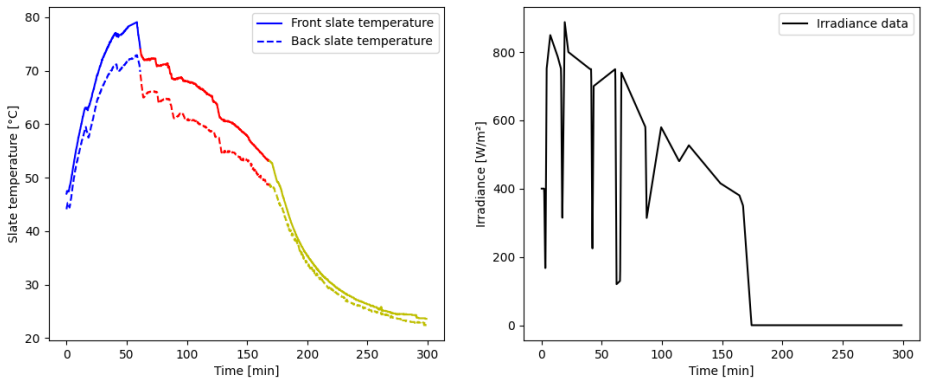

Figure 3.5: Front and back slate temperature (left) and Irradiance data (right)

The ΔT_m measured at the front of the slate are therefore higher, which implies that for the same power, the data will be located at a higher abscissa. Consequently, the heat transfer coefficients will be lower if the measurement is taken at the front of the slates compared to the back (see fig. 3.6).

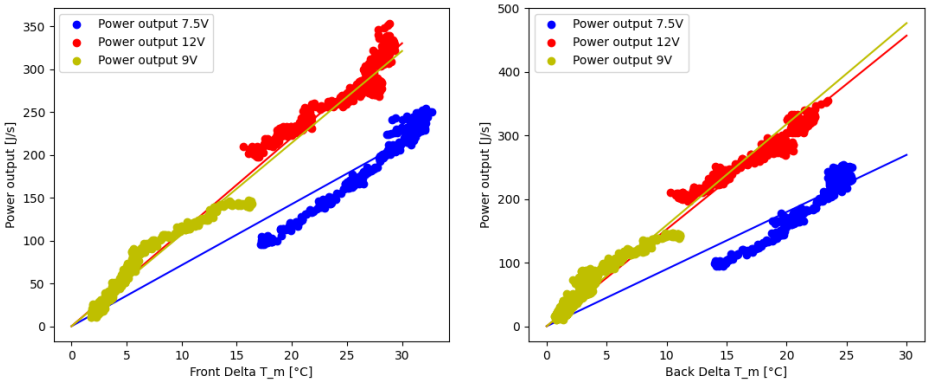

Figure 3.6: Power output w.r.t ΔT_m

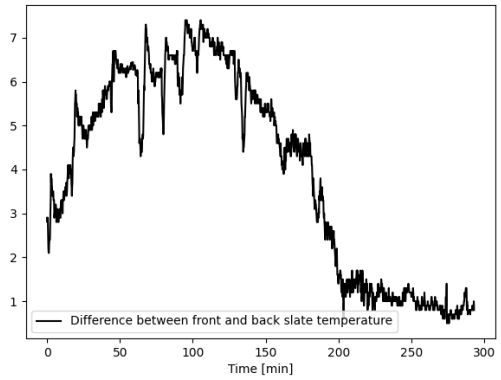

Figure 3.7: Slate temperature gap between front and back surfaces

Observing the relationship $\dot{Q} = U \times A_{slate} \times \Delta T_m$ when the measurement is taken on the contact surface of the heat exchanger, the analysis still shows a certain non-linearity. This non-linearity arises from the error made when not considering that the slate temperature differs at the inlet and outlet of the heat exchanger.

Experiment on Small Collector

The same experiment was conducted with the small collector. For this other collector, with the same irradiance data as Figure 3.5, the slate temperatures at different measurement points and the gap between these temperatures are available in Figure 3.8. For the small collector, the delay remains similar to that of the large one. The average temperature gap slightly increases to 4.06 $[°C]$. For all the graphs in this analysis, the blue part indicates the increase in slate temperature (front or back) and the red part represents the decrease.

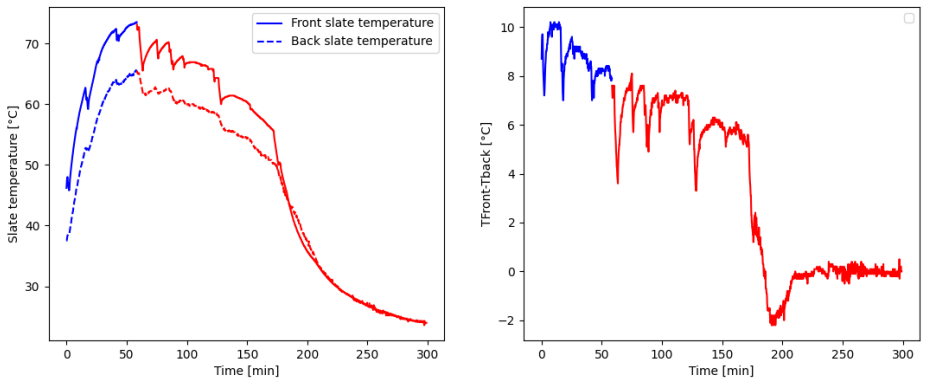

Figure 3.8: Slate temperature (left) and Gap (right)

These temperatures lead to the heat exchanges shown in Figure 3.9. It is also evident that approximating by considering only one measurement point per surface results in a certain non-linearity.

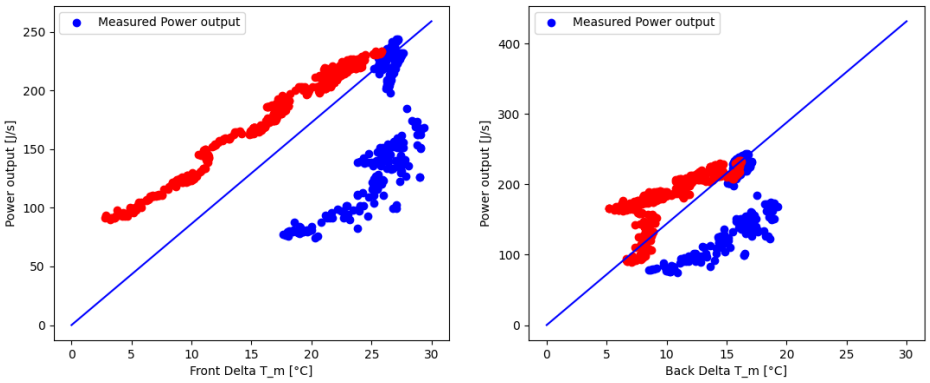

Figure 3.9: Heat exchanges based on ΔT_m

3.2.3 Losses assessment and correction factor

The following graphs compare the simulated absorber temperature with the measured one and highlight the sharing of the losses through the collector. The simulation has been performed for two different days for the small collector design with slate absorber in the 7 baffles configuration with a polystyrene insulator for the 18th May and without for the 21th May, and for the large collector, using the measured irradiance during the considered days. The small collector

had a mass flow rate of 0.00541 $[\frac{kg}{s}]$ for both days, the aluminum one 0.00540 $[\frac{kg}{s}]$ and the large one 0.00802 $[\frac{kg}{s}]$ the 18th of May and 0.00559 $[\frac{kg}{s}]$ the 21th of May.

For the sake of the reader, we plotted the optical losses with the global losses to not overload the graphs.
For the same reason, there is no legend on the graph highlighting the proportion of each losses, the colors are the same for each loss for all the graphs.
This analysis allows to asses the precision of the theoretical losses computation in order to simulate better the behavior of a solar thermal collector in a new situation.

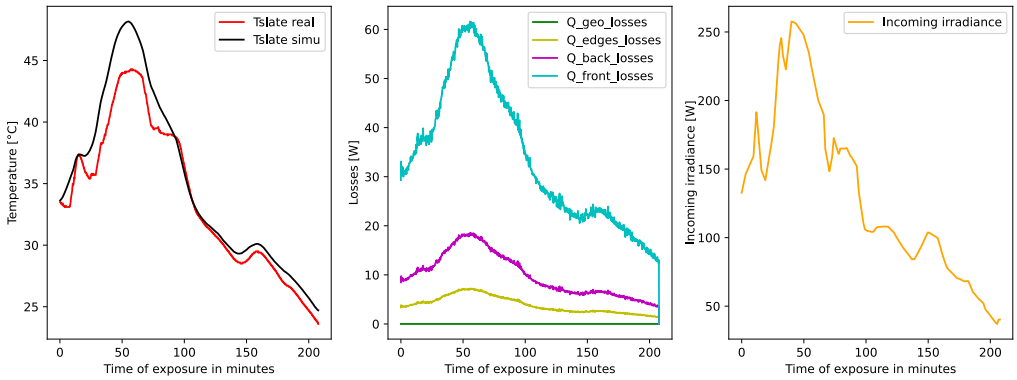

Figure 3.10: Losses simulation small collector with 7 baffles 18 may

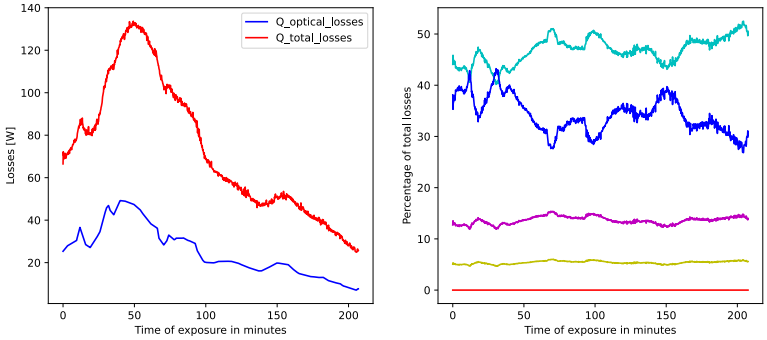

Figure 3.11: Percentage of each losses in the small collector insulated, with 7 baffles 18 may

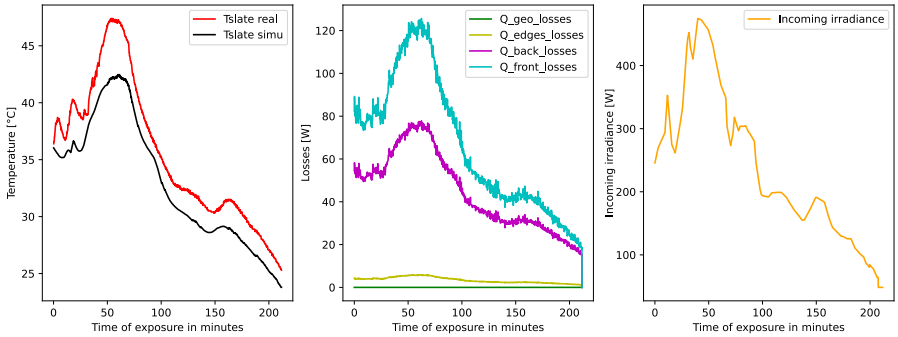

Figure 3.12: Losses simulation large collector 18 may

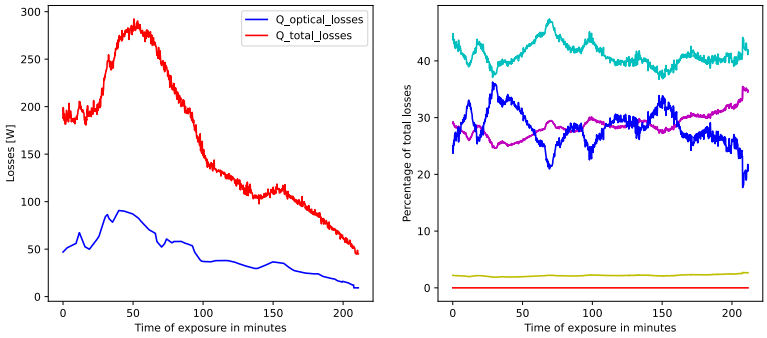

Figure 3.13: Percentage of each losses in the large collector 18 may

The optical losses represent a constant fraction of the incident irradiation. However, the small collector being well insulated at its back as at the front since no convection is considered, the optical losses become paramount and represent a higher sharing of the losses than for the large collector.

The simulated slate temperature follows the same trend as the real one but does not exactly fit it. The losses have actually been systematically divided by two at each iteration. This correction factor seems to be constant since it gave similar results for every case.

However, one has to keep in mind that since this correction is done at each iteration and not at the end, the evolution of the losses is improved in the way that it allows the slate to reach higher temperature which causes in turn higher losses but at the right temperature at which they really occur. The mass flow rate is constant and the measured outlet temperature is used to compute the heat transfer to the air. Therefore, the more the simulated slate temperature curve fits the real one, the more the losses reflect the real ones.

The main difference for the collectors in losses computation is for the front losses. Indeed, the air layer thickness between the absorber and the cover showed via non-dimensional numbers that convection is negligible for the small collector but not for the large one.
The correlations used are designed for a closed rectangular enclosure. However, the slates are not contiguous. This is of a prime importance. It implies that the air actually flows in front and at the back of the absorber. Due to the summer hatch, although closed, the front enclosure communicates with the back of the collector. A non-negligible amount of the heat captured at the front side of the absorber is therefore converted into useful heat, as the latter flows towards the outlet of the collector, therefore modifying actual front losses and increasing the convective heat transfer coefficient.
However, the whole simulation uses theoretical formulas and correlations that might overestimates the real heat transfers in our case.

The reason why the simulated curves don't perfectly fit the real ones can be explained as follows :

- The slate temperature is systematically the one of the upper left corner slate/absorber surface. This has several consequences : We know that the temperature is not uniformly distributed in the absorber. Indeed, the upper part of the absorber is likely to be slightly warmer than the lower part since it is in contact with higher air temperature. Moreover there is a gradient of temperature through the thickness of the absorber which is characterized by the inertia of the absorber. However, the code computes the absorber temperature as the average temperature for the whole absorber, there is therefore an inevitable slight mismatch between the measurements and the simulation, the simulated temperature being likely to be lower.

- As previously mentioned, the slates of these collectors are not contiguous which alters the actual front losses which are designed for a closed enclosure

i.e. contiguous slates and communication from the front to the back thanks to the hatch. For the small collector, only conduction and radiation are considered through the air layer. However, one can assess that convection therefore also occurs and increases the heat losses. The black curve should therefore be lower to match our experimental setup, which is however not the ideal.

- The mass flow rate is evaluated applying to the log-tchebycheff method. Indeed, due to pressure losses, one cannot rely on the theoretical mass flow rate. However, this method induces a lot of uncertainty in the results.
- The irradiance data. The device used doesn't record the irradiance and one has to manually encode it. Data is often recorded (each 1 to 10 minutes) and especially each sudden change in irradiance is recorded. However, due to the fluctuating nature of irradiance, one can expect better results with the exact one.

- The mass flow rate computed at an ambient working temperature is considered constant in every regime. However, at higher absorber temperature, one can expect to have a slight increase in the mass flow rate due to the increasing in the buoyancy effects.
- The losses computation rests on theoretical physical models which model the actual phenomena but possibly don't exactly reflect the reality.

In the figure 3.14, the temperature probe has been stuck at the outlet back face of the slate. One can see that the fitting is quite good. In fact this temperature is closer to the average temperature of the slate,thus, it is desirable that it matches our results.

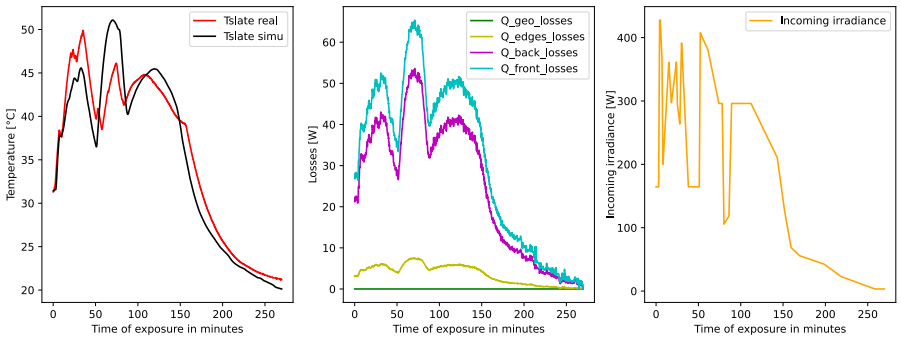

Figure 3.14: Losses simulation small collector with 7 baffles 21 may

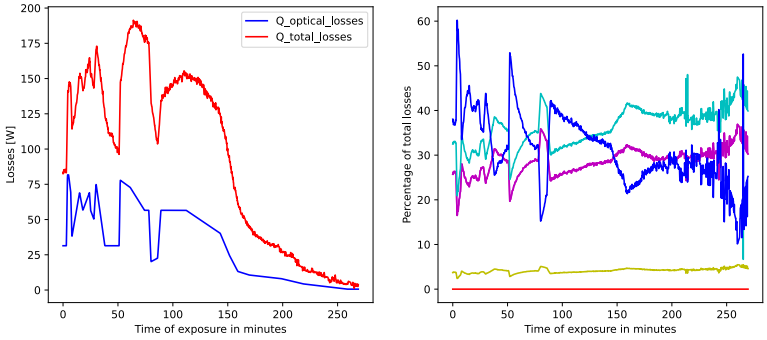

Figure 3.15: Percentage of each losses in the small collector with 7 baffles 21 may

In this configuration, the collector was not insulated at its back. This can be obviously seen since the back losses are more as important as the front losses. The sharing of the losses is not constant and follows a different trend at the end of the exposure time. In fact, due to the inertia of the absorber, when the latter doesn't receive any irradiance anymore, the front of the slate starts to cool down while heat is still spread through its thickness towards the back of the slate. The back of the absorber thus cools down slower. Even if eventually, the heat transfer will be inverted and going from the warmer part (the back) to the coldest one (the front), the back of the absorber will be momentarily warmer. Since the buoyancy-driven

effects are primarily due to a difference of temperature and that the front slate temperature tends to the ambient temperature, the convection in the front enclosure is therefore highly reduced and these losses drop significantly. Indeed, the Rayleigh number :

$$Ra = \frac{g \cdot \beta \cdot (T_{slate} - T_{outside}) \cdot L^3}{\nu \cdot \alpha} \tag{3.1}$$

For a temperature delta of around 1°C with air at 21 degrees, the Rayleigh number becomes 3924 instead of 85242 in the working conditions as evaluated in the methodology.

On the other hand, the back losses occur between the back slate temperature and the atmosphere. Since it is higher than the atmosphere temperature and the base being just an 18 mm thickness MDF wood board, back heat losses become leading.

For this configuration (Figure 3.17), we decided to take the temperature measurements at the inlet and the outlet of the collector. This is likely to give a more accurate estimation of the mean temperature by averaging these two values.

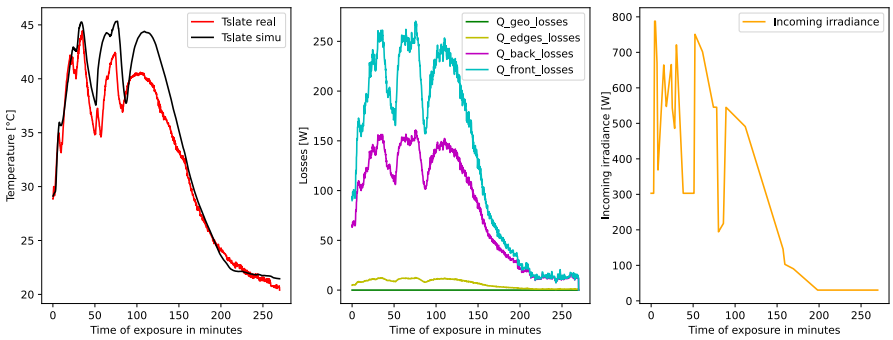

Figure 3.16: Losses simulation large collector 21 may

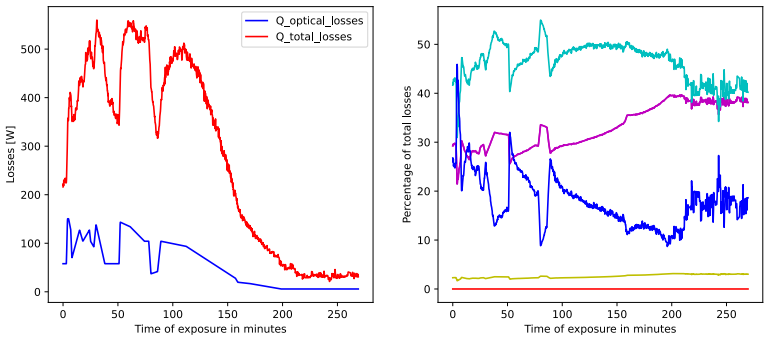

Figure 3.17: Percentage of each losses in the large collector 21 may

As one can see, the slate temperature is now slightly above the real one while it was under the real curve for the previous day for the large collector (Figure 3.18). If we could have a very precise aveage slate temperature, we could find the exact correction factor that matches reality. However, this variable absorber temperature distribution is beneficial to the collector and is what allows the air to reach higher temperature than the mean absorber temperature. We can therefore not simulate exactly the real losses of the collector but we can still have a good approximation. To verify the impact of the losses on a collector with another configuration, one computed the losses and absorber temperature evolution for the aluminum absorber collector.

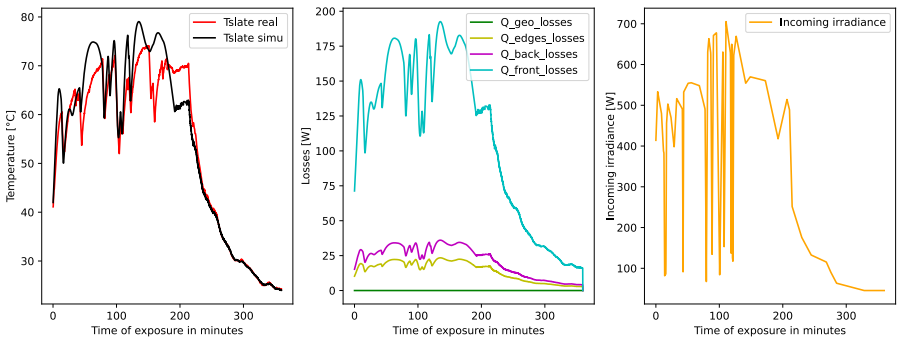

Figure 3.18: Losses simulation aluminum absorber collector 5 may

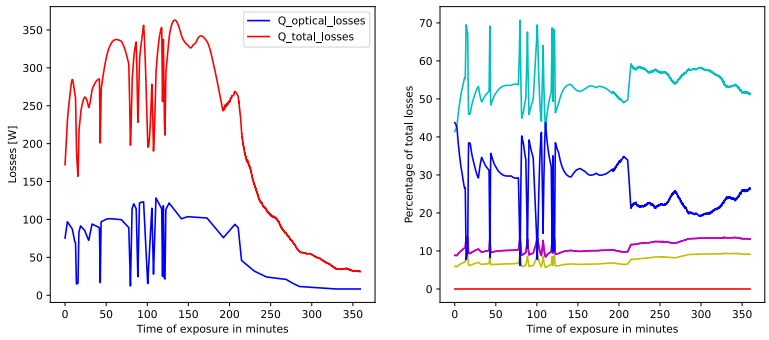

Figure 3.19: Percentage of each losses in the aluminum absorber collector 5 may

Once again, front losses are leading and especially in this configuration for which the collector is very well insulated at its back.

This table gathers the main results one can extract from these graphs using the simulated slate temperature. The first line of a specific loss always corresponds to the May 18_{th} and the following one to the May 21^{st} May. For the aluminum absorber collector these results are dated from the May 5^{th}. The geometrical losses have been intentionally set to zero since there was no shadowing on the collectors these days :

The observations one can draw from this tabular should be the following ones :

- The front losses are leading either way we consider convection in the front enclosure or not. They represent though a 11.6% increase of the sharing when convection is taken into account for the collectors the 21th of may. The 18th of may is not relevant for this comparison since the back insulator modifies the sharing of the losses. The front losses become therefore almost of the same order of magnitude of the back losses. For the large collector although, as expected, the sharing of the front losses doesn't vary significantly.
  The front losses share for the aluminum collector is very high since the back face is well insulated and that optical losses are lowered thanks to the lower reflectivity of the black painted aluminum (0.10 versus 0.11 for slates (20)). They take a smaller sharing of the losses, therefore allocated to the front heat losses.

Collector	Losses	Total [kWh]	% of losses	% of irradiation
Small one	Front losses	0.117	46.4	25.6
		0.139	34.0	18.7
	back losses	0.034	13.6	7.5
		0.112	27.4	15.1
	Edges losses	0.014	5.4	3.0
		0.016	3.9	2.1
	Optical losses	0.087	34.6	19.1
		0.142	34.7	19.1
	Total losses	0.252	100	55.2
		0.410	100	55
	Incoming irradiation	0.457	/	100
		0.745	/	100
Large one	Front losses	0.235	41.5	27.8
		0.453	45.6	35.5
	back losses	0.158	27.9	18.7
		0.275	27.6	21.5
	Edges losses	0.012	2.1	1.4
		0.021	2.1	1.6
	Optical losses	0.161	28.5	19.1
		0.244	19.7	19.1
	Total losses	0.566	100	67
		0.993	100	78.3
	Incoming irradiation	0.844	/	100
		1.277	/	100
Aluminum one	Front losses	0.655	52.9	32.3
	back losses	0.129	10.4	6.4
	Edges losses	0.086	6.9	4.2
	Optical losses	0.369	29.8	18.2
	Total losses	1.239	100	61.1
	Incoming irradiation	2.029	/	100
All of them	Geometrical losses	0	0	0

Table 3.1: Losses analysis and comparison between collectors

- The optical losses are proportional to the irradiation and only dependent on glass and absorber features. We save 0.9% of the irradiation using an absorber with a reflectivity of 0.10 instead of 0.11.
- For a lower irradiation, one expects that the losses to irradiation ratios are lower, due to a lower temperature reached by the absorber for the same mass flow rate. For the large collector, this effect is accentuated since on the low irradiation day (18th), the mass flow rate is higher than on the other day. This prevented the absorber to reach high temperatures and increased thus this difference of absorber temperature reached between these days. For the small collector the slate temperature curves overestimates the real one (being already higher than the average absorber temperature), leading to higher losses, which counteract this effect.
- The use of the polystyrene foam enhances clearly the insulation since the back losses proportion drops from 27.4 to 13.6 % of the share. The global losses doesn't decrease for the reason previously mentioned.
- The small collector in general looks more efficient than the two other ones. This can be explained by the reduced front losses but also by the fact that it was working at a more optimal mass flow rate than the other collectors. Indeed, between the 18th and 21st may, the large collector works with 0.00802 $\frac{kg}{s}$ the 18th and 0.00559 $\frac{kg}{s}$ the 21st while the irradiation increased. The absorber reached similar temperatures but for a twice larger surface the mass flow rate is not twice higher and a larger amount of losses therefore occurred. The aluminum absorber collector received a huge amount of irradiation while working at a mass flow rate of 0.00540 $\frac{kg}{s}$, equivalent to the one of the small collector (0.00540 $\frac{kg}{s}$). Knowing that the aluminum absorber was 2mm thick versus 4mm for the slate and with a heat capacity of 897 $\frac{J}{kgK}$ for aluminum and 837 $\frac{J}{kgK}$ for the slate, aluminum in this configuration reaches quicker high temperature (70-80 °C) and losses are therefore consequent.

One can conclude that :

- The edges don't need a particular insulation. For the small collector they are 4.5 cm in width and thick, and for the large one, 7 cm. While the losses don't represent exactly the same share of the losses, they are approximately of 15-20 [Wh] for the periods. This is quite negligible and a frame thickness of a 4.5 cm is enough to shrink these losses while not overloading the collector. The aluminum absorber collector has however a higher contact surface and a lower thickness 2.5 which is why one observe that these losses reach a higher

sharie of the total losses.

- The back of the collector should always be insulated, this cheap upgrade is highly profitable. Combined with a reflective foil to shrink to radiative heat losses from the slate to the base, these effects add up since the related electrical resistances are in series2.7 and the back losses are efficiently decreased.

- The front face is subject to a huge amount of losses, which can nevertheless not easily be reduced. Opting for design parameters limiting the convection while keeping a good greenhouse effect and joining well the slates to prevent front warm air flows against the glass can help reducing these losses.

- One should use a cover with qualitative properties (high transmittance) and use an absorber with an absorptivity as high as possible if reducing optical losses is sought.
- As long as the outlet temperature is still acceptable to heat the dwelling, one should always aim at setting the highest mass flow rate achievable by the fan in order to keep the absorber temperature as low as acceptable which therefore reduces the subsequent heat losses.

To have a better insight of the computation effectiveness of the front losses, we did the following analysis.
The main loop of the front losses code iterates until the inside glass temperature is guessed. Afterwards, the different convection/radiation heat transfer coefficient can be calculated. To verify this process, we decided to measure the inside glass temperature of the large collector and to compare it to the simulated one :

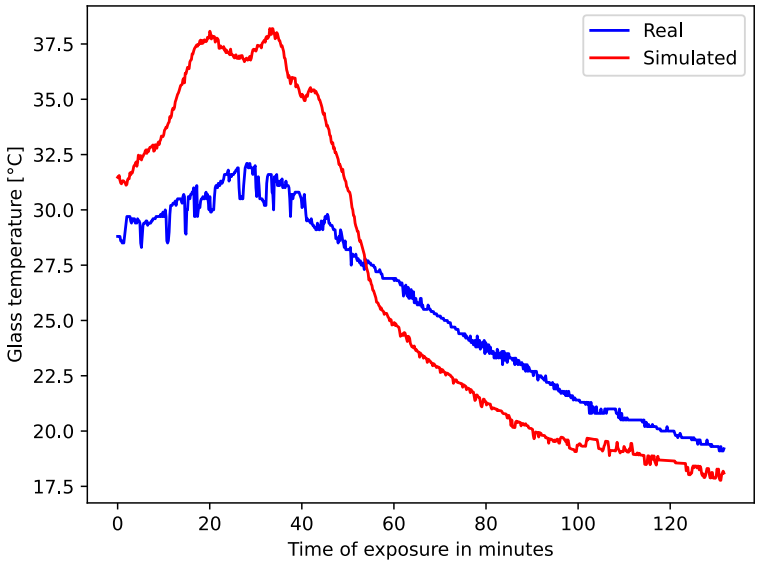

Figure 3.20: Inside glass temperature evolution

While this difference is not negligible, the impact on the slate temperature simulated is quite limited.

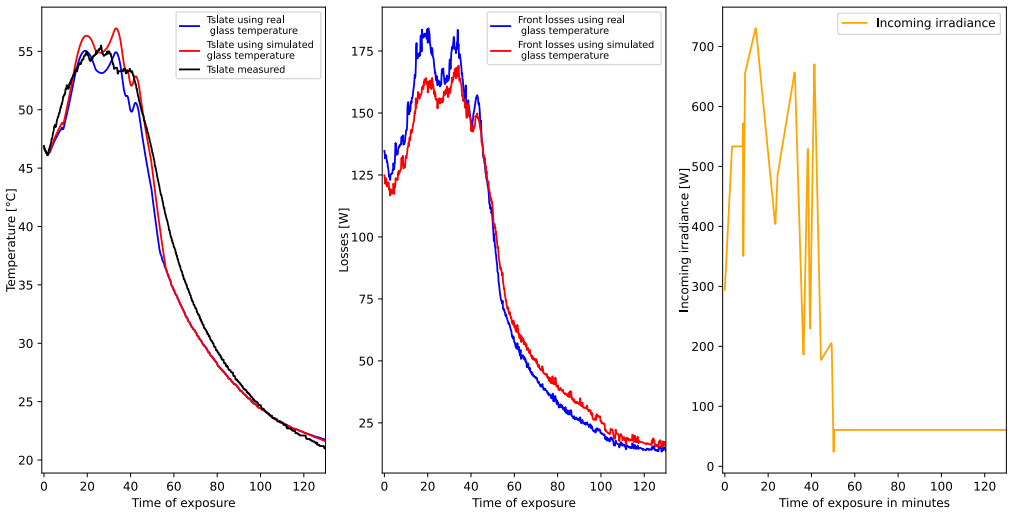

Figure 3.21: Slate temperature and losses comparison

These results are obtained again by dividing these front losses by two at each iteration. The simulated curve is slightly closer to the reality using the glass temperature measured. However, while the front losses theoretical approach don't exactly follow the real behavior of the collector, the error remaining after using a correction factor is low enough to have a good approximation of the behavior of the collector.

3.2.4 Analysis of the heat transfer coefficients

To have a better understanding of the heat transfers that occur in the collector, we will take the small collector configuration and analyse the impact of some design choices. The heat transfer coefficients are always averaged over the whole simulation.

First of all, one needs to find the outlet temperature at each iteration and not use the measured one like in the previous analysis. Doing this, one can truly assess the impact of each modification. In order to do that, we will use the heat transfer coefficient for the modeled heat exchanger that the absorber and the air represent. For the small collector, we will simulate it on the 18 of may using the two heat transfer coefficients for the 7 baffles configuration and with the slate temperature measured on the front face of the absorber 3.18. The simulation is processed like explained in the subsection 2.6.2 A paramount limitation of the simulation is that it considers the slate temperature as an average from our hypothesis. However, the temperature is not distributed evenly. When there is irradiance, the front face is warmer, and the bottom slates are always cooler than the top ones. This is of paramount importance. The air can therefore heat up to a higher temperature since it always follows the back slates temperature with a few degrees gap. However by considering the absorber temperature as an average, the air reaches lower temperature since it cannot be heated up higher than at the average temperature. One would need three-dimensional heat spread analysis to increase the accuracy of the real outlet temperature.

The analysis will be done on the 18 of may data. Since the results will slightly differ from the one of the previous subsection here is the new graph of the simulation on which these coefficients are based :

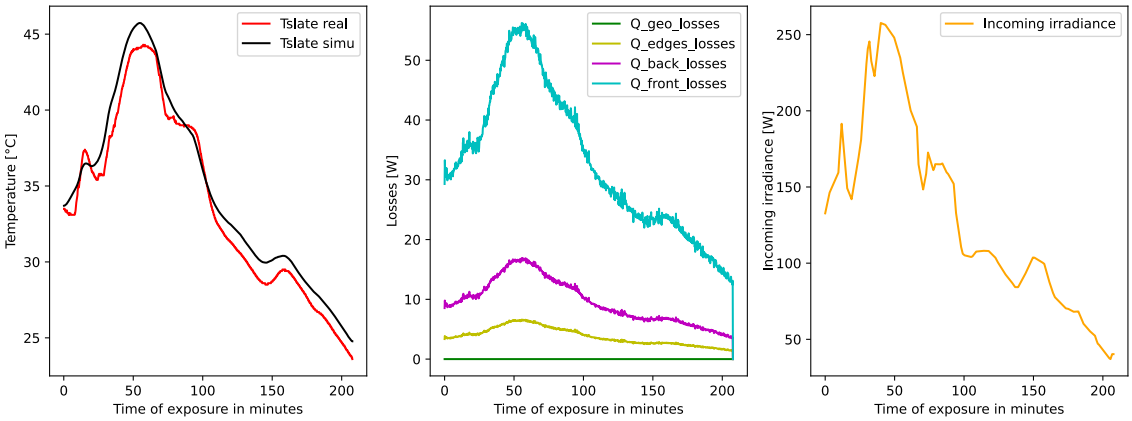

Figure 3.22: Losses and slate evolution computing Toutlet

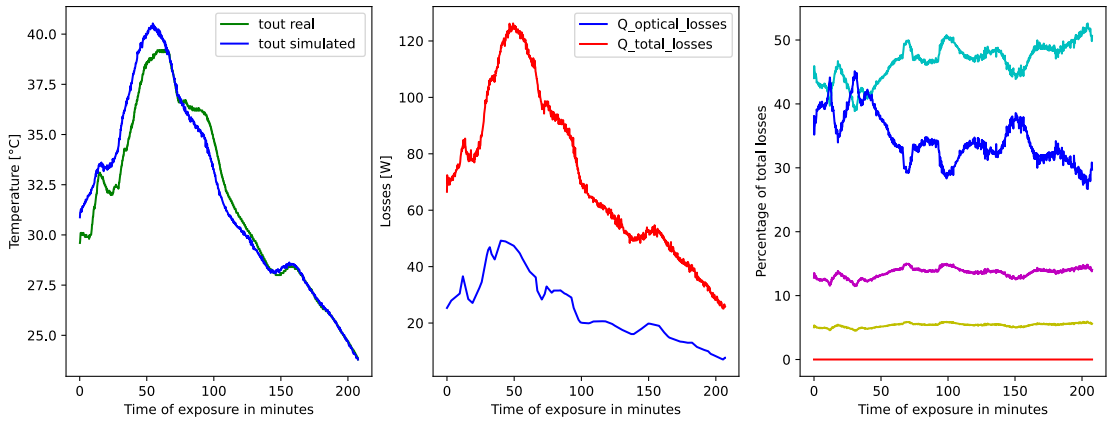

Figure 3.23: Outlet temperature comparison and sharing of the losses

Heat transfer coefficient (HTC) in $[\frac{W}{m^2}]$	Small collector 7 baffles
Radiative HTC atmosphere-cover	209.3
Convective HTC atmosphere-(cover, edges, base)	21.8
Conductive HTC cover	166.7
Radiative HTC cover-absorber	5.45
Conductive HTC cover-absorber	2.36
Radiative HTC absorber-base	0.33
Convective HTC absorber-base	21.2
Conductive HTC edges	3.11
Rdiative HTC edges	139.9
Conductive HTC base	7.78
Conductive HTC insulator	2.11
Radiative HTC base-atmosphere	122.6

Table 3.2: Heat transfer coefficients (HTC) $[\frac{W}{m^2}]$ insulated small collector

To compute the heat transfer through one face of the collector, the inverse of these coefficients have to be added up or calculated as two parallel resistances as shown on the electrical circuit 2.7 and then re-inverted to have the global heat transfer coefficient.

The resulting resistance of two series resistances is their sum and of the one of two parallel resistances is $\frac{1}{\frac{1}{R1}+\frac{1}{R2}}$, which means that the resulting resistance is always smaller than the smallest of the two resistances. Since we invert the resulting resistance back, the result is the opposite for the heat transfer coefficients. Two heat transfer coefficients that can be seen in parallel add up, and two heat transfer coefficients that can be seen in series simplify as $\frac{1}{\frac{1}{U1}+\frac{1}{U2}}$.

Front face : The outside radiative resistance is really high which is due to the fact that the sky is considered as a blackbody i.e. its emissivity is equal to 1 and that the glass emissivity is 0.9 (20). This heat transfer coefficient is responsible for most of the outside heat losses. It is in parallel with the outside convective coefficient thus the resulting heat transfer coefficient is 231.1 $[\frac{W}{m^2}]$.

The cover HTC is also very high, meaning that its inside temperature is almost equal to its outside temperature. Its main interest rests on the greenhouse effect and the protection it offers against outside convection and weather conditions.

Inside, conduction is considered instead of convection, which offers good

insulation. However, radiative exchanges from the absorber to the cover are the main heat exchange and increases the global losses from the absorber to the cover. The resulting HTC is 7.81 $[\frac{W}{m^2}]$.

The global front HTC is therefore the parallel of these 3 heat transfer coefficients and is equal to 7.22 $[\frac{W}{m^2}]$.

Edges : Once more the outside radiative heat transfer coefficient is really high but less than for the cover since the edge's temperature is lower while wood and glass emissivity are equal. The resulting heat transfer coefficient is 161.7 $[\frac{W}{m^2}]$.

The global HTC is therefore 3.05 $[\frac{W}{m^2}]$, which highlights the fact that edge losses occur almost only by conduction.

Back : Inside, the heat transfer is mainly driven by convection induced by the airflow. Since there is a reflective aluminum foil, the radiative exchange is very low and nearly does not impact the losses. The resulting heat transfer coefficient is 21.53 $[\frac{W}{m^2}]$.

The conductive resistance is also what characterizes the insulation here, since the resulting coefficient is 1.66 $[\frac{W}{m^2}]$. We can note that without the polystyrene this coefficient is therefore 4.69 times higher !

Eventually, the outside coefficient is 144.4 $[\frac{W}{m^2}]$. The radiative HTC is lower than for the edges because the polystyrene foam has a lower emissivity (0.60 (20)) than the wood and that the surface temperature is also likely to be lower than the edges since the conductive HTC is lower.

The global HTC is therefore 1.52 $[\frac{W}{m^2}]$.

With 7.22 $[\frac{W}{m^2}]$, the front heat transfer coefficient is leading followed by the edges with 3.05 $[\frac{W}{m^2}]$ and eventually the back with 1.52 $[\frac{W}{m^2}]$. However, the edgesexchange surface area is much lower than that of the back or front face, which explains why these losses are low. The global heat transfer coefficient adapted to the front surface area is :

$$7.22 + 3.05 \cdot \frac{A_{edges}}{A_{front}} + 1.52 \cdot \frac{A_{back}}{A_{front}} = 9.53[\frac{W}{m^2}]$$

And the heat transfer rate is $9.53 \cdot A_{front} = 6.275[W]$.

We also understand the major role the insulator plays by shrinking the back losses and also why for some applications, selective materials are used to reduce the front heat losses.

Impact of design parameters on the losses and heat transfer coefficients

We will discuss somehow some design choices influence the losses and the heat transfer coefficients, based on the same configuration previously discussed 3.2.4. The graph of the slate temperature and losses evolution is available in figure3.22 and here below is the tabular gathering the numerical values. In order to increase the accuracy of the results, we added to the global irradiation the energy that represents the difference of initial and final absorber temperature and divided it by the optical yield (0.809). This ensures that losses and power output are not overestimated :

Losses	Total [kWh]	% of losses	% of irradiation
Front losses	0.114	45.5	23.9
back losses	0.036	14.3	7.6
Edges losses	0.013	5.2	2.7
Optical losses	0.087	35.0	19.1
Total losses	0.249	100	53.3
Q output	0.222	/	46.7
Incoming irradiation	0.475	/	100

Table 3.3: Losses small collector 7 baffles

Aluminum reflective foil

In the table 3.2, the aluminum foil was taken into account since every collector is built that way. If we don't use this reflective foil, the radiative heat transfer coefficient between the absorber and the base rises from 0.33 to 5.88 $[\frac{W}{m^2}]$ and the other coefficients remain unchanged. The global heat transfer coefficient is thus 28.08 // 1.66 // 144.4 = 1.55 instead of 1.52 $[\frac{W}{m^2}]$ previously computed. In fact in terms of losses the impact is really limited, the heat transfer coefficient decreases by 2 % when the reflective foil is not used. In term of global losses, the losses increase from 0.2495 to 0.2498 [kWh] which corresponds to an increase of 0.1 % and a decrease of 0.1 % of the yield as well.

While it seems totally useless at first sight, one has to qualify these results. Here is a subjective reasoning : The heat transfer coefficient of the heat exchanger might be influenced since this reflective aluminum foil allows the radiation coming from the slate to be reflected back to the slate, crossing therefore twice the air and transferring it more heat. The global heat transfer coefficient of the heat exchanger in this configuration might have thus slightly decreased which would have in turn reduce the outlet temperature for a fixed mass flow rate. This reduces the heat taken from the slate. The latter would have thus a higher temperature, likely to

induce more losses but to heat up more the air as well, limiting this negative impact !

Another factor to take into account is the insulator. If one considers the collector without insulator we end up with a coefficient of 28.08 // 7.78// 144.4 = 5.845 $[\frac{W}{m^2}]$ without the foil instead of 21.53 // 7.78 // 144.4 = 5.497 $[\frac{W}{m^2}]$ with the aluminum foil which corresponds to a decreasing of 6 % of the heat transfer coefficient, therefore totally not negligible !

Eventually, if one disposes of a variable speed fan and has an insulated collector, the advice would be to increase the mass flow rate as long as the outlet air is warm enough so that it limits the absorber temperature. In this situation, the reflective aluminum foil used would not be useful.

Contribution of a polystyrene insulator to the back of the panel

In various literatures, collector configurations include an insulating material at the back of the collector to enhance the air collector's efficiency. This insulator can either be a separate material or the wall of the house itself. In this analysis, we will evaluate experimentally the use of the insulator and afterwards, we will compute the theoretical losses analysis according the previous configuration 3.3.

Concerning the cover, it's not necessarily a good idea to use double-glazing to increase the insulation, as it's often more expensive, heavier and more cumbersome, and the overall solar factor which is the fraction of solar radiation that reaches the absorber, will be poorer.
This is why this analysis focuses on a polystyrene foam added to the back of the small collector.

*Measurement Implementations To ensure comparable data, for the measurement on the insulated small collector another air collector without insulation was placed beside it, with measurements taken simultaneously. During the measurement period, both collectors had 7 baffles and a mass flow rate imposed by their respective fans that are 0.005411 and 0.00559, respectively for the small insulated and large collector. The average irradiance for this period measurement is 597.76$[\frac{W}{m^2}]$, as one can see on figure 3.24.

*Advantage on Power Output The objective is to use these two collectors to compare the energy extracted from a collector when it has a polystyrene foam insulation at the back and when it does not.

For this purpose, the recorded measurements were taken using the irradiance data shown in Figure 3.24. It can be observed that the small insulated and large

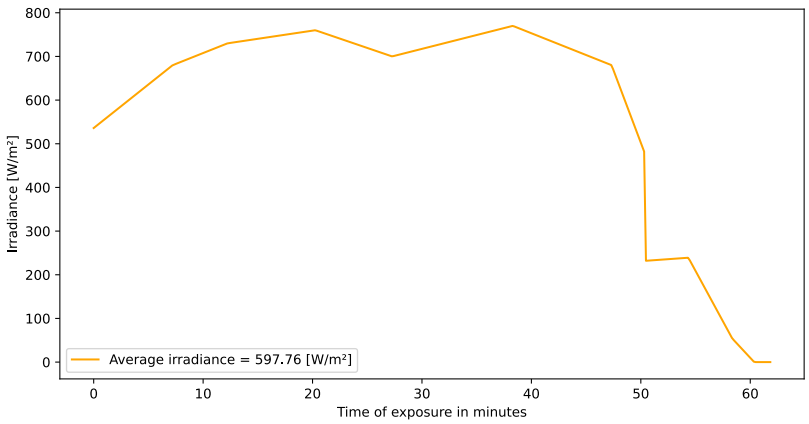

Figure 3.24: Irradiance Data

collectors exhibit slate temperatures (Figure 3.25) with quite similar dynamics, but with a higher slate temperature for the larger collector.

To calculate the output powers and compare the efficiency, we use the heat exchange system again: $\dot{Q} = U \times \text{Area} \times \Delta T_m$. The graphs in Figure 3.26 provide an initial indication that the insulation is beneficial. For the same ΔT_m, the thermal power of the small collector is slightly higher than that of the large collector. In contrast, it was lower than the large collector when the small collector did not have the polystyrene foam.

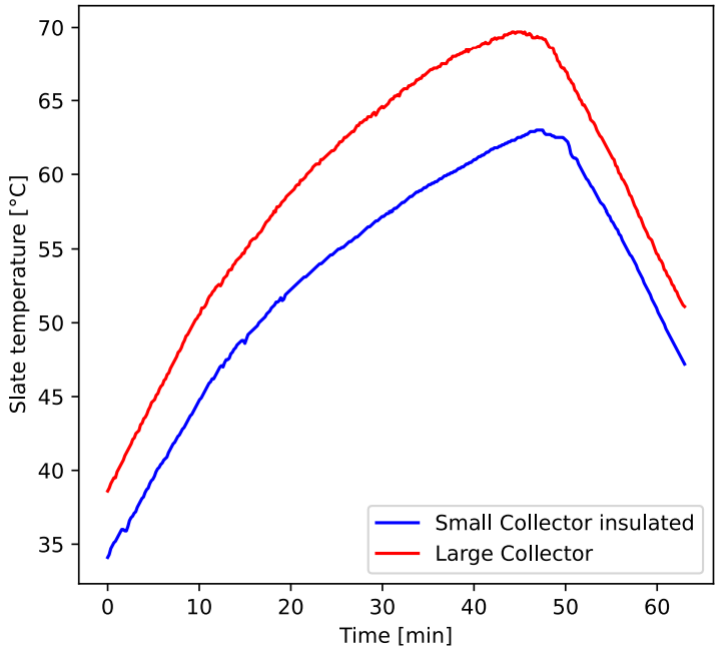

Figure 3.25: Slate temperature through time

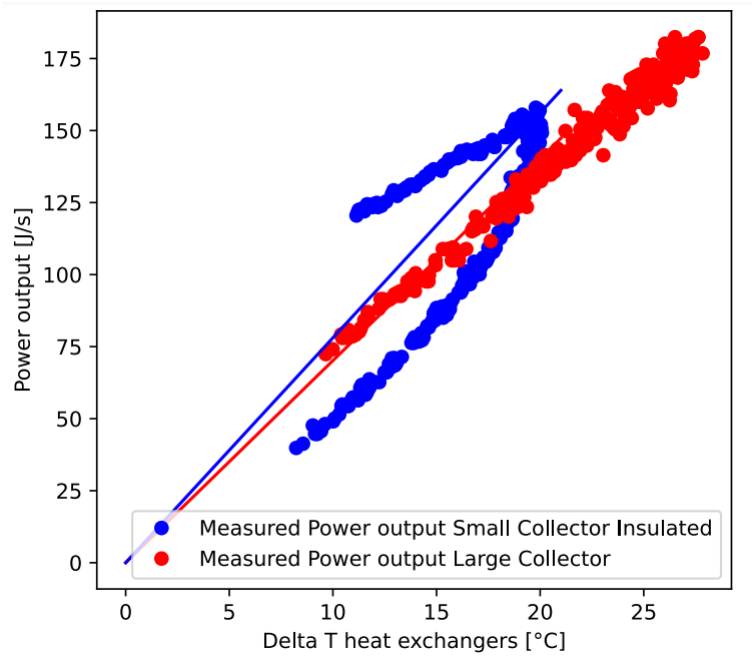

Figure 3.26: Model of the heat exchange between air flow and slate

This ultimately helps for the calculation of the power extracted from the panel. Using the mass flow rates determined in Section 2.5, the power is calculated as $\dot{Q} = \dot{m} \times C_p \times (T_{out} - T_{in})$, leading to the graphs shown in Figure 3.27.

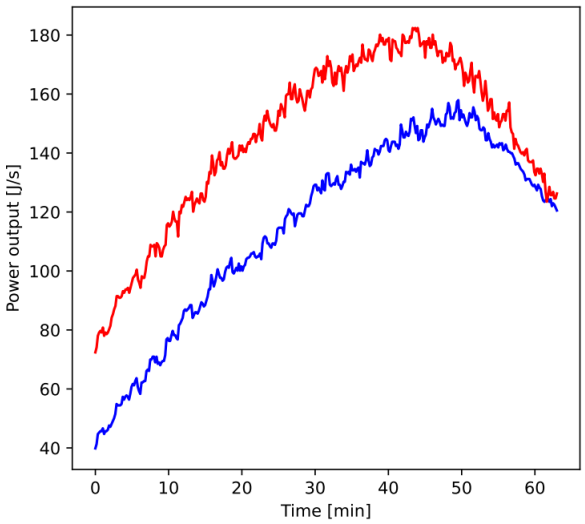

Figure 3.27: Power output through time

Thus, we can analyze the effect of the polystyrene foam based on the thermal energy extracted from each. The thermal energy extracted is obtained by numerically integrating the power output curve. These numerical integrals are performed using the trapezoidal rule method (Table 3.4).

Average irradiance	$597.76W(m^{-2})$
Non-Insulated large collector	$166.77[Wh]$
Insulated small collector	$121.07\ [Wh]$

Table 3.4: Energy (Wh) with insulation

It can be observed that 1.38× more energy was extracted from the collector without insulation compared to the one with polystyrene foam insulation for the same duration and irradiance. However, the non-insulated collector has a larger surface area than the insulated collector, and it is known from subsection 3.2.6 that for

an average irradiance of 597.76$[\frac{W}{m^2}]$, the large non-insulated collector will extract 1.6186× more energy than the own-constructed small collector (outperformance of 61.86%). Therefore, it is easy to imagine that for this measurement period, the energy extracted from the non-insulated small collector (NISC) would have been:

$$E_{NISC} = \frac{E_{LC}}{1.6186} = \frac{166.77}{1.6186} = 103.03[Wh] \tag{3.2}$$

Now it is possible to compare the energy extracted from a small collector with and without insulation, which allows finding the advantage η of using insulation.

$$\eta = \frac{E_I}{E_{NI}} = \frac{121.07}{103.03} = 1.1751 \tag{3.3}$$

Finally, one can deduce that insulation allows extracting 17.51% more energy for the same duration and an average irradiance of 597.76$[\frac{W}{m^2}]$.

In the previous configuration 3.3, the polystyrene foam is used. If we take it off the equation the back heat transfer, as said before, becomes 21.53 // 7.78 // 144.4 = 5.497 $[\frac{W}{m^2}]$, which is 3.61 higher than the 1.52 $[\frac{W}{m^2}]$ previously computed and lead to a global HTC and heat transfer rate of 13.51 $[\frac{W}{m^2}]$ and 8.89 [W]. The losses tabular becomes :

Losses	Total [kWh]	% of losses	% of irradiation
Front losses	0.096	33.6	20.1
back losses	0.092	32.1	19.3
Edges losses	0.011	3.8	2.3
Optical losses	0.087	30.5	19.1
Total losses	0.286	100	60.8
Q output	0.187	/	39.2
Incoming irradiation	0.477	/	100

Table 3.5: Losses small collector 7 baffles without foam insulator

The impact is significant, the yield drops from 47.3 % to 39.2 % and the back losses are multiplied by 2.67, increasing from 36 [Wh] to 96 [Wh] for the period. Insulating the collector resulted in a gain of 8.1% of the irradiation, which corresponds to an increase of 20.6% in its energy yield [1] which confirms our experimental based

[1] $\frac{47.3}{39.2}$

results showing that insulating the collector increase its yield of around 17.5 %. The polystyrene thickness is 18 mm with a conductivity of 0.038 $[\frac{W}{mK}]$ (20) in our case.

Let's see what would be the gain to double this thickness. The conductive heat transfer coefficient through the insulator drops logically from 2.11 to 1.055 $[\frac{W}{m^2}]$ and the global heat transfer coefficient through the back is therefore 21.53 // 0.93 // 144.4 = 0.885 $[\frac{W}{m^2}]$. The table becomes :

Losses	Total [kWh]	% of losses	% of irradiation
Front losses	0.118	49.0	24.9
back losses	0.022	9.2	4.6
Edges losses	0.014	5.6	2.9
Optical losses	0.087	36.2	19.1
Total losses	0.286	100	51.5
Q output	0.230	/	48.5
Incoming irradiation	0.477	/	100

Table 3.6: Losses small collector 7 baffles with a double thickness foam insulator

Compared to the single insulation layer, the one goes from 46.7 % to 48.5 % of yield which represents an increasing of 4.3 % of the yield and a gain of 1.8 % of the irradiation. The improvement is logically proportionally reduced than for one layer. Seen the price of an insulator foam, we advise therefore that the use of one layer is paramount but that the one for a second layer can be done if the thickness of the collector is not a design parameter to optimize and that one does not encounter problem to hang the collector. However for a third layer the yield goes from 48.5 % to 49.34 % which represents an improvement of 1.7 %, one let the reader make up his mind if this is worth it in his situation.

3.2.5 Forced convection

The air flowing along the slate is heated and circulates by natural convection, which helps to warm the tiny house. Intuitively, one might think that installing a fan allows the air to circulate faster and thus heat the room more quickly. However, as the amount of heat provided by the slate also increases with the mass flow rate, imposing a flow rate prevents the slate from reaching high temperatures. Therefore, the objective is to analyze the impact of mass flow rate in forced convection on the extracted power, heat transfer, and efficiency.

Heat transfer coefficient analysis

The initial phase of the analysis centered on comparing the heat transfer coefficient of the collector, with a focus on the effects of altering the mass flow rates for the same air collector.Experimental measurement are obtained on the self-constructed large collector, with a particular flow rate set using a fan placed at the inlet of the collector. To manipulate the mass flow rates, the input voltage of the fan was varied to values of $7.5, 9$, and 12 [V]. These settings correspond to the different mass flow rates investigated in this study:

Voltage [V]	7.5	9	12
Mass flow rate $[kg.s^{-1}]$	0.00802	0.00882	0.01265
HTC $U[W/(m^2K)]$	19.54	7.76	20.35

Table 3.7: Heat transfert coefficient (HTC) for different mass flow rate

The goal is to observe the variation of the power provided by the collector $\dot{Q}$ as a function of the given flow rate. Consequently, the following graphs are obtained for the mentioned voltages (and mass flow rates), representing the extracted power as a function of the log-mean temperature difference between the slate and the air (3.28a). Similar analyses are then conducted for the irradiance data over time (3.35b):

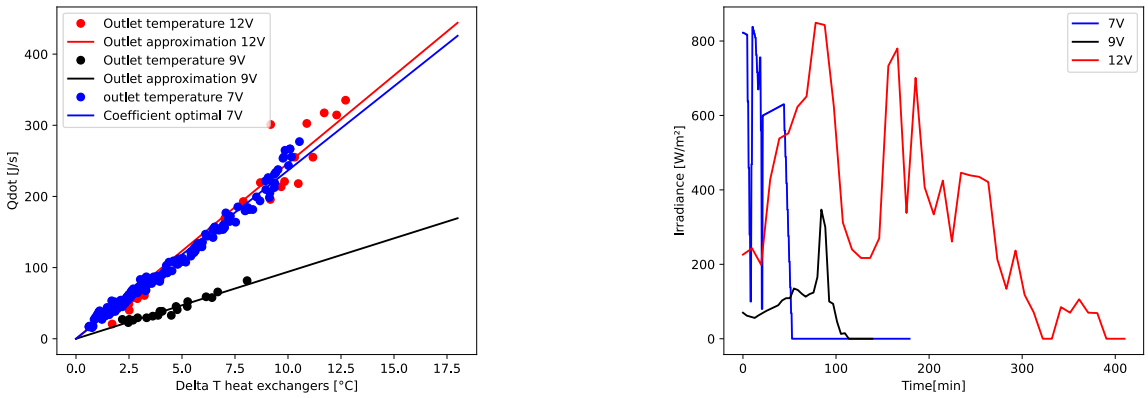

(a) Power output w.r.t ΔT_m

(b) Irradiance Data

Figure 3.28: Heat exchanger model for different mass flow rate

The most significant transfer coefficient is the one for a supply voltage of $12[V]$,

which implies that for a material at a certain temperature, the highest power can be extracted at the highest flow rate.

Analysis of power output

It is now known that collectors operate differently depending on the temperature. Therefore, to compare which flow rate yields a better efficiency, we will use experimental data taken with a flow rate of $0.00802\frac{kg}{s}$ on an air collector with an area of 1.212m^2 and simulate, for the same irradiance, the power output if this same collector had a flow rate of $0.00559, 0.00882$, or $0.01265\frac{kg}{s}$. The irradiance during these measurements is shown in Figure 3.29.

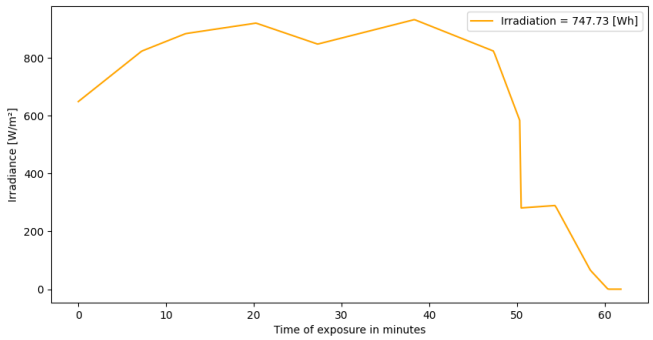

Figure 3.29: Incoming irradiance data

This incoming irradiance allows us to measure or simulate the different power outputs for the various mass flow rates analyzed in this report, namely $0.00559, 0.00802, 0.00882$, and $0.01265\frac{kg}{s}$. These power output data are presented in Figure 3.30. The data shown in the legends represent the extracted energy expressed in Wh for each mass flow rate.

In order to analyze the temperature efficiency, one can now compare the energy extracted from the collector over a measurement period to the solar energy captured by the collector, both expressed in Wh. The objective was to find the optimal flow rate. These energies are obtained by integrating the power extracted from the panel (respectively, irradiance multiplied by the collector's area) using the trapezoidal integration method. The energy is then converted into Wh to obtain the energy provided by the panel (respectively, captured by the panel).

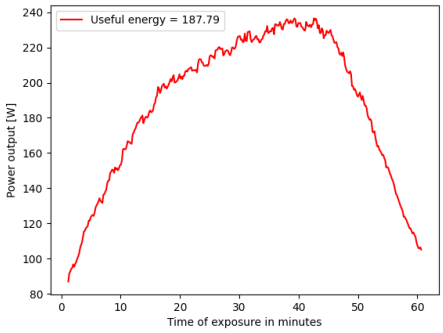

(a) Power output for $0.00559\frac{kg}{s}$

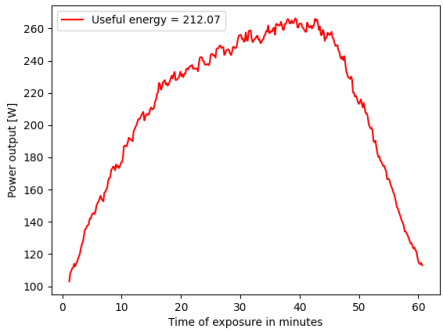

(b) Power output for $0.00802\frac{kg}{s}$

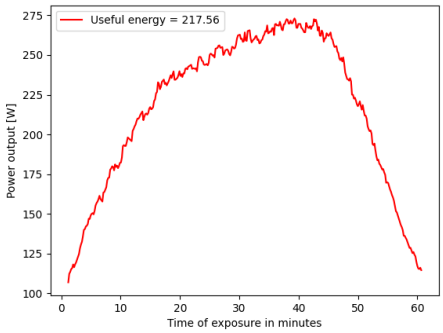

(c) Power output for $0.00882\frac{kg}{s}$

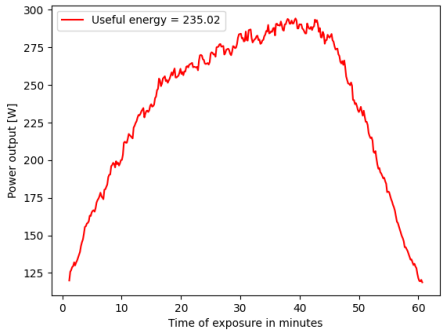

(d) Power output for $0.01265\frac{kg}{s}$

Figure 3.30: Power output with respect to time

Irradiation$[Wh]$	747.73			
Voltage $[V]$	6	7.5	9	12
Mass flow rate $[kg.s^{-1}]$	0.00559	0.00802	0.00882	0.01265
Energy extracted $[Wh]$	187.79	212.07	217.56	235.02
Efficiency $[\%]$	25.11	28.36	29.09	31.43

Table 3.8: Extracted energy and efficiency as a function of mass flow rate

We observe a linear trend for efficiency as a function of mass flow rate.

3.2.6 Influence of area

The solar power captured by a slate is proportionally dependent on its area. However, the extracted power is necessarily higher with a larger collector, given the longer air path length, which increases the instantaneous heat losses from the

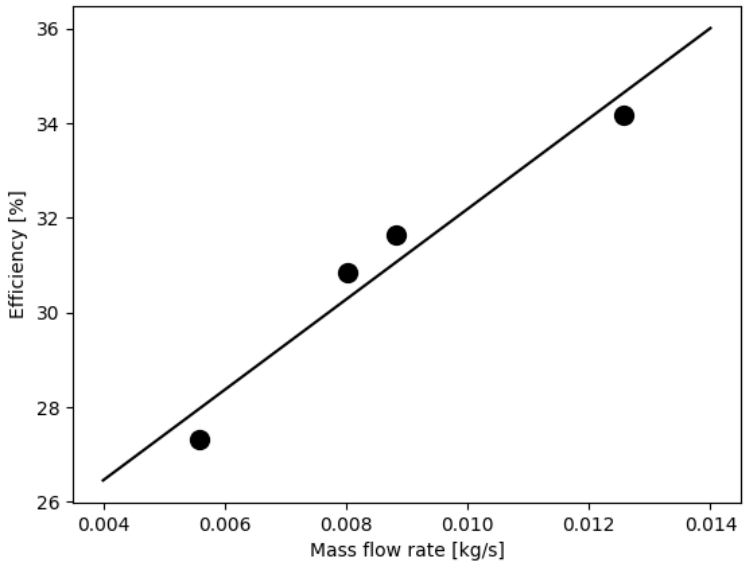

Figure 3.31: Efficiency

slate. Therefore, this section aims to observe the influence of the area of a collector on its efficiency.

Experimental procedure

To compare the impact of this parameter, the energy extracted from the two panels constructed for this thesis, with respective sizes of $0.658[m^2]$ and $1.212[m^2]$, was observed over two measurement sessions, with almost identical mass flow rates (0.005411 and $0.00559[\frac{kg}{s}]$, a difference of 3%). During both measurement periods, the irradiance was the same for both collectors. The objective is ultimately to understand what power ratio can be obtained for a slate area 1.84× larger.

Experimental results and conclusion

The irradiance data used for the two irradiance measurements are those from figure 3.32.

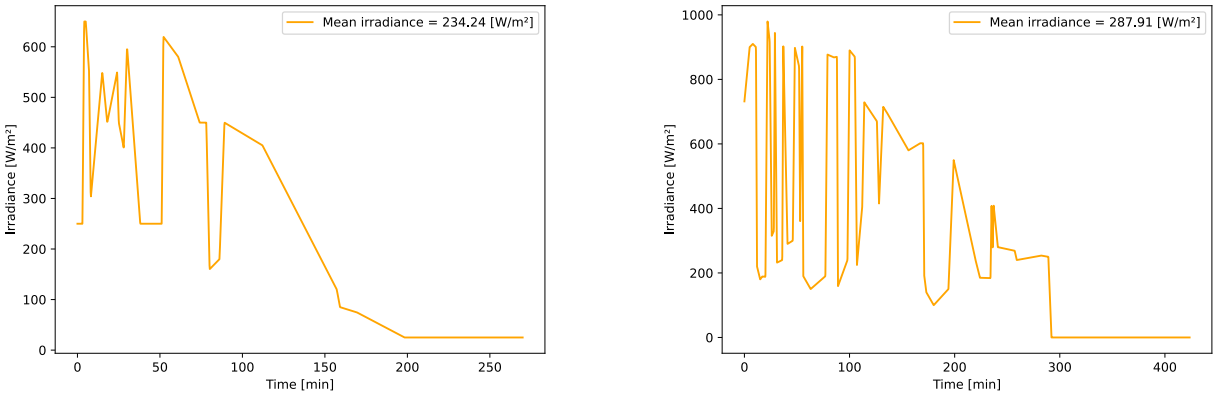

(a) 1^{st} period (b) 2^{nd} period

Figure 3.32: Irradiance data

The first irradiance data, with an average value of $234.24[\frac{W}{m^2}]$, allow for higher useful power on the larger collector (see figure 3.33a). The second measurement, with a 22% increase in average irradiance ($287.91[\frac{W}{m^2}]$), demonstrates that the heat power extracted is now much more significant for the larger collector (see figure 3.33b). As mentioned in the graph legends of figure 3.33, the blue curve represents the measured power output on the large collector, while the red curve represents that on the small collector.

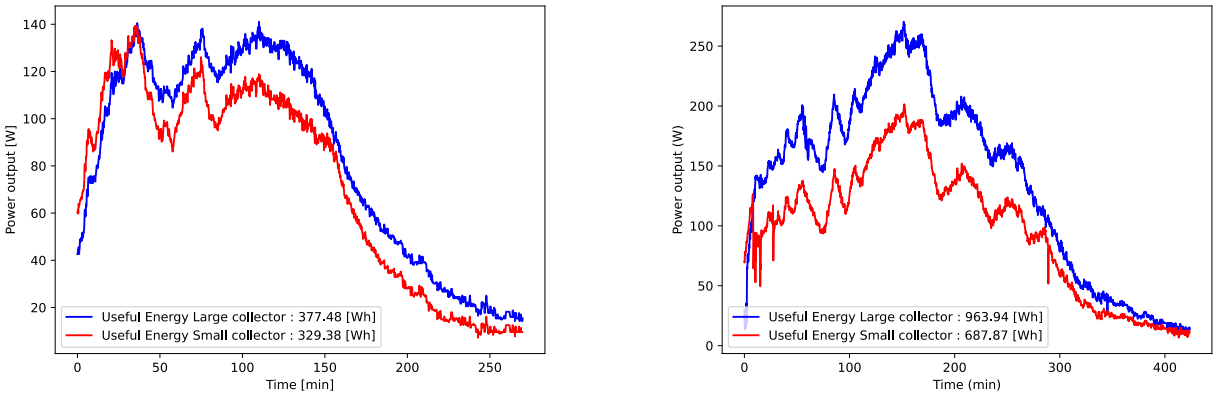

(a) 1^{st} period (b) 2^{nd} period

Figure 3.33: Power output w.r.t time

In terms of extracted energy, it is observed that for the same irradiance and at

a similar flow rate, the larger collector outperforms the second for an average irradiance of $234.24[W/m^2]$, and the advantage of using a larger slate surface tends to increase as the irradiance rises. From these measurements, the figures presented in Table 3.9 can be derived. The three experimental periods each have different durations, which implies that the total energy may be lower despite a higher average irradiance.

Mean irradiance	$234.24[W.m^{-2}]$	$287.91[W.m^{-2}]$	$597.76[W.m^{-2}]$
Small collector : $0.658[m^2]$	329.38	687.87	116.56
Large collector : $1.212[m^2]$	377.48	963.34	188.67

Table 3.9: Energy extracted (Wh) as a function of area and average irradiance

By analyzing these data, for the irradiance of the first measurement range, the energy extracted from the larger collector is 1.146× greater than the energy extracted from the small collector, which corresponds to an outperformance of 14.6%. For the second measurement period, it is similarly observed that one can extract 1.4013× more, which corresponds to an outperformance of 40%.

Mean irradiance $[W.m^{-2}]$	234.24	287.91	597.76
Outperformance [%]	14.6	40.13	61.86

Table 3.10: Outperformance w.r.t mean irradiance

It is evident that no collector can outperform another when the irradiance is zero. Therefore, we approximate the data points using a linear approximation passing through the origin (0,0) to estimate the performance improvement of a panel with a surface area that is 1.84× larger. As an example, it is observed that for a surface 1.84× larger and with an average irradiance of $256.1[\frac{W}{m^2}]$, the extracted power will be 1.25× higher.

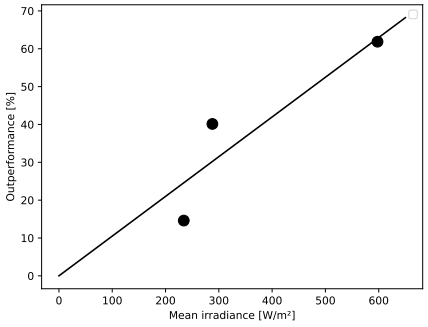

Figure 3.34: Outerformance of the large collector compared to the small one

3.2.7 Influence of the baffles

One technique to ensure that the air stays along the slate for a longer duration is by introducing baffles. This forces the air to follow a much longer path than if it were to simply rise directly. Therefore, the purpose of this analysis is to understand the impact on output power and efficiency based on the number of baffles.

Measurement Implementations

The measurements for this experiment were conducted on a panel with a surface area of 0.658 $[m^2]$. The mass flow rate of the air is controlled by a fan at the inlet of the air collector, powered at a voltage of 6 $[V]$, which results in a mass flow rate of 0.00418, 0.005411 and 0.00684 $[\frac{kg}{s}]$, respectively for 5,7 and 9 baffles. Initially, measurements were taken on a collector with 5 baffles, and then a modification was made so the collector had 7 baffles and eventually had 9 baffles.

Influence on the power output

As mentioned in the previous paragraph, we want to observe once again the influence of the number of baffles on the power output and the ratio of this power to the solar power captured by the collector. We will again rely on the measurements taken to characterize the heat exchange between the slate and the air for the different configurations. Les mesures de la slate temperature afin de calculer le ΔT_m de la configuration à 5 chicanes ont été faites en prenant un point à l'entrée et un autre à la sortie. Les mesures de la température d'ardoise pour les configurations à 7 et 9 chicanes sont prises avec un point sur l'avant de l'ardoise et considérant l'ardoise constante pour toute la surface. Cela implique que le coefficient de transfert sera plus important étant donné que pour une même puissance, le ΔT_m calculé sera inférieur avec la première méthode de mesure plutôt que la deuxième. This implies

that the transfer coefficient will be higher since, for the same power, the calculated ΔT_m will be lower with the first measurement method compared to the second. This simply changes the value of the heat transfer coefficient U that the user should use when utilizing the results of this thesis. However, it does not affect the relevance of the comparisons of efficiency, extracted heat over time, and irradiance data. The results obtained are as follows:

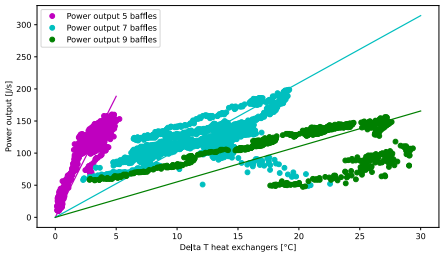

(a) Power output w.r.t ΔT_m

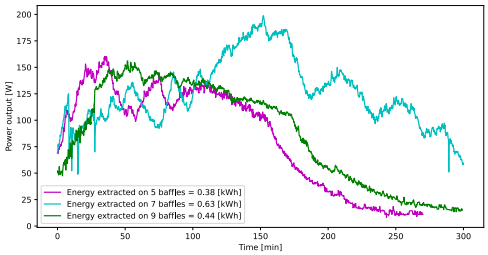

(b) Power output w.r.t time

These results are obtained from the irradiance data presented in Figure 3.36.

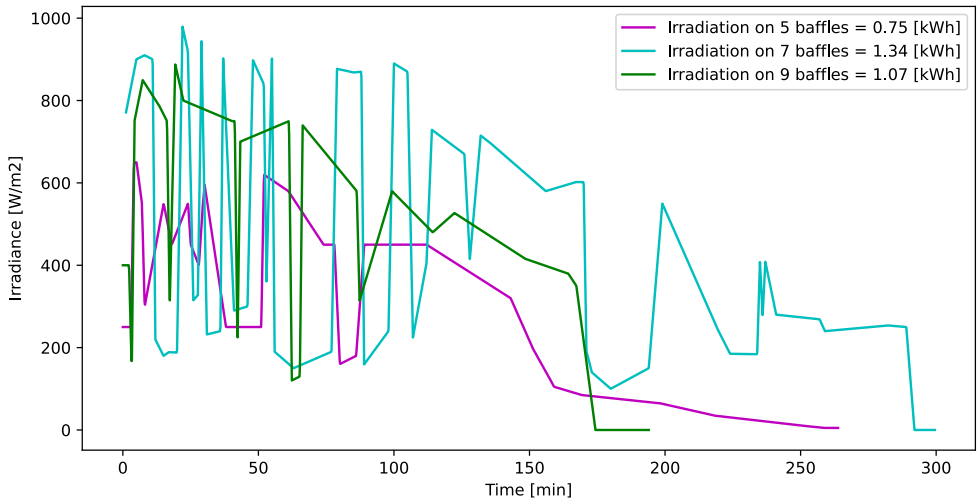

Figure 3.36: Irradiance data

By analyzing the irradiance captured by the small collector and the power extracted from it over time for the three tested configurations (5, 7, 9 baffles), we can determine the ratio of energy converted into useful heat relative to the energy available in

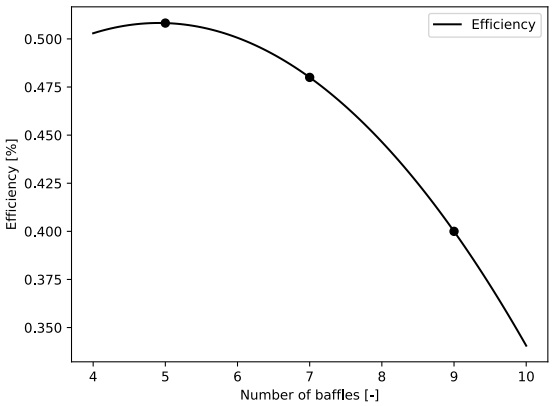

Figure 3.37: Efficiency based on the number of baffles

the solar resource. These energies are respectively calculated by integrating the power output and irradiance curves, multiplied by the area of the collector used, over the entire measurement period. The integration is again performed using the trapezoidal numerical integration method. For the previously taken measurements, we obtain the values:

Baffles [-]	Irradiation [kWh]	Useful energy [kWh]	Efficiency [%]
5	0.75	0.38	50.82
7	1.34	0.63	47.57
9	1.07	0.44	40.47

Table 3.11: Comparison of efficiency based on the number of baffles

The three measured efficiencies are then interpolated using a second-degree function (fig 3.37). It is observed that this function has a theoretical maximum at 4.8 baffles with an efficiency of 50.84%. In practice, for a collector of similar size to the one used, the optimal efficiency is achieved with 5 baffles and is 50.33%. Therefore, one can observe that for an average irradiance between 280 and 510$[\frac{W}{m^2}]$ (May in Belgium 2024), the reduction in flow rate due to the higher number of baffles has a greater impact on the output power than the benefit provided by a longer air path due to the baffles. These data are specific to Belgium, but the optimal number of baffles tends to increase if the average irradiance is in a higher range.

3.2.8 Natural convection

Making use of these collectors without any flow rate controller presents one noticeable advantage: the passivity of the device. Indeed, this enhances resilience to electricity shortages or component failures, which is particularly relevant in dwellings such as tiny houses. It also avoids the low background noise created by the fan. As can be seen below, however, the power output is much lower, and this configuration should be used only under specific conditions.

Evaluation of the mass flow rate

The evaluation of the mass flow rate is much more challenging in natural convection since it is no longer constant. As seen before, the mass flow rate depends on the square root of the temperature difference between the absorber and the inlet. Following the Log-Tchebycheff methodology, we could evaluate the flow rate at some working points, measuring the outlet air speed with a hot wire anemometer. Afterwards, one just needs to multiply the flow rate computed by the outlet air density to have the mass flow rate.
The fitted square root function allows to compute the mass flow rate for any temperature difference. To reproduce these results, the absorber temperature has to be taken on the front top left quarter of the absorber.
The collector used for the following analysis is the one with the aluminium absorber whose design parameters can be found in the section 4.5. The following graphs highlight the mass flow rate evolution and the temperature (inlet, outlet and absorber). The x abscissa is the time during which the collector is exposed to the specific irradiance. The outlet and aluminum absorber temperatures start around 33 degrees due to the few minutes needed to install the setup and begin recording measurements. These measurements are dated from the 11 may.

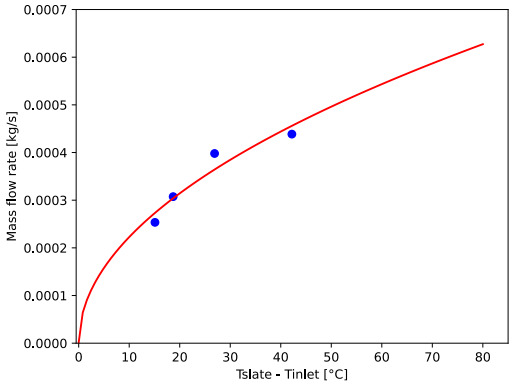

Figure 3.38: Mass flow rate evolution for the aluminum collector

The equation of the function is :

$$6.998 \cdot \sqrt{\Delta T_{inlet}} + 1.346e - 6$$

In natural convection, the mass flow rate is a factor 10 lower than in forced convection, which is in compliance with the theoretical computation of the mixed convection flow with a low impact of the natural convection.

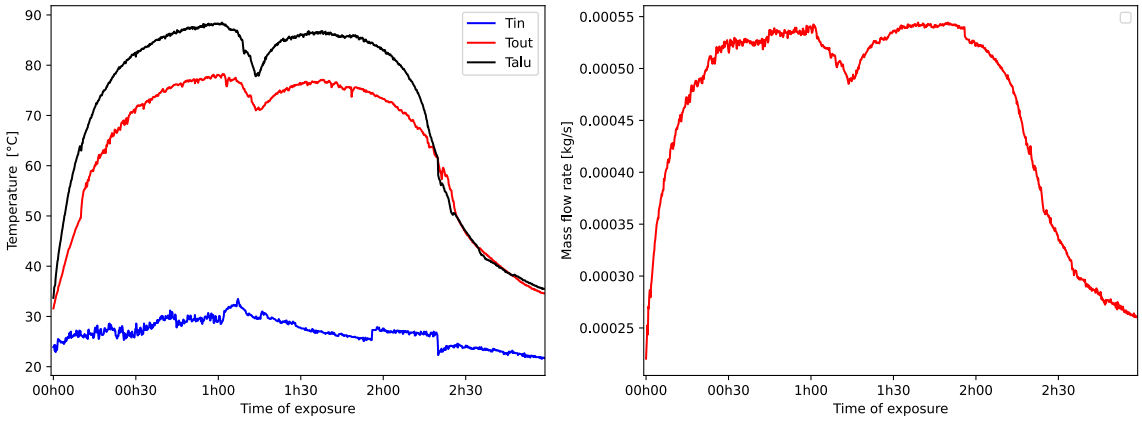

Figure 3.39: Temperatures and mass flow rate evolution

These graphs depict the power output of the collector with the aluminium absorber. On the left one can see the instantaneous power given to the air and on the right the incoming irradiance times the area of the collector.

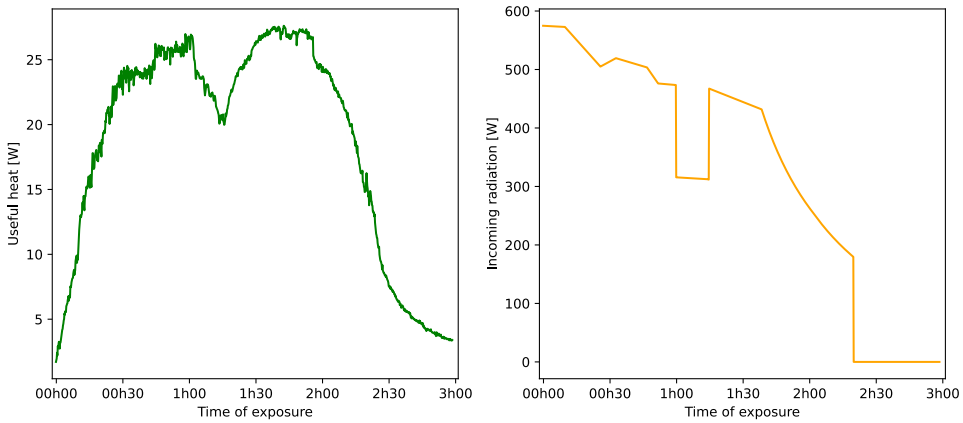

Figure 3.40: Power output vs power incoming

The results of these graphs are gathered in the table here below. On the right column are the results obtained in forced convection for the same collector a different day. Results obtained for the small slate absorber collector for the same day have been written down as well for the temperature comparison since the behavior of the collectors is highly fluctuating.

	11 may NC[2]	5 may FC[3]	11 May FC slate absorber
Power output	55.73 [Wh]	793.77 [Wh][4]	864.8 [Wh][5]
Irradiation	970.0 [Wh]	2027 [Wh]	1521 [Wh]
Yield	5.75 %	39.16 %	56.8 %
Hourly average mass flow rate	0.166 [kg/h]	16.48 [kg/h]	25.36 [kg/h]
Average absorber temperature	71.95 [°C]	52.84 [°C]	68.30 [°C]
Average increase in air temperature	37.64 [°C]	29.38 [°C]	32.12 [°C]

Natural convection usually leads to higher outlet temperature for same conditions since the mass flow rate is of a factor of 100 times lower than in forced convection which takes thus less heat from the absorber. While a higher absorber temperature however leads to higher heat losses, it also potentially heats up more the fluid. Since the air flows slowly along the absorber, it has time to heat up and reach high temperatures.

However this higher outlet temperature cannot compensate for the low mass flow rate observed. This is why we end up with a yield of 5.75 %, around 14.7% of the potential power output one could have achieved using a mass flow rate controller, based on the 39% yield (the 56.8% yield being far above the average observed, one shouldn't expect that as usual).

Assuming that using the same fan to control the flow rate one would have thus achieved a yield of 39 %, this would have led to an increase of the actual power of 322.57 Wh on the period. The fan consumes a power of $12[V \cdot 0.17 = 2.04[W]$ which corresponds to 6.12 Wh electric for the period. To draw a parallel with a heat pump, this increasing of heat produced, consuming 6.12 Wh would correspond to heat pump with a COP of 52.7!
This very simplistic comparison aims just to highlight that the use of a fan to increase the flow rate is undoubtedly beneficial. One inevitably will have to face the drawbacks related such as the loss of resilience to electricity shortage, one is then less autonomous, to the maintenance of such a device and to the background noise.

3.2.9 Yearly Analysis

Eventually, to characterize in a practical manner the power output of the air thermal collector, we need to evaluate the auxiliary heat provided throughout the year. As we experimented, the collectors are really sensitive to any change of irradiance and their behavior can therefore not be simulated with a large granularity.

This is why we ran the simulation with a 10 seconds precision.
The data input for the wind speed, atmosphere temperature and irradiance are given every five minutes from the Solcast website (24) and taken constant over that period.
The working of the function is explained in the methodology 2.6.2.

The characteristic of the simulation has been gathered in the table.

Feature	value
Collector	small collector 7 baffles
Insulation	Polystyrene foam 18mm thickness
Tilt angle	90 [°]
Azimuth angle (w.r.t. south)	0 [°]
Mass flow rate	variable (NC to 0.00987 $[\frac{kg}{s}]$)
Wind speed	$v(z) = v_{10} \cdot (\frac{z1}{10})^{\alpha}$

Table 3.12: Characteristics of the simulation

The design characteristics of the small collector with 7 baffles can be found here 2.4. We saw before that the 5 baffles configuration was optimum, but this is for the mass flow rate considered of 0.00541 $\frac{kg}{s}$. However, in this simulation the mass flow rate evolve throughout the iterations depending on the slate and temperature output.

We plotted the different temperatures, power, losses and mass flow rate evolution for 4 different weeks evenly spaced along the year, the first week of January, April, July and October with the main results gathered in tables. Eventually we will gather the results for the whole year. the irradiance striking the surface of the collector has been taken in order to compare easily this graph in [W] to the losses and power output.

[2]Natural convection

[3]Forced convection

[4]Where one balanced the initial and final energy of the absorber for the recorded time i.e. Talu=41.2 °Cat the beginning and 24.2 °Cat the final step so we deducted 17.83 Wh

[5]Similarly, 14.8 Whhave been added since the slate ended at a temperature of 8.8 degrees higher.

One has to keep in mind that the inlet air is the outdoor air and that the power outputs have been computed based on the heat given to this air. One cannot simply consider that the following power outputs completely contribute to the heating of the dwelling. The electricity consumed by the fan is simply its current times the power set times the time during which this power is set (scheme for each iteration).

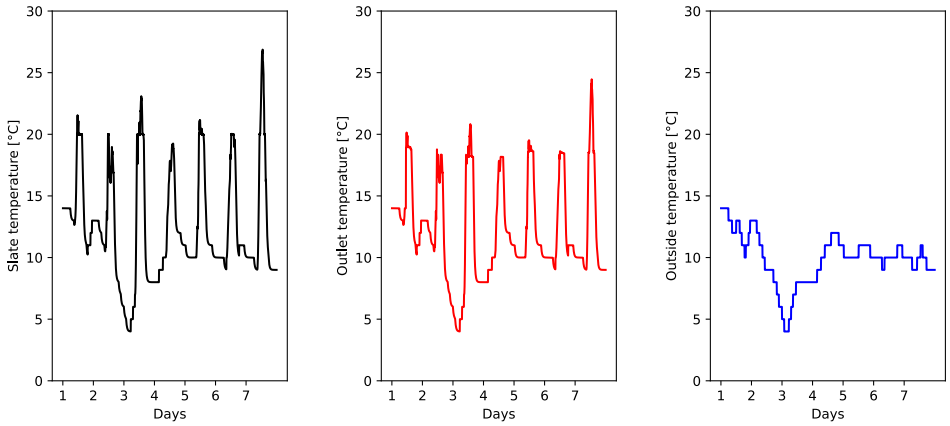

Figure 3.41: Absorber, outlet and inlet temperature evolution for the first week of January

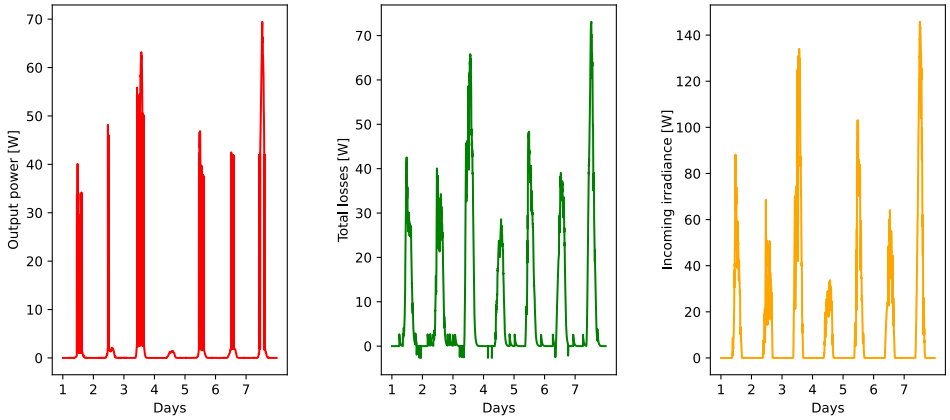

Figure 3.42: Power output and losses evolution for the first week of January

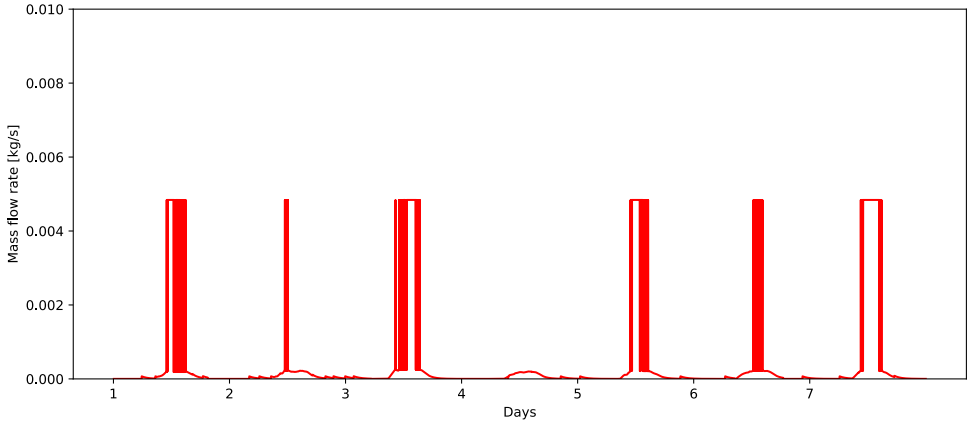

Figure 3.43: Mass flow rate evolution for the first week of January

Results	Value [KWh]
Front losses	0.73
Back losses	0.27
Edge losses	0.10
Optical losses	0.41
Total losses	1.51
Power output	0.63
Yield	29.56
Irradiation	2.14
Electricity consumed	0.018

Table 3.13: Power output and losses for the first week of January 2023

While the simulation optimizes the mass flow rate to the actual conditions, the yield obtained stays quite low for this week.
This is because the slate and outlet temperature don't rise high. The natural convection mass flow rate is therefore constantly switching from the first mass flow rate imposed by the fan to natural convection, which results in colored bars on the graph. The power consumed by the fan is thus almost insignificant.
However, the mass flow rate in natural convection is very low. The power output therefore also varies a lot, as seen on the fully colored evolution, while the losses oscillate less and stay at the high position which is however similar for the losses and the power output. The integral of the losses is obviously higher. The outlet temperature is very close to the slate temperature since the latter is low. The

atmosphere temperature is around 10 °C and even if the power output is not significant, an effective air replacement in the dwelling can be done without seriously cooling it.

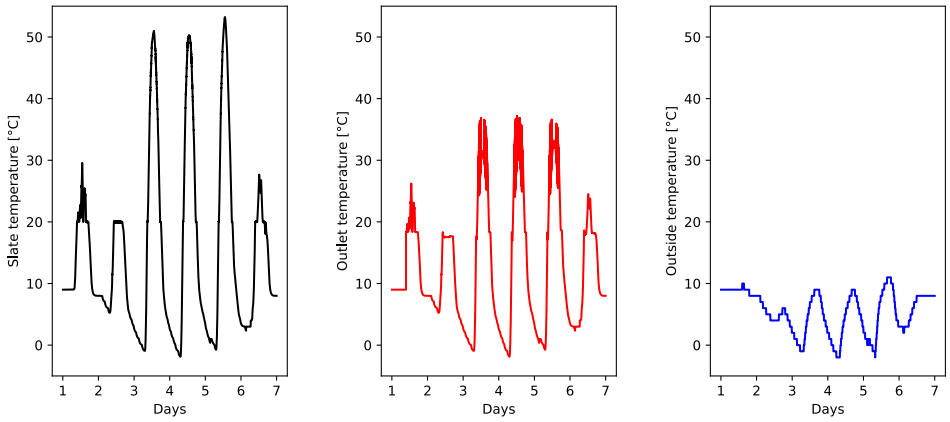

Figure 3.44: Absorber, outlet and inlet temperature evolution for the first week of April

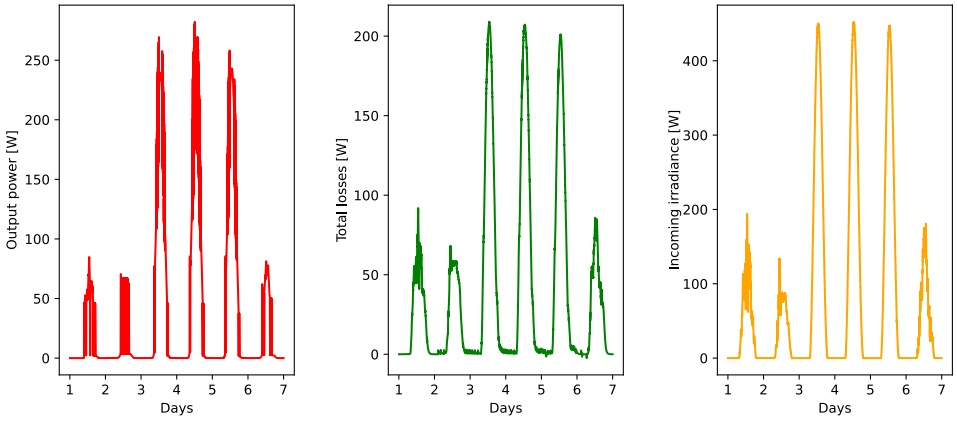

Figure 3.45: Power output and losses evolution for the first week of April

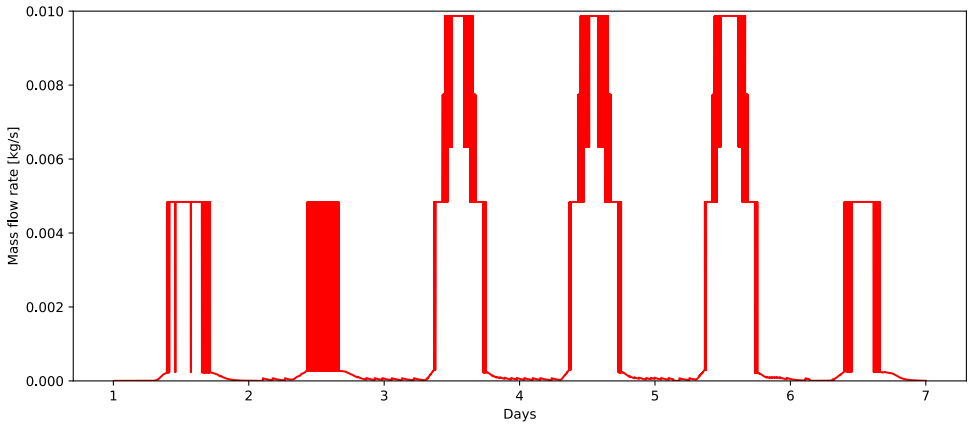

Figure 3.46: Mass flow rate evolution for the first week of April

Results	Value [KWh]
Front losses	2.34
Back losses	0.88
Edge losses	0.31
Optical losses	2.04
Total losses	5.57
Power output	5.10
Yield	47.78
Irradiation	10.67
Electricity consumed	0.072

Table 3.14: Power output and losses for the first week of April 2023

The yield is consequently increased while the atmosphere temperature is even lower than previously which could induce high heat losses. However, the peaks of irradiance combined with a high flow rate allowed for a good harnessing of heat from the panel. The output power is quite significant and seen the outdoor temperature, the collector would be of a great use to heat up the dwelling during this period of the year. In fact inter-season weeks such as this one, with a low atmosphere temperature but a relatively high enough irradiance, one can have a really useful heat supply.

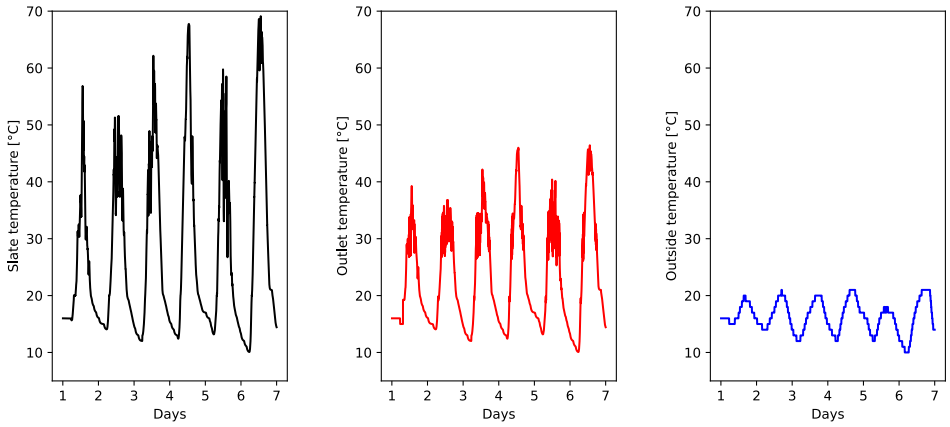

Figure 3.47: Absorber, outlet and inlet temperature evolution for the first week of July

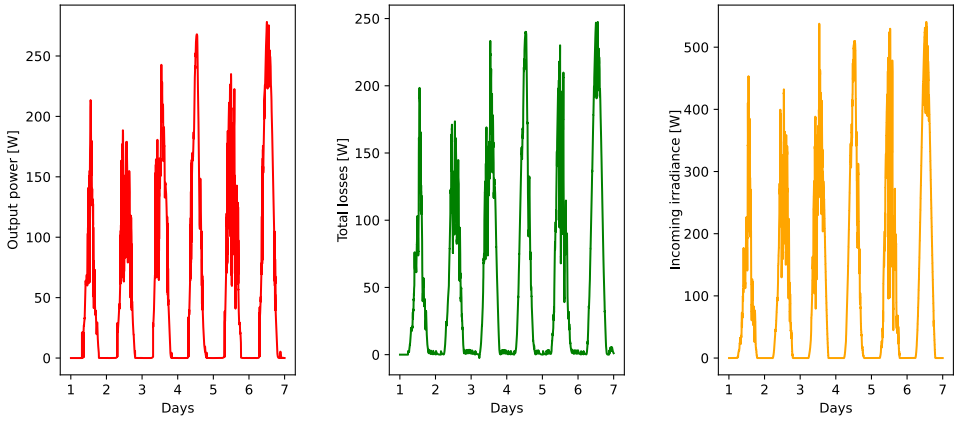

Figure 3.48: Power output and losses evolution for the first week of July

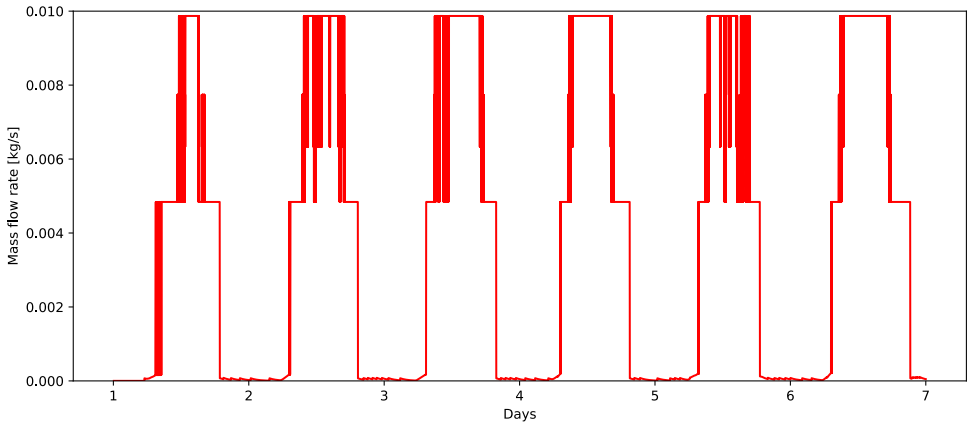

Figure 3.49: Mass flow rate evolution for the first week of July

Results	Value [KWh]
Front losses	2.99
Back losses	1.05
Edge losses	0.36
Optical losses	2.90
Total losses	7.30
Power output	7.88
Yield	51.9
Irradiation	15.18
Electricity consumed	0.152

Table 3.15: Power output and losses for the first week of July 2023

The yield increased a bit more since the slate is most of the time warmer than 20 °C, allowing for an efficient mass flow rate to harness energy from the absorber. The power output over the week is consequent while the outdoor temperature is already sufficient to maintain a comfortable inside temperature during the day. The collector is therefore more likely to be useful by the end of the day, the flap being kept opened and the outlet closed during the day. The power consumed by the fan is higher than for the previous periods, however, this corresponds to 0.32 % of the heat produced which does not decrease the system profitability.

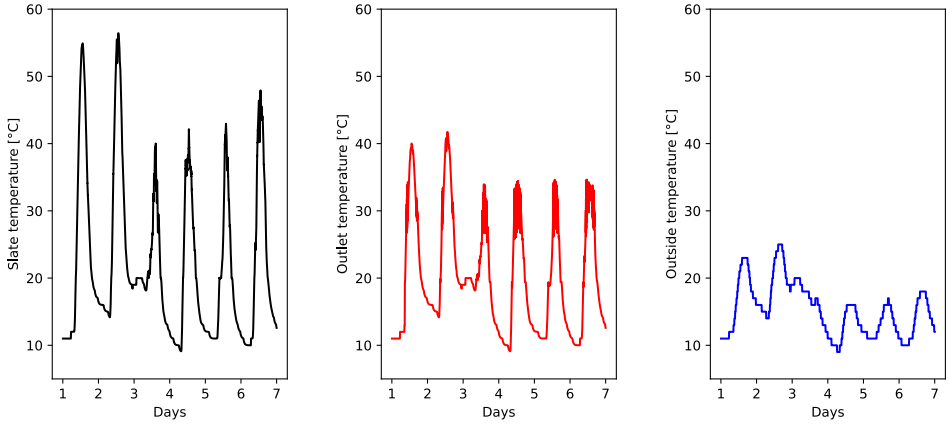

Figure 3.50: Absorber, outlet and inlet temperature evolution for the first week of October

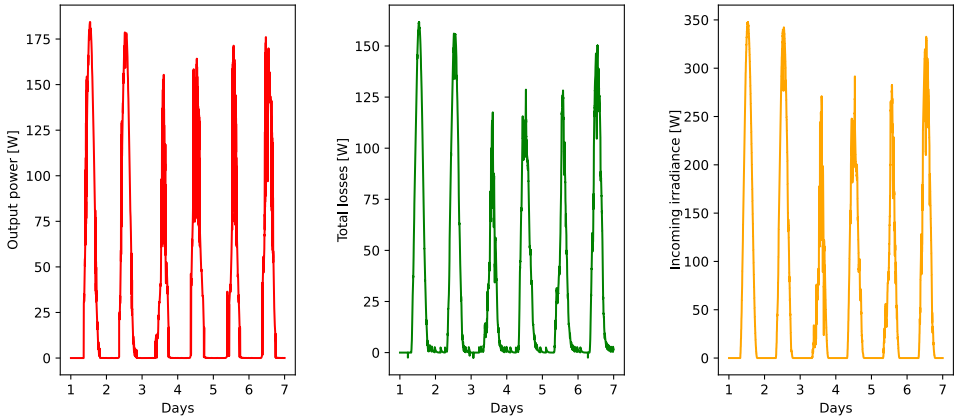

Figure 3.51: Power output and losses evolution for the first week of October

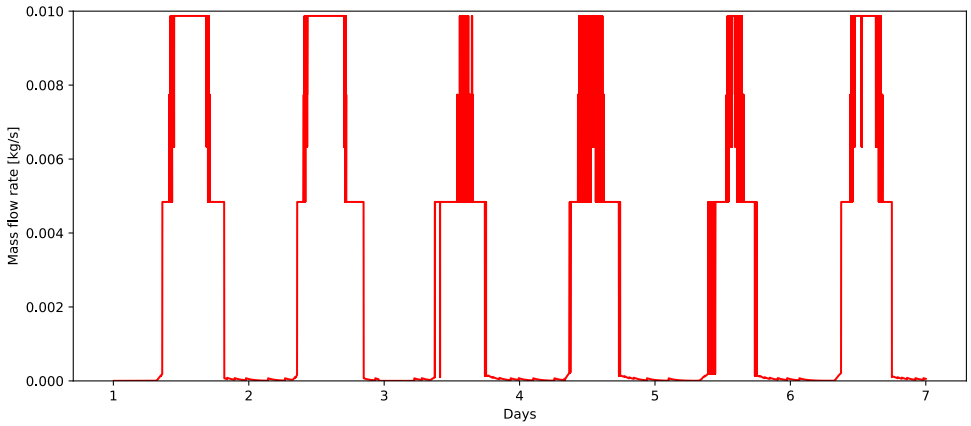

Figure 3.52: Mass flow rate evolution for the first week of October

Results	Value [KWh]
Front losses	1.80
Back losses	0.65
Edge losses	0.23
Optical losses	1.74
Total losses	4.42
Power output	4.68
Yield	51.44
Irradiation	9.10
Electricity consumed	0.110

Table 3.16: Power output and losses for the first week of October 2023

The two first days of the week, the absorber reaches high temperatures due to a significant irradiation and atmosphere temperature (which reduces thermal losses). While the collector won't be useful during these days, it still is interesting by the end of the day. For the following days, outdoor temperature drops and the collector keeps an average power of 150 [W] during the day.

the results for the whole year are gathered in the table below. The global yield is 49.54 %, fluctuating therefore from values around 30 % to more than 50%. We can assess that the thermal collector is a good device to harness solar energy while consuming a low level of electricity consumed, around 0.33 % of the power output.

Results	Value [KWh]
Front losses	119.05
Back losses	43.07
Edge losses	15.01
Optical losses	107.95
Total losses	285.08
Power output	280.84
Yield	49.54
Irradiation	565.9
Electricity consumed	5.59

Table 3.17: Power output and losses for the whole year of 2023

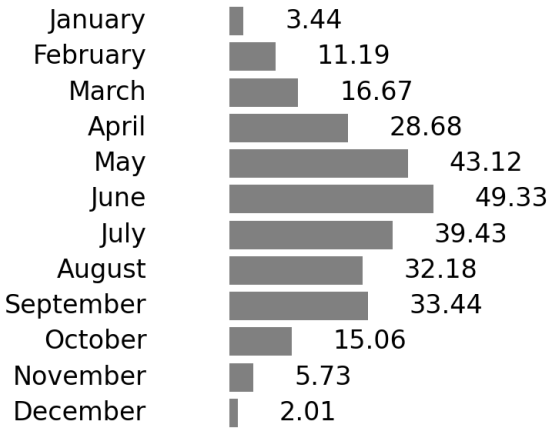

Figure 3.53: Monthly share of the power produced [kWh]

For this size of collector (0.658 [$m2$]), these results are well optimized thanks to the variable air flow. We see that the mass flow rate often saturates to its high position, however, we cannot ensure that a higher mass flow rate would be more beneficial. Indeed, the heat transfer coefficient of the heat exchanger is likely to decrease at a higher flow rate due to the lack of time to heat up correctly the air. A configuration with a higher surface or with more baffles and thus a longer path would increase this contact time and improve the heat transfer coefficient of the heat exchanger at a high mass flow rate. The heat provided in summer is as expected much higher than in winter. Nevertheless, during inter-season months such as April or September the collector could greatly contribute to the heating, adapting its dimension or number to the volume of the dwelling.

3.2.10 Impact of the orientation

The orientation and tilt cannot always be chosen when setting a solar collector, yet they have an important impact on the power harnessed. For the azimuth angle, which defines the orientation of the collector, we computed for the evolution of the total irradiation striking the collector, the power output and the yield for the first week of April analyzed before. We chose this week since this is an inter-season week during which one still needs to warm up the house but during which irradiation can be significant enough to produce heat thanks to the collector.

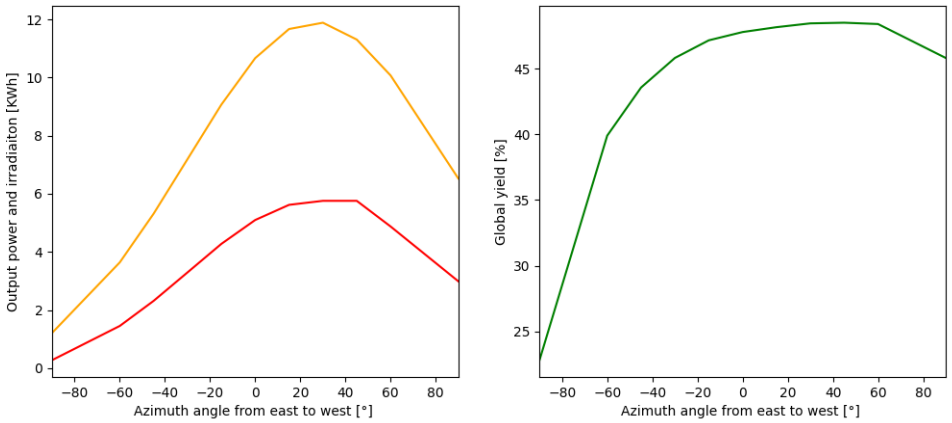

Figure 3.54: Evolution of the irradiation, power output and yield in function of the azimuth angle

There seems to be an optimum for the yield around 30 degrees from south to west which can be explained by the fact that solar irradiance is higher in the afternoon when the sun is in the west, compared to the morning when it is in the east which also explains the evolution of the irradiation curve . This is for a tilt angle of 90 ° and for the first week of april. The optimum tends to be facing completely the south for the whole year, with a good efficiency at small azimuth angle from south.

3.3 Discussion of the assumptions

1. Heat flow through the cover is one-dimensional. The heat transfer of the glass cover is 166.67 for the small collector 3.2. The impact of the cover itself is non-existent and does not change the global heat transfer coefficient. This is totally valid.

2. One-dimensional heat flow through back insulation for the same reason as mentioned before. This assumption does not impact our experiments as we got similar results by simulation and experimentally. Actually the way the heat flows through the insulator is not paramount in this case because it doesn't represent the main heat transfer and the surface temperature can be simulated knowing the absorber and atmosphere temperature. therefore the total heat transfer through the insulation can be evaluated, but not its spreading.

3. The absorber and base planes can be approximated by infinite parallel plates. It eliminates edge effects and makes it easier to apply theoretical models for the heat transfers. The edges behave differently than the center. For the absorber this assumptions induces uncertainties due to the heat gradients, the edges are colder than the center, and it induces pressure losses. In fact, all the edges on which air flows induces pressure losses as we evaluated here 2.9. some are regular losses, along the surfaces, but every turning and flow against the walls induces singular pressure losses which are not negligible as we saw. However, since we measured experimentally the mass flow rates this does not influences importantly our results.

4. Surfaces can be assumed to be diffuse and gray. Considering them as diffuse means that they scatter radiation uniformly in all directions. It simplifies the radiative heat transfer calculations since the directional dependence of radiation can be ignored. Considering them gray means that the surfaces have constant emissivity and absorptivity. They are independent of wavelength which simplifies the calculations since it allows the use of average values for these properties. However, the material temperature can vary from 0 or lower to 90-100 degrees. In this range of temperature, emissivity and absorptivity can decrease of around 5 % (20) (when increasing in temperature) which is not negligible and could be taken into account. The radiative heat transfer coefficient of the front face is not negligible as seen before 3.2 hence we cannot ensure that assuming diffuse and gray surfaces is totally valid but we can suppose that its impact would be though really low.

5. Sky is considered as a blackbody. It simplifies the modeling of radiative heat exchange between the collector and the sky since we can use the blackbody radiation laws for the sky.The sky consists of various gases, aerosols, and water vapor that interact with sunlight in different ways. These interactions include absorption, scattering, and emission, which deviate from blackbody behavior.

The emissivity is therefore not uniform neither. One could develop greybody models which account for emissivity less than 1 and can approximate some aspects of atmospheric radiation.

6. Uniform Solar Radiation. Allows for a uniform calculation of the absorbed solar energy across the entire surface of the collector. A solar panel is oriented in one same direction and receive thus a similar amounts of sunlight. if we were to consider a small scale area farm of solar collectors for instance this would become less valid.

7. The absorber temperature is uniform. Combined with the previous hypothesis, this simplifies the heat transfer. This reduces the complexity of the heat transfer equations and leads to a single spatial dimension which is easier to solve but we saw that this supposition is far from being true and would need a tri-dimensional analysis to better simulate the heat transfers occuring.

3.4 Exchanger heat transfert coefficients for different topologies

Small collector: $0.658[m^2]$						
$\dot{m}$	Nbr of baffles	Material	Isolation	Mean ΔT_m	Measurement	Transfer Coefficient
0.00684	5	Slate	✗	2.30	In/Out	45.4
0.00541	7	Slate	✓	6.26	Front	14.04
0.00541	7	Slate	✓	16.53	Front	10.66
0.00541	7	Slate	✗	8.62	Front	12.67
0.00418	9	Slate	✗	15.19	Front	7.91
0.00418	9	Slate	✗	20.55	Front	8.39
0.00418	9	Slate	✗	12.24	Back	13.99

Table 3.18: Exchanger heat transfer coefficient $[\frac{W}{m^2K}]$ small collector (0.658 m^2)

Large collector: $1.212[m^2]$						
$\dot{m}$	Nbr of baffles	Material	Isolation	Mean ΔT_m	Measurement	Transfer Coefficient
0.00559	7	Slate	✗	11.29	Front	7.49
0.00802	7	Slate	✗	4.44	Front	6.64
0.00802	7	Slate	✗	18.96	Front	6.64
0.00802	7	Slate	✗	21.79	Front	6.44
0.00882	7	Slate	✗	11.56	Front	8.03

Table 3.19: Exchanger heat transfer coefficient $[\frac{W}{m^2K}]$ large collector (1.212 m^2)

3.5 Conclusion

Our research on the performance of low-tech solar collectors for tiny houses yielded significant insights into their efficiency and behavior under various conditions. The key findings from our simulations and experimental measurements are as follows:

We assessed the heat exchanger transfer coefficients for two collectors with different areas, various mass flow rates, temperature differences (ΔT_m), and probe locations. One can therefore simulate and predict his collector behavior throughout the year by using the most appropriate coefficient to the design of the new one. Values range from 6.64 to 45.4, which are quite low compared to water-air heat exchangers that typically have coefficients ranging from 200 to $[\frac{W}{m^2K}]$(25). However, this application performs quite well despite the absorber not storing a large amount of energy,only 363.5 kJ for an 80°C slate in 20°C atmospheric air for the small collector,therefore, a very high heat transfer coefficient is not necessary for achieving good efficiency.

Through experiments, we achieve yield ranging from 20 to 55 %, which is a large span. The reason of this fluctuation comes mainly from the irradiance data. An analysis showed that for a given mass flow rate, a collector with an area 1.84 times larger than another one outperforms the smaller collector by 14.6 % at a mean irradiance of 234 $\frac{W}{m^2}$ and this performance rises linearly increasing to 61.86% of additional power output with a mean irradiance of 598 $\frac{W}{m^2}$. However, 598 $\frac{W}{m^2}$ being already a quite high value for an average, we cannot easily expect a linear increase of power output with the surface in this configuration. The mass flow rate must be increased. Indeed, the outlet temperature is in general close to the back last slate temperature (5-8 degree difference approximately). For mass flow rate, the contact area it thus 1.84 larger but the higher temperature reached cannot compensate for the power linearly.

An efficiency improvement of up to 20 % is achievable through the insulation of the collector. Subsequent insulators improve much less the yield. The second 18 mm polystyrene insulator improve proportionally the yield of 4.3 % which represent 1.8 % more of irradation captured. It is still beneficial but for a mounted collector one has to assess the insulation brought by the wall.

An overview of the heat transfer coefficient characterizing the losses teaches us (small collector values) that edges have a heat transfer coefficient of 3.05 $\frac{W}{m^2}$, the back of the collector a coefficient of 1.52 $\frac{W}{m^2}$ with insulator and 3.61 times lower without insulator, and the front 7.22 $\frac{W}{m^2}$.
This highlights that losses through the front face are leading and they represent on average more than 40 % of the total losses. This values is diminished if only conduction and radiation are considered in the front layer air thickness between the absorber and the cover. It represents a higher share of the losses if the back is

insulated.
Due to the low insulation of the cover, the drop of temperature is low between its outer and inner part. Therefore there is a high gradient of temperature between the absorber and the cover. Combined with the high emissivity of the surfaces, one obtains a high heat transfer coefficient through the front air layer thickness of 5.45 which highly decreases the effective conductive insulation of the air (k/e = 2.36). The use of selective materials could shrinks the radiative losses and drastically reduce the global heat losses through the front. The global heat transfer for the losses is found to be 6.275 [W] on average for the 0.658 m^2 collector. This evolves in function of the delta of temperature between the absorber and the atmosphere and characterize the graph 3.22.
A natural convection setup experimentally achieved a yield of 5.75 %. This is far from being efficient but can still have an interesting impact to refresh the air. The use of the fan greatly improves the yield while consuming a really low power.

We also assessed experimentally the optimal number of baffles to 5 for the collector of 0.658 m^2 which leads to an expected yield of 50.82 %. For the other configurations, pressure losses were higher and therefore reduce the mass flow rate. To gain in increased contact time with the absorber does not outperform the loss in flow rate. We found a yield of 47.57 % with 7 baffles and 40.47% with 9 baffles. For a higher flow rate, this optimum could switch to 7 baffles for instance. Indeed, the main simulation over the year is working with the 7 baffles configuration and with variable mass flow rate. The global yield is actually found to increase with the mass flow rate and can be kept constant around 50 % of the irradiation from spring to autumn by forcing a variable mass flow rate thanks to a small fan. the inter-season is the period when the collector can be the most useful due to the low outside temperature and the sufficient irradiance. One can harness 28.68 kWh and 53.12 kWh in April and May. With such a small collector this is not negligible. In this configuration, a collector with an area of 0.658 m^2 harnesses 280.84 [kWh] throughout the year with a global yield of 49.54 %.

For the first week of April, an azimuth angle of 30 ° from south to west is found to be optimal. Indeed, we can see that the irradiance is higher in the afternoon i.e. to the west than in the morning i.e. to the east. At our latitude, it is common to have periods where this is the case. However for a full year optimum one need to face the collector to the south.

The absorber inertia is characterized by its opposition to a sudden variation of temperature which corresponds here to how long it provides heat when there is no irradiance anymore and how fast heat is spread through the material. As seen on the graph, depending on how warm the slate is when irradiance stops, one can expect to have a decreasing power output during one to two hours. The

rear surface temperature lags by 50 seconds, indicating that when the front of the slates experiences a rapid temperature increase, this peak reaches the rear surface after 50 seconds. Additionally, the rear slate surface is, on average, 3.96 $[°C] cooler than the front$.

In conclusion, while low-tech solar collectors cannot fully replace traditional heating systems due to the intermittent nature of solar radiation, they provide a substantial supplementary heating solution that enhances energy efficiency and sustainability in tiny houses.

3.6 Recommendations

To further develop the research, here are some essential future recommendations and improvements that we suggest. A potential feature that could be added to the collector is honeycombs between the glass and the absorber. The interest is to allow an increase of the cover-absorber gap while reducing the convection in the air layer while , making conduction the main heat transfer in this air layer and thus improving the insulation.

In order to have a long living collector, one could make it in a different way. Using the router, it is possible to dig a notch on an horizontal plane in the thickness of the frame. Therefore, it is possible to slide the base in these notches by assembling 3 sides of the frame only, then sliding the base, then closing the frame with the fourth side. This allows to avoid the large contact zone between the base and the frame that experiences rain infiltration and whose fixing can wear out. Moreover it strengthens the panel and allows the fixing of the insulator within the frame thickness right behind the base for a better aesthetic aspect.

Future research should focus on optimizing material properties and collector designs such as selective materials or cover with higher transmittance or low emissivity etc.

An interesting analysis could be on the uncertainty of the results. Indeed there are uncertainties linked to the instrumentation and to the measurements that influence the results. Quantifying them and their cascade impact would give a confidence interval to interpret these results.

Further experimental analysis should be performed using several identical collectors and changing one feature at a time and repeat the experiment several times to confirm the results.

A computational fluid dynamics would undoubtedly improve the model. This

would help studying the distribution of airflow around obstacles, such as baffles, and identifying areas of turbulence or stagnation that could be improved. The temperature distribution obtained would help identify areas of uneven heating, allowing for adjustments in the design to improve overall thermal performance. As previously mentioned, the code considers the absorber temperature as an average. The air reaches lower temperature since it cannot be heated up higher than at the average temperature. The tri-dimensional heat spread analysis would increase the accuracy of the real outlet temperature. Other parameters such as the spacing and size of the baffles or the shape of the collector frame would be better understood.

Bibliography

[1] NightHawkInLight, *Easy heat from DIY solar thermal panels*, https://www.youtube.com/watch?v=Tg44ndqPTGQ

[2] LENVI2007, https://moodle.uclouvain.be/course/view.php?id=4982

[3] Claire Heather Trease, *Design and development of novel absorber coating for solar collector applications*

[4] Solar Radiation, Michigan Technological University, Available at: https://pages.mtu.edu/~jstallen/courses/MEEM4200/lectures/solar/Arici_Chp_VII.pdf

[5] TSI Inc., *Traversing a Duct*, https://tsi.com/getmedia/1a11d344-0a58-4ca6-94fe-65721825686b/AF-106%20Traversing%20a%20Duct?ext=.pdf

[6] JPC Inc., *Fan and Blower Datasheet*, https://www.e-jpc.com/wp-content/uploads/fanblower2007.pdf

[7] A. A. Ghoneim, *Performance Optimization of Solar Collector Equipped with Different Arrangements of Square-Celled Honeycomb*, https://www.researchgate.net/publication/245074160_Performance_optimization_of_solar_collector_equipped_with_different_arrangements_of_square-celled_honeycomb

[8]

[9] Saad M. K. Ismail, Nabaz G. Hasan, and Bnar S. Mahdi, *Estimation of Global Solar Radiation in Duhok City and Characterization of Two Types of Silicon Solar Cells*, https://www.researchgate.net/publication/362082143_ESTIMATION_OF_GLOBAL_SOLAR_RADIATION_IN_DUHOK_CITY_AND_CHARACTERIZATION_OF_TWO_TYPES_OF_SILICON_SOLAR_CELLS/figures?lo=1

[10] Saad M. K. Ismail, *Green House Effect vs Infrared Radiation Emissions*,

https://www.researchgate.net/publication/302923000_Green_House_Effect_vs_Infrared_Radiation_Emissions

[11] Physics Forums, *What is the Difference Between Emissivity and Reflectivity?*, https://www.physicsforums.com/threads/what-is-the-difference-between-emissivity-and-reflectivity.340828/#:~:text=Materials%20with%20high%20emissivity%20tend,significant%20amount%20of%20incoming%20light

[12] Guy Isabel, *Les capteurs solaires à air*

[13] Yunus A. Cengel, Robert H. Turner, John M. Cimbala, 3^{rd} edition, *Thermal-Fluid sciences*

[14] Noureddine Mechi, *Global Solar Radiation on Tilted Surfaces in Tunisia: Measurement, Estimation, and Gained Energy Assessments*, https://www.researchgate.net/publication/324502848_Global_solar_radiation_on_tilted_surfaces_in_Tunisia_Measurement_estimation_and_gained_energy_assessments/figures?lo=1&utm_source=google&utm_medium=organic

[15] Olga Stryzhak and Oksana Bryl, *The Influence of Machining Parameters on Surface Roughness of MDF in Milling Operation*, https://bioresources.cnr.ncsu.edu/resources/the-influence-of-machining-parameters-on-surface-roughness-of-mdf-in-milling-ope

[16] Ahmed A. E. and Ali H. H., *Effect of the Air Channel Depth on the Efficiency of Photovoltaic/Thermal Sensor with a Parabolic Concentrator*, Available at: https://studylib.net/doc/18182641/effect-of-the-air-channel-depth-on-the-efficiency-of-phot...

[17] Frank P. Incropera, David P. DeWitt, Theodore L. Bergman, Adrienne S. Lavine, *Fundamentals of Heat and Mass Transfer, 6th Edition*, Available at: https://hyominsite.wordpress.com/wp-content/uploads/2015/03/fundamentals-of-heat-and-mass-transfer-6th-edition.pdf pages 587-590

[18] Convective Heat Transfer. Available at: https://www.engineeringtoolbox.com/convective-heat-transfer-d_430.html

[19] OMEGA Engineering. Emissivity of Common Materials. Available at: https://www.omega.co.uk/literature/transactions/volume1/emissivityb.html

[20] Emissivity Coefficients. Available at: https://www.engineeringtoolbox.com/emissivity-coefficients-d_447.html

[21] Fresnel Equations. Available at: https://www.rp-photonics.com/fresnel_equations.html

[22] Published by IIETA. Available at: https://iieta.org/journals/psees/paper/10.18280/psees.010101

[23] MDPI. Available at: https://www.mdpi.com/2071-1050/15/13/9932

[24] Solcast. Available at: https://solcast.com

[25] ASHRAE Handbook - Fundamentals (2017 Edition, Chapter 14)

Appendix A

Log-Tchebycheff method : detailed tabulars

circle	6V	7.5V	9V	12V
small circle average	0.687	0.855	0.872	1.455
medium circle average	0.575	0.888	1.013	1.392
large circle average	0.478	0.740	0.865	1.117
Average speed	0.580	0.833	0.917	1.321

For the first configuration of the small collector (5 baffles), one obtains these results :

circle	6V	7.5V	9V	12V
small circle average	0.820	1.158	1.405	1.730
medium circle average	0.833	1.028	1.235	1.570
large circle average	0.632	0.720	0.882	1.308
Average speed	0.762	0.969	1.174	1.536

For the second configuration of the small collector (7 baffles), one obtains these results :

circle	6V	7.5V	9V	12V
small circle average	0.583	0.668	0.972	1.252
medium circle average	0.465	0.647	0.788	0.908
large circle average	0.487	0.695	0.882	0.972
Average speed	0.512	0.572	0.853	1.044

For the third configuration of the small collector (9 baffles), one obtains these results :

circle	6V	7.5V	9V	12V
small circle average	0.347	0.447	0.472	0.580
medium circle average	0.338	0.465	0.502	0.612
large circle average	0.355	0.478	0.538	0.687
Average speed	0.347	0.463	0.504	0.626

For the last collector horizontally designed, with an aluminium absorber one obtained the following results :

circle	6V	7.5V	9V	12V
small circle average	0.682	0.887	1.230	1.548
medium circle average	0.417	0.612	0.802	1.100
large circle average	0.397	0.598	0.817	1.030
Average speed	0.499	0.699	0.950	1.226

UNIVERSITÉ CATHOLIQUE DE LOUVAIN
École polytechnique de Louvain
Rue Archimède, 1 bte L6.11.01, 1348 Louvain-la-Neuve, Belgique | **www.uclouvain.be/epl**